UNIVERSITY OF CALIFORNIA
RIVERSIDE

Magnonic Holographic Devices

A Dissertation submitted in partial satisfaction
of the requirements for the degree of

Doctor of Philosophy

in

Electrical Engineering

by

Frederick Gertz

March 2015

Dissertation Committee:
Dr. Alexander Balandin, Co-Chairperson
Dr. Alexander Khitun, Co-Chairperson
Dr. Roger Lake

The Dissertation of Frederick Gertz is approved:

_____

_____

Committee Co-Chairperson

_____

Committee Co-Chairperson

University of California, Riverside

Acknowledgements

As the saying goes, it takes a village, and the work contained in this dissertation is no different. There is a considerable amount of gratitude owed to a multitude of people who all have helped me accomplish the process of both assembling this dissertation and performing the research contained within. Everyone mentioned here-in is greatly appreciated for supporting me through this process and while I know that saying thanks can in no way repay the kindness given to me I hope that it will go some small way to covering the debt I owe.

First I want to acknowledge my advisor Dr. Alexander Khitun, who has worked with me for several years, and taken a keen interest in my development. I'm quite sure this process would not have completed, or even perhaps begun without his input, and I think there is no appropriate way for me to show how grateful I am for his advice and mentorship over the last years.

Second, I must thank my family, who have supported me in this endeavour with their love and their belief in me.

Third, I think it's necessary to also address the gratitude that I owe to the cleanroom staff, Mark Heiden and Dexter Humphreys, both have been enormously helpful, and the physical realizations of these devices I firmly believe would not have happened without them.

Fourth, and certainly not least is it is necessary for me to thank the contribution of Dr. Yuri Filimonov and Dr. Alexander Kozhevnikov who both have taken time to mentor me as well as collaborate with me, and whose experience made much of this work possible

Finally I want to thank the NSF/SRC/NEB for providing funding for this research, their financial support was most appreciated.

Dedicated to my Mother

ABSTRACT OF THE DISSERTATION

Magnonic Holographic Devices

by

Frederick Gertz

Doctor of Philosophy, Graduate Program in Electrical Engineering
University of California, Riverside, March 2015
Dr. Alexander Balandin, Co-Chairperson/Dr. Alexander Khitun, Co-Chairperson

For the past 50 years technological advancement has been dominated by semiconducting technologies. Transistors have gone from macro scale to micron scaled devices to nanoscale, and CMOS technology has continuously improved to keep up with the aggressive shrinking of these logic and memory devices. However, with the release of CMOS features of 22nm and CMOS manufacturers already researching 5nm die features for devices, it is just a matter of time before CMOS and transistor technology reaches the end of what it can be scaled down to. Also with each scaling power consumption by the device as well as power dissipation from the device, especially due to waste heat becomes an increasing concern[1]. With this in mind, many new technologies have been proposed to either redesign current transistor technology to extend its future or to completely replace it with alternative technologies all together. Contained here-in is a proposed device with the possibility to replace or enhance current transistor design and CMOS processing using Spin Wave systems. The devices comprise a magnetic matrix and spin wave generating/detecting elements placed on the edges of the waveguides. The matrix consists of a grid of magnetic

waveguides connected via cross junctions. Magnetic memory elements are incorporated within the junction while the read-in and read-out is accomplished by the spin waves propagating through the waveguides. Presented in this work is experimental data on spin wave propagation through NiFe and YIG magnetic crosses. The obtained experimental data show prominent spin wave signal by the external magnetic field, where both the strength and the direction of the magnetic field define the transport between the cross arms. Also presented is experimental data on the 2-bit magnonic holographic memory built on the double cross YIG structure with micro-magnets placed on the top of each cross. It appears possible to recognize the state of each magnet via the interference pattern produced by the spin waves.

Contents

List of Figures

1 Introduction

1.1 Research Motivation

"The complexity for minimum component costs has increased at a rate of roughly a factor of two per year.

…this rate can be expected to continue, if not to increase."

- ***Gordon Moore (1965)***

Nearly half a century ago in 1965, Gordon Moore made the above quote[2]. This statement would become known as Moore's Law and is usually reduced to the statement that computing power will double every 12 to 18 months. Since this statement the semiconductor industry has grown to exceed $300 billion in annual revenues[3], while keeping pace with Gordon Moore's bold prediction. To accomplish this goal has required advances in material science, physics, manufacturing and nanotechnology. As this technology has advanced and devices have shrank problems relating to cost, effectiveness, and physical limitations have arisen and thus, to continue to keep pace with Moore's Law the industrial and academic community has begun looking for technologies beyond Silicon based transistor technology and Complimentary-Metal Oxide Semiconductor (CMOS) Processing. To deal with the expected end of the CMOS technology life cycle, several technologies have been proposed.

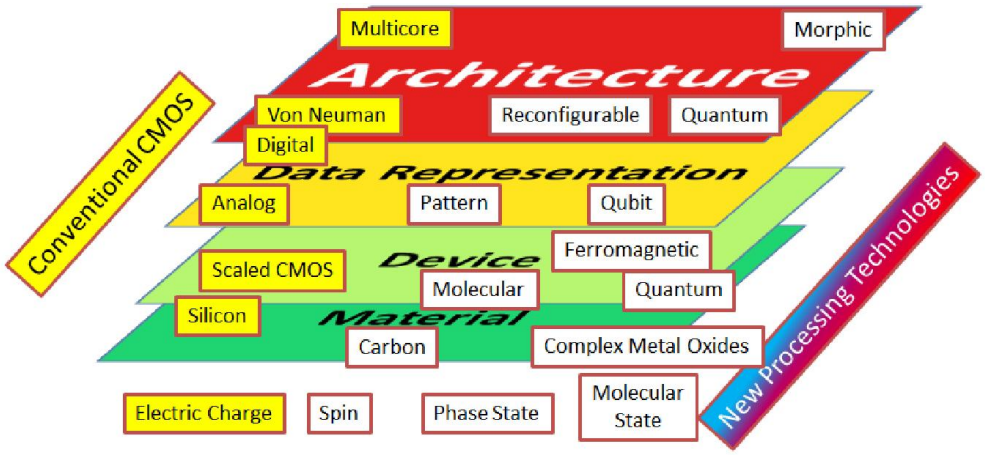

Figure 1 – Proposed roadmap for the future semiconductor technologies with conventional technologies highlighted in yellow.

To this end many different technologies have undergone development in the last decade, with much focus on reducing the power requirements of the next-generation of technologies. This focus on highly efficient designs as well as improved computing performance has led to exploration of exotic materials and designs such as three dimensional heterostructures and graphene to help mitigate the current inefficiencies of silicon technology. One area of exciting research that has grown out of this exploration has been the area of spintronics, the idea of using technologies based on electron spins. The majority of spintronic devices however require the utilization of either difficult processing techniques or the use of electric current to perform their function. This requirement for the use of electric current, in some cases, very high current places many limitations on the development and integrations of spintronic devices with current technology. To this end spin waves have shown much promise in research for their ability to produce large signals as well as being proposed with the ability to be voltage controlled. As a collective excitation technology spin waves do not rely on small signal quantum effects, and have the robustness to be used in a real world settling at room-temperature. Several technologies have been

proposed and of recent interest has been technologies that utilize spin wave interference or their processing technique.

1.2 Background

1. Introduction to Computer Logic

Most commonly computers are constructed using binary elements, either "on" or "off" to perform the functions it is required. To obtain higher order functions it is necessary to combine elements in such a way that they can complete there computation. For binary elements, the best tool for this is the use of Boolean algebra to build logic circuits[5]. Boolean algebra has changed some since its inception by George Boole in the 1800's, but its essence has remained the same. At the heart of Boolean algebra are three logical operators, NOT, OR, and AND. These logical operators, when combined together are said to be universal, in that using some combination of these, any mathematical function can be reproduced. NOT logic is simplest in that it always just outputs the inverse of its input. To be pedantic "on" states (represented by a 1) when undergoing a NOT operation change to an "off" state (represented by a 0). OR logic involves two inputs, and when either input is "on" or both are "on" then the output from a single output terminal is simply "on", otherwise it is off. Lastly, AND logical operators output an "on" state only when both input terminal are "on" otherwise it is "off". Simple diagrams and truth tables have been provided below. The inverse of the OR and AND operators are simply known as NOR and NAND and have truth tables in which the output is the opposite of the truth tables shown below.

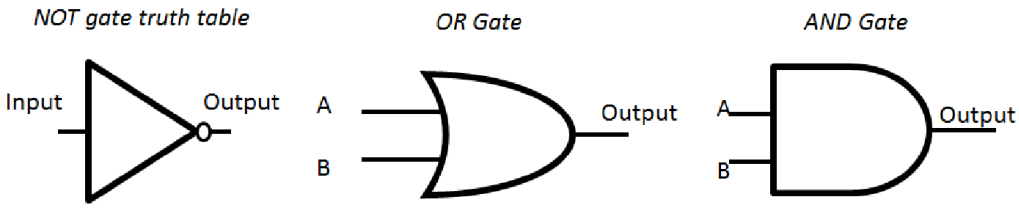

Input	Output
0	1
1	0

A	B	Output
0	0	0
0	1	1
1	0	1
1	1	1

A	B	Output
0	0	0
0	1	0
1	0	0
1	1	1

Figure 2 - Shows diagrams and truth tables for NOT, OR and AND operators[5]**.**

Various forms of computers/calculators have been used in the past two centuries by a variety of people. These range from the all-mechanical calculator style computers that could solve specific functions such as Charles Babbages Difference Engine and his Analytic Engine[6], to electro-mechanical switching, which was replaced by vacuum tubes, and finally to transistor and it's modern CMOS form. The transistor, considered by many to be the most important invention of the twentieth century has for the last 40 years represented almost all logic devices.

The transistor was invented in 1956 by Shockley, Bardeen, and Brattain at Bell. Using germanium and gold foil they were able to produce a device known now as the point-contact transistor and were able to control the flow of current between the slit in the gold foil. The device acted as a simple solid-state switch and soon it soon replaced the vacuum tube in active circuit design. The first transistor made use of germanium as the semiconducting material; however, modern transistors (in excess of 95% of all transistors) use silicon as the primary semiconducting material. The current method of producing transistors is CMOS technology, standing for Complementary Metal Oxide Semiconductor

process. This process makes use of photolithography techniques to form patterns in the silicon material as well as the other metals and dielectrics associated with the building of a modern transistor.

Modern transistors are of the MOSFET (Metal Oxide Semiconductor field-effect transistor) type, and are three terminal devices that use voltage on a gate terminal to control the flow of current from the source to the drain terminal. This switching action when connected in various ways to other transistors can be used to recreate the Boolean logic gates that were shown above, and are the backbone of modern computing. However, it can take several transistors, and a large area to create a gate.

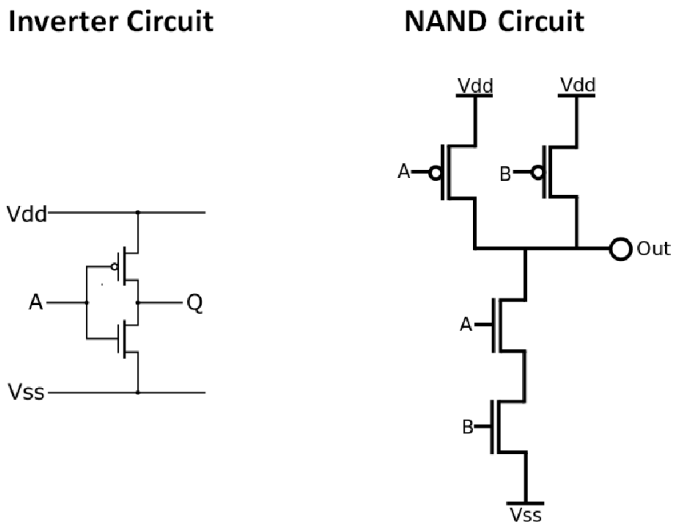

Figure 3 - Circuit diagrams for CMOS interpretations of NOT and NAND logic operators Source: http://en.wikipedia.org/w/index.php?title=File:CMOS_NAND.svg License: Creative Commons Attribution-Sharealike 3.0,2.5,2.0,1.0 Contributors: JustinForce[5]**.**

Currently the computer logic industry grows in accordance with Moore's Law, which states that the speed/number of devices on silicon chips will double every 18 months. At this rate and assuming the scalability of current technology, Moore's law will no longer be achievable using current CMOS technology by around 2020[7]. For this reason it has become increasingly important to replace the modern transistor with a new technology that

lacks the problems we are quickly approaching for it, i.e. scalability, waste heat removal, etc. The current unit size of a transistor is about 22nm, which already stretched the capabilities of modern day photolithography sizes, and soon the transistor will begin to enter realms where effects such as quantum tunneling, and other producers of noise begin to dominate. Even with the development of 3D transistors such as the FINfet, the modern implementation of the transistor will soon be at an end.

Several replacements have been proposed, as well as many promising proposals for the enhancements of current technology. Many allow for the use of single electrons, or of using polarized spin currents to transfer data. It has been suggested that the focus of the new technology be two-fold: one design devices with lower energy consumption, two: design devices with higher throughput in mind. Higher throughput can be achieved by creating devices which natively perform the logical operations such as AND, OR, NOT, and NAND, or even higher order logics such as ADDER circuits instead of having to combine many elements to perform the task. To this end we propose the use of a multiferroic based spin wave technology that incorporates the field of emerging field of “straintronics”.

1.2.1 Ferromagnetism

It is a well-known that some simple metallic objects contain a property that makes them attracted to one another. When materials contain this property of perpetual magnetism, or the ability to maintain a magnetic field without the assistance of outside energy sources they are known to be ferromagnetic. This property is one of the states of magnetism along with antiferromagnetism, diamagnetism, paramagnetism, and ferrimagnetism. As this document is not meant to be an all-inclusive treatise on all magnetic

states we will limit our conversation to that of ferromagnetism, which is handily the one most known to lay men and also the one most helpful in this discussion of applications.

The simplest model of ferromagnetism can be described by using the Bohr model of the atom, in which a negatively charged electron is orbiting a positively charged nucleus. Due to the Pauli Exclusion Principle only so many electrons may exists within an orbital. Electrons themselves have a dipole term causing them to act themselves as small magnets with a “north” and “south” end. This is an effect of the quantum property of the electron known as its spin. Electrons can have either a spin “up” or a spin “down” property. Like large scale macroscopic magnets, spin up electrons are attracted to spin down electrons, and same spins will repel each[8]. Electron orbitals will fill with evenly numbered electron that are paired, one spin up with one spin down, in the event that an orbital has an odd number of electrons, or a number of unpaired electrons than that gains a magnetic moment over the entire atom. Materials with these unpaired electrons are known as ferromagnetic and can have their magnetic properties used for any number of applications.

1.2.2 Spin Waves

Spin Waves are a collective excitation of electrons in a ferromagnetic lattice. In a lattice system these quantized excitations are known as magnons, and represent quantized excitations of electrons[9], much the same way that phonons represent the quantized vibrations of the crystal lattice. When spins in an ordered ferromagnet are disturbed they will precess around their axis. (see figure below).

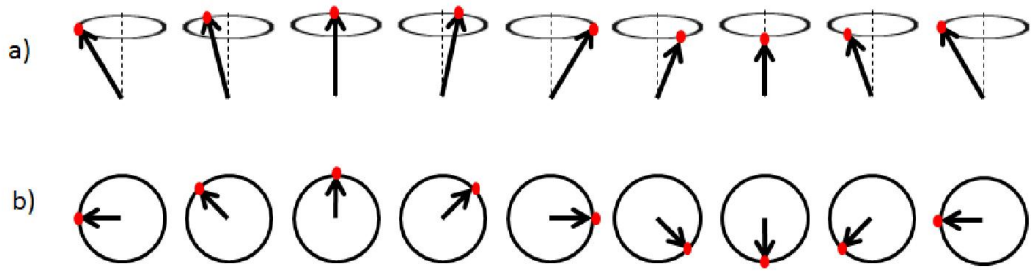

Figure 4 - Precession of spins around their axis. a) Side view b) Top view of the same system.

This motion causes a wave that can travel for microns and even millimeters under the right circumstances. Like phonons, magnon dispersion relations are found for ω with respect to *k*.

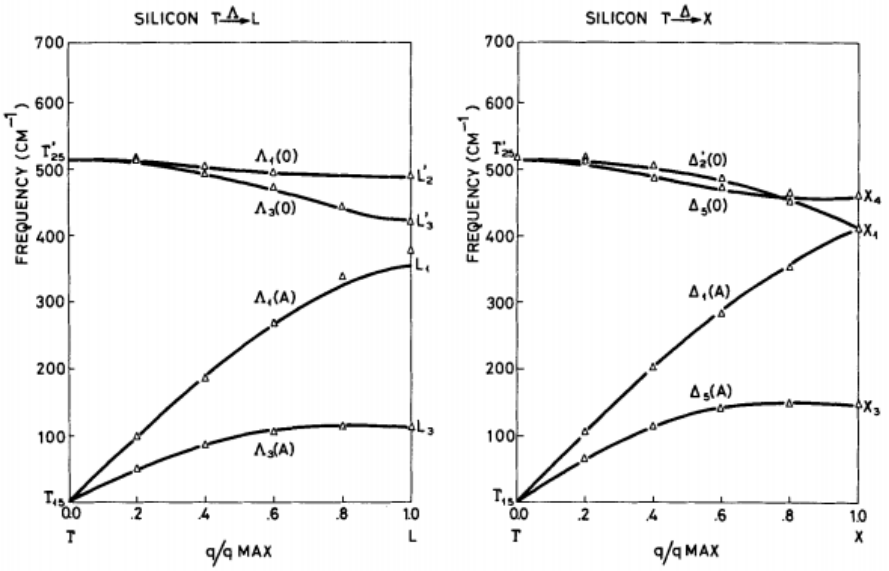

Figure 5 – Phonon dispersion graph for silicon is shown above. Lattice Dynamics and Spectroscopic Properties by a Valence Force Potential of Diamondlike Crystals: C, Si, Ge, and Sn Tubino, Riccardo and Piseri, Luigi and Zerbi, Giuseppe, The Journal of Chemical Physics, 56, 1022-1039 (1972), DOI:http://dx.doi.org/10.1063/1.1677264 Copyright 1972, AIP Publishing LLC.

Spin Waves are typically analytically described using the Landau-Lifshitz-Gilbert (LLG) equation. Magnetization dynamics with respect to time are written in the form of[10] :

$$\frac{d\vec{m}}{dt} = -\frac{\gamma}{1+\alpha^2}\vec{m} \times \left[\vec{H}_{eff} + \alpha\vec{m} \times \vec{H}_{eff}\right]$$

Where **m** is the unit magnetization vector, ***Ms*** is the saturation magnetization, **γ** is the gyromagnetic ratio, and **α** is the phenomenological Gilbert damping coefficient. The $\mathbf{H_{eff}}$ term can be expanded also as follows[10]:

$$\vec{H}_{eff} = \vec{H}_d + \vec{H}_{ex} + \vec{H}_a + \vec{H}_b$$

$$\vec{H}_{eff} = -\nabla^2\Phi + \frac{2A}{M_s}\nabla^2\vec{m} + \frac{2K}{M_s}(\vec{m}\cdot\vec{e})\vec{e} + \vec{H}_{pulse}$$

When a wave packet approximation is used then the magnetization component can be solved. So a wave packet with Gaussian distribution of wave vectors centered around *k0* propagates in the y-direction the magnetization amplitude is given by[10]

$$M_y = \frac{Ce^{-\frac{t}{\tau}}}{\delta^4 + \beta^2 t^2} e^{\left[\frac{-\delta^2(y-vt)^2}{4(\delta^4+\beta^2 t^2)}\right]} \times \cos(k_0 y - \omega t + \phi)$$

This gives a very good result especially when fitted to experimental data, as Covington et. al. [10]was able to do when exciting localized spin wave packets in a permalloy film. The result shown below from that work, shows an almost perfect overlay of experimental and theoretical values, establishing that the LLG equation provides an excellent resource for understanding and predicting spin wave phenomena.

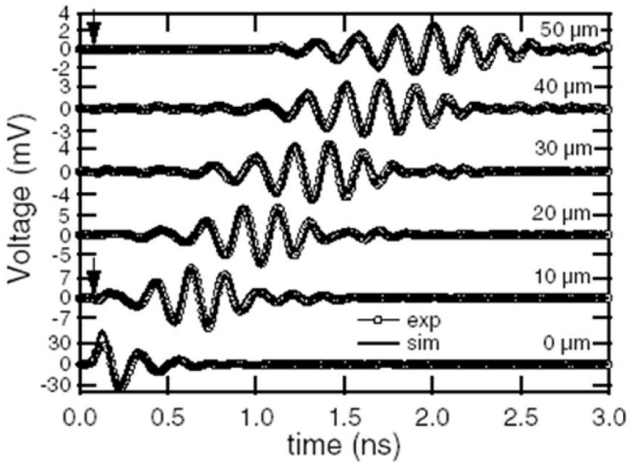

Figure 6 - Work by Covington et. al. [10]showing theoretical and experimental overlay of data for time-resolved spin wave experiments. Dots in the graph represent experimental data and the solid black lines represent simulation data. Results are shown as detected by 5 different waveguide detectors placed at 10, 20, 30, 40 and 50 um away from the excitation waveguide represented as 0 um. "Reprinted figure with permission from: M. Covington, T.M. Crawford and G.J. Parker, Physical Review Letters, 89, 237202,2002. Copyright 2002 by the American Physical Society."

1.2.3 Magnonic Holographic Devices

1.2.3.1 Current Spin Wave Device Designs

Since 2005 there has been several designs and realization of spin-wave logic devices that have been made public. The first of these is based on Mach-Zehnder type spin wave interferometer[11]. This logic device design utilized a power splitter, and two controlled phase shifters that lead into a ferromagnetic mixing device. Inside the mixing device the signals from each of the controlled phase shifters is able to either constructively or destructively interfere and the output read from the device is just the amplitude of the signals. Using this scheme it is possible to construct both NOT and XOR gates, as seen in Fig. 6 , and the experimental device operated stably at room temperature at frequencies of about 7 GHz.

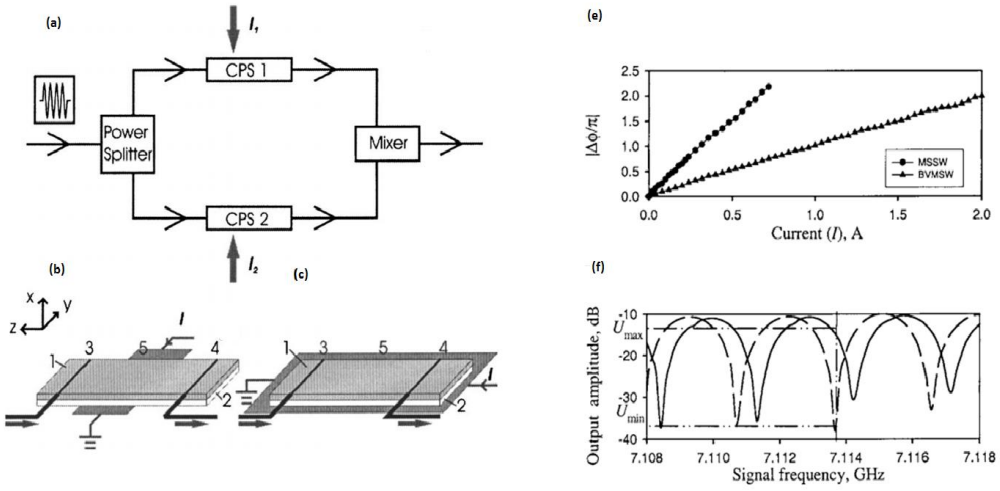

Figure 7 - Mach-Zehnder Type Spin Wave Interferometer. a) Diagram showing components of interferometer. b) A diagram showing the layout of the planar spin wave device with the intent to transmit MSSW Spin Waves from one antenna to another. C) similar to b, but with the intent of transmitting BVMSW. e)Graph showing the relationship between phase-shifts in the devices signal and current. f) Graph showing output in dB of a device with respect to frequency. The dashed line is the result of current applied to cause a phase shift in the signal. "Reprinted with permission from [11]. Copyright 2005, AIP Publishing LLC."

This scheme makes use of two different types of spin wave to perform different logical operations, Magnetostatic Surface Spin Waves (MSSW) being used for the logical XOR argument and Backward Volume Magnetostatic Spin Waves (BVMSW) being used for the logical NOT. Although it was shown that both types of waves could be used in both operations.

Another proposed method, related to the first uses a similar style of interferometer to create universal gates [12]. This design uses the same Mach-Zehnder style interferometer to create constructive and destructive interference, but proposed is both a smaller design (on the order of nanometers) and the use of permalloy instead of YIG waveguides. Like the previous design a single element could be used to produce a logical NOT device. In this device a bifurcated waveguide is split by a nanoscale conducting wire (see Figure 7). When there is no current present in the wire then the two branches of the waveguide constructively interfere and the output is one. When a currents density of 2 x 10^{11}A/m^2 (which represents a logical state of 1) is applied to the conducting wire a phase

shift occurs causing the magnetic signal to destructively interfere and thus yielding an output of zero. Thus the output of the magnetic state in such a system is always the inverse of the input of the current carrying wire. It should be noted as shown in figure 7 that these devices can require as much as almost a full ampere of current to result in a phase shift of π.

This setup can be further enhanced by placing units in both series and parallel. By placing the units in series it is possible to realize NOR logic and by placing units in parallel the observed logic is NAND, thus making these connections universal.

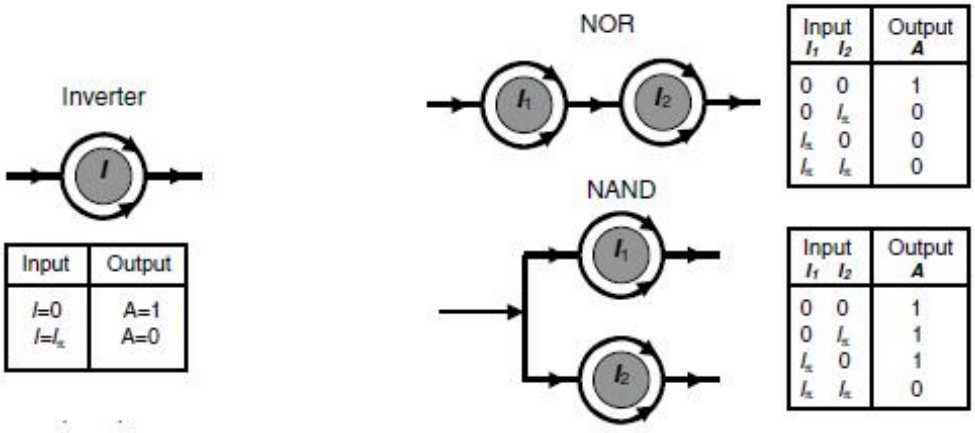

Figure 8 - Shows Mach-Zender Interferometer diagram as well as logic associated with both single and cells as well as cells setup in parallel and series. (Diagram from Khitun et al, J. Phys. D, Apply. Phys. (2010)) © IOP Publishing. Reproduced by permission of IOP Publishing. All rights reserved

A third proposed field utilizes phase-based logic implemented through ACPS style waveguides positioned over a spin wave bus (see figure 9) [13], [14].

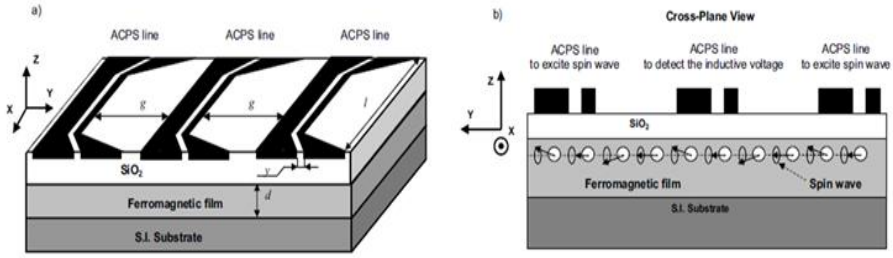

Figure 9 - a) top view of ACPS resting on top of a ferromagnetic film that is utilized as a spin-wave bus b) Side view with overlay of spin wave in ferromagnetic media. "A. Khitun and K. L. Wang, "Nano scale computational architectures with Spin Wave Bus," *Superlattices Microstruct.*, vol. 38, pp. 184–200, 2005., with permission from Elsevier."

Information is stored in the phase of the spin wave with 0 representing the "off", state (0) and π representing the "on", state (π). Several different logic gates can be constructed via this method. For example the implementation of a NOT gate, or an inverter circuit only requires that the length of the waveguide be half of the wavelength of the excited spin wave, thus any initial phase will be 90° out of phase upon reaching the output (see figure 9). Also a structure can be constructed that allows for the making of a majority gates[15].

The group also presents some experimental data, of which a selection is shown below that shows the inductive voltage response to in-phase and out-of-phase devices at different frequencies.

Majority gates in this design are simply three terminal devices in which the input is either 1 or 0 and the output matches whatever input is most common over the three input terminal. This "voting" style of logic allows for much higher order logic than is observed with simple Boolean algebra and allows for more input terminals.

All of the designs mentioned above make use of a similar excitation method. The use of a microstrip antenna is used to excite spin waves in a ferromagnetic medium.

This design has numerous advantages including ease of design and manufacture. However, this design ultimately is a strong limitation for the future use of spin wave devices. Microstrip antennas have several problems within spin waves systems, the two most important being efficiency and scalability. Microstrip antennas work by coupling with the ferromagnetic media to create a spin wave signal, however, microstrips can also produce direct coupling with each other. This "cross-talk" can be many times the amplitude of the spin wave signal and the best way to avoid it is simply by placing the antennas far enough apart that they do not interfere as strongly[16]. However, as devices scale down it would become increasingly important to place antennas near each other, enhancing this direct coupling and eventually causing the spin wave signal to be unreadable. As for efficiency, using these microwave antennas to excite spin waves only converts approximately 1% of the energy supplied to the microstrip into spin waves. This incredibly low-yield takes away one of the advantages of spin wave logic, notably its efficiency. To best utilize the design mentioned above, and any other future spin wave device design it becomes necessary to find a better method for exciting spin waves.

To this end synthetic multiferroics used to form magnetoelectric cells offer a very good opportunity at solving this problem. Multiferroics are materials which exhibit both ferroelectric properties as well as mechanical piezoelectric properties. In the case of spin waves it would be desirable to have devices that could change a magnetic state via voltage control and preferably with higher efficiency than is observed with microstrip excitation methods. To this end, "synthetic" multiferroics have been utilized to change magnetization states. The term synthetic is used here to denote materials that work due to an interface between two different materials, so as to gain a coupling between the piezoelectric and ferromagnetic effect, as opposed to "natural" multiferroics whose inherent

structure within one material exhibits both of these properties. In this proposal we will consider the multiferroics system of nickel thin films deposited onto PZT (Lead Zirconium Titanate) films. PZT is a well-known piezoelectric material that is used in a wide range of research and commercial applications. Nickel is a magnetic material that exhibits a magnetostriction effect[17], in short, when strain is applied to nickel film it results in a change of its magnetic state and vice versa[18]. Many studies have been conducted on this PZT/Nickel system and its properties are now well known. The Carmen group at UCLA has gone so far to show the reversal of a bi-stable element of nickel deposited on top of a PZT substrate that is capable of both controlled domain wall motion [19] as well undergoing a complete magnetic reversal[20] by applying voltage across the multiferroics device.

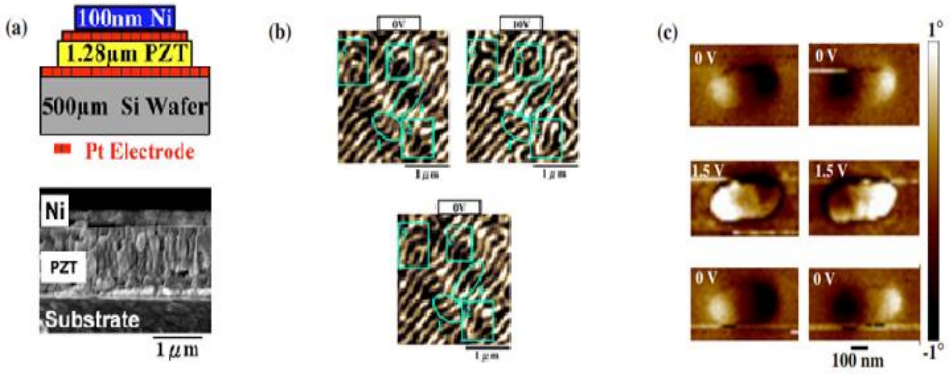

Figure 10 - Results from Carmen group publication. a) Layout and SEM image of structure. c) Domain wall motion due to applied electric field. c) Complete reversal of Nickel nanomagnet showing bi-stability. "Reprinted with permission from T.-K. Chung, S. Keller, and G. P. Carman, "Electric-field-induced reversible magnetic single-domain evolution in a magnetoelectric thin film," *Appl. Phys. Lett.*, vol. 94, no. 13, p. 132501, Mar. 2009. Copyright 2005, AIP Publishing LLC."

This capability has led to research into this type of structures ability to create oscillations within a ferromagnetic media, and such spin wave excitations have recently been observed. Recently another group has shown excitation of spin waves[21] using these multiferroics elements to both create spin waves as well as detect them.

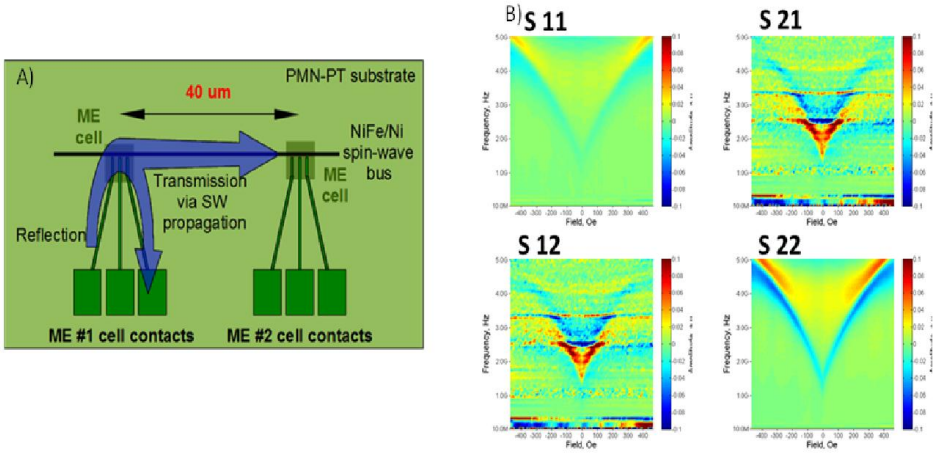

Figure 11 – A) a schematic depicting the excitation and detection of a spin wave signal via multiferroic elements. B) Experimental data obtained from a Network Analyser depicting the read-out of the analyser as a function of the applied magnetic field strength and direction.

With this in mind it is easy to expand upon this to design magnetoelectric cells, which we propose to use in conjunction with spin wave buses to create logic. Shown below is a design of majority gate utilizing magnetoelectric cells to excite spin waves and using phase-based logic to interfere and form the function of a majority gate[22]. The design allows for easy incorporation into modern technology as it still uses already commercialized materials and standard photolithography processing. Since the input and output of the device is nothing more than voltage, these devices can be incorporated into hybrid CMOS/straintronics systems.

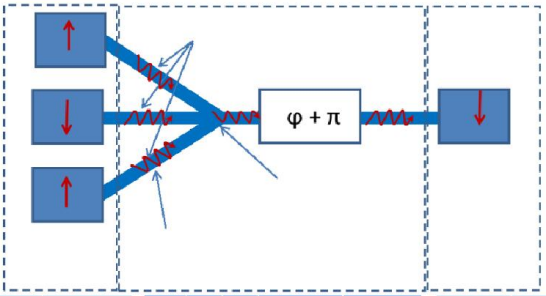

voltage	phase
+ 10mV	0
- 10mV	π

A	B	C	Junction	Inverter
0	0	0	0	π
0	0	π	0	π
0	π	0	0	π
0	π	π	π	0
π	0	0	0	π
π	0	π	π	0
π	π	0	π	0
π	π	π	π	0

phase	voltage
0	+ 10mV
π	- 10mV

Figure 12 - Diagram of Magnetoelectric cells being used in a Majority Gate spin wave system, accompanied by truth tables, where π is used to denote the tyical "on" or 1 state. "Reprinted with permission from [22]. Copyright 2010, AIP Publishing LLC."

The electric field required to switch these elements is on the order of ~1MV/m and allows for much higher efficiency for the excitation of spin waves, since the magnetoelectric elements use a piezoelectric effect to efficiently mediate force to the magnetic elements. This eliminates the problems of direct-coupling between devices as well since there will be no wireless communication elements.

1.2.3.2 Proposed Magnonic Holographic Device Design and Features

Spin waves have played an important role in magnetics research for the better part of the last century, as well as providing exciting and unique research opportunities in the last decade. Much of this research has been driven by interest from the spintronics community and has led to much deeper exploration of both theoretical and experimental phenomena. Phenomena such as: spin wave interferometry[23], multiferroics[24] and magnonic crystals[25], [26]. And as such, many proposed devices utilizing magnetization dynamics

including spin wave technologies have been proposed[27][12], [28]. Interest in nanoscale magnetic phenomena has implications far outside the field of spintronics as understanding and control of dynamic magnetization could have interesting impacts in proposed technologies in the fields of cellular biology[29], [30], MRI[31], and microwave technologies[32], just to name a few. To-date one of the many shortcomings of magnetic device technologies is both a reliance on Amperian fields, as well as a difficulty in efficiently performing read-out of a magnetic state[33][34]–[37]. To wit, devices with high sensitivity to changes in magnetic state are desirable, as currently most reading of micromagnetic objects is done using either Magnetic Force Microscopy (MFM) or Giant Magnetoresistance (GMR) probes, which while accurate require physical manipulation to work effectively. Recently the spin wave community has begun taking a great interest in spin wave interference[23], [38]–[41][42], with several devices utilizing the phenomena being proposed. Borrowing much from the research involving light interference the recently developing field of spin wave interference has the potential to open many doors into the understanding of spin waves.

Spin waves like all other wave phenomena have the ability to form interference patterns, and borrowing from the language of optics, interference patterns in which the wave interferes with an "object" are referred to as holograms. Holography is usually associated with images being made from light; however, this is only a narrow field of holography. Any interfering coherent wave source can be used to form a hologram, and several technologies exist utilizing the detection of objects using acoustics waves, seismic waves and microwaves. And indeed the first proposal of holography by Dennis Gabor intended for the use to be with coherent electron waves[43]. Magnonic Spin Wave interference devices have been proposed and tested, as designed in previous works, in

which Spin Wave Interference (some refer to spin waves as magnons, the quasiparticle representation of a spin wave) is used to detect a spatially non-uniform magnetic field in close proximity to a ferromagnetic waveguide. One proposal suggests the utilization of a ferromagnetic element placed on a grid of waveguides to create a local non-uniformity for the realization of a highly efficient, highly parallelized memory device[44]. This device design constitutes a Magnonic Holographic Matrix (MHM) device and has several unique properties including the use of spin wave bus, a similarity to nanofabric designs[45], and the ability to use as well as study spin wave interference, using common materials as well as being performed at room-temperature.

Recently proposed in literature was the idea of a new form of spin wave interference device which took advantage of magnonic holography as it's mechanism for work. Holography is usually associated with images being made from light; however, this is only a narrow field of holography. Any interfering coherent wave source can be used to form a hologram, and several technologies exist utilizing the detection of objects using acoustics waves, seismic waves and microwaves,. And indeed the first proposal of holography by Dennis Gabor intended for the use to be with coherent electron waves[43]. Interest in this structure stems from early experiments conducted by Kozhanov[42], who explored properties of spin wave propagation within a CoTaZr ferromagnetic cross structure that exhibited spin wave interference effects. Also within the community of spin wave interference that has been much interest in the design of spin wave devices that are both non-reciprocal as well as low in energy, which the results provided will explore. The cross is tangentially magnetized, so predominant modes of spin wave propagation should be Magneto-static Spin Waves as well as Backwards Volume Spin Waves, but this in turn arises an interesting question. Since the junction of the cross represents a scattering area for the

propagating spin waves, in what way will the spin waves propagate, if at all into orthogonal arms.

This is especially of interest to the community as there have been several studies recently of spin waves around bends and "turning a corner". Several interesting questions arise in a system such as these, such as the efficiency of propagating waves to turn a corner, as well as the ability of the spin waves, to change direction not only spatially with regard to the original direction of propagation but also with regard to the direction of the applied field. Studies in cross devices have centered on some of these propagation characteristics, and thus our study shall begin with some characterization of the device using only the junction as the scattering area. The schematics of MHM are shown in Figure 13. The core of the structure is a magnetic matrix consisting of the grid of magnetic waveguides with nano-magnets placed on top of the waveguide junctions. Without loss of generality, we have depicted a 2D mesh of orthogonal magnetic waveguides, though the matrix may be realized as a 3D structure comprising the layers of magnetic waveguides of a different topology (e.g. honeycomb magnetic lattice). The waveguides serve as a media for spin wave propagation – spin wave buses. The buses can be made of a magnetic material such as yttrium iron garnet $Y_3Fe_2(FeO_4)_3$ (YIG) or permalloy ($Ni_{81}Fe_{19}$) ensuring maximum possible group velocity and minimum attenuation for the propagating spin waves at room temperature. The nano-magnets placed on top of waveguide junctions are the memory elements holding information in the encoded in the magnetization state. The nano-magnet can be designed to have two or several thermally stable states for magnetization, where the number of states defines the number of logic bits stored in each junction. The spins of the nano-magnet are coupled to the spins of the junction magnetic wires via the exchange and/or dipole-dipole coupling affecting the phase of the propagation of spin waves. The phase change received by

the spin wave depends on the strength and the direction of the magnetic field produced by the nano-magnet. At the same time, the spins of nano-magnet are affected by the local magnetization change caused by the propagating spin waves.

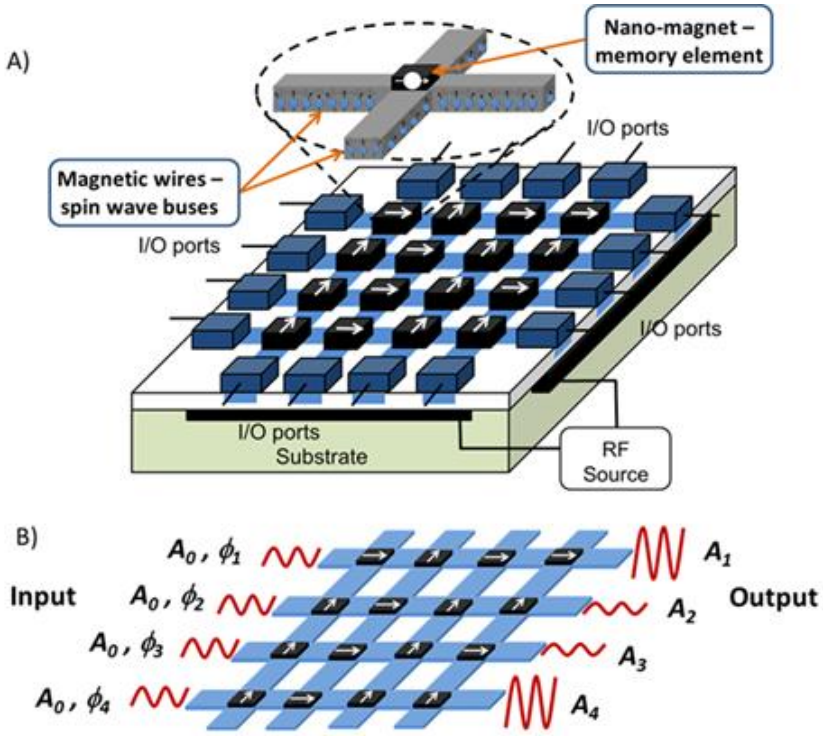

Figure 13 – (A) Schematics of Magnonic Holographic Memory consisting of a 4×4 magnetic matrix and an array of spin wave generating/detecting elements. For simplicity, the matrix is depicted as a two-dimensional grid of magnetic wires with just 4 elements on each side. These wires serve as a media for spin wave propagation. The nano-magnet on the top of the junction is a memory element, where information is encoded into the magnetization state. The spins of the nano-magnet are coupled to the spins of the magnetic wires via the dipole-dipole or exchange interaction. (B) Illustration of the principle of operation. Spin waves are excited by the elements on one or several sides of the matrix (e.g. left side), propagate through the matrix and detected on the other side (e.g. right side) of the structure. All input waves are of the same amplitude and frequency. The initial phases of the input waves are controlled by the generating elements. The output waves are the results of the spin wave interference within the matrix. The amplitude of the output wave depends on the initial phases and the magnetic states of the junctions"Reprinted with permission from [44]. Copyright 2005, AIP Publishing LLC.".

Estimates exist on the devices effectiveness, with several predictions being made as to potential applications as well performance. To benchmark the performance of the

magnonic holographic devices, we apply the charge-resistance approach as developed in Ref. [35] The details of the estimates and the key assumptions are given in literature. According to the estimates, MHM device consisting of 32 inputs, with 60nm separation distance between the inputs would consume as low as 150μW of power or 72fJ per computation. At the same time, the functional throughput of the MHM scales proportional to the number of cells per area/volume and exceeds 1.5×10^{18} bits/cm^2/s for 60nm feature size. It is interesting to note, that holographic logic units can be used for solving certain NP class of problems (i.e. finding the period of the given function). The efficiency of holographic computing with classical waves is somewhere intermediate between the digital logic and quantum computing, allowing us to solve a certain class of problems fundamentally more efficient than the general-type processors but without the need for quantum entanglement [36]. Image recognition and processing are among the most promising applications of magnonic holographic device exploiting its ability to process a large number of bits/pixels in parallel within a single core. Of great interest is the idea to combine the efficiency of multiferroic elements with the multi-frequency capability of other wave based proposals. A device of this sort would be completely voltage driven, capable of integrating with current produced devices, extremely efficient, as well as having a data throughput that is potential far higher than that of standard CMOS circuitry. This style of device since it offers the greatest potential as a beyond CMOS device will be the focus of the research presented here-in. Section, we discuss the fundamental limits and the technological challenges of building multi-bit magonic holographic devices and present the estimates on the device performance.

The advantages of using YIG for spin wave research are well known and have been established[46]. The length of the whole structure is 3mm, the width of each arm of the waveguide is 360μm with a thickness of 3.6μm. To excite spin waves, micro-antenna

structures have been fabricated at the edges of each arm. Microwave voltage signals can be transmitted and received using the micro-antenna structures, and spin waves are excited by the well-established inductive voltage method. The input and the output micro-antennas are connected to a Hewlett-Packard 8720A Vector Network Analyzer (VNA). Since the basic prototyped structure requires a wave front that has the same frequency and amplitude, signal from the VNA is split across all the exciting antennas, resulting in an equivalent signal for all output structures. To conform to standard optical language we refer to the magnetic element as the "magnetic object", and it represents an analog to the optical object reconstructed in an optical holograph. The objects in our example are small microscale ferromagnetic elements with a length of 1.1mm and a width of 360μm, and a coercivity of 200-500 Oersted (Oe), produced on a silicon substrate with a cobalt based magnetic thin film produced via plasma sputtering by Paramount Sensors. However, any variety magnetic elements could be used including multistate ferromagnets and electromagnetic field producing wires. The phase change received by the spin wave depends on the strength and the direction of the magnetic field produced by the magnetic object, as a result of the localized change in the external magnetic field.

The VNA generates an input RF signal up to 20 GHz and measures the S-parameters showing the amplitude and the phases of the transmitted and reflected signals.

We start the discussion with the choice of magnetic material for building spin waveguides. Spin wave transport in nanometer scale magnetic waveguides has been intensively studied during the past decade[10], [47]–[49]. There are two most popular magnetic materials: permalloy $Ni_{81}Fe_{19}$ and YIG used for spin wave devices prototyping. The coherence length of spin waves in permalloy is about tens of microns at room temperature [10], [47], while the coherence length in a non-conducting YIG exceeds millimeters[46]. The

attenuation time for spin waves at room temperature is about a nanosecond in permalloy and a hundreds of nanoseconds in YIG [46]. However, the fabrication of YIG waveguides require a special a special gadolinium gallium garnet (GGG) substrate. In contrast, a permalloy film can be deposited onto a silicon platform by using the sputtering technique. Though YIG has better properties in term of the coherence length and a lower attenuation, permalloy is more convenient for making magnonic devices on a silicon substrate.

The system proposed is sensitive to the phase of the spin wave signal, and the final output intensity is a result of the accumulated phase shift. Magnonic waveguide systems have an inherent phase shift within the system, where the phase output is determined by κ, the wave vector as[50]

$$\phi = \kappa \cdot l + \phi_0$$

Here l is the distance the spin waves have traveled through the waveguide. The phase difference, $\Delta\phi = \phi - \phi_0$, is also affected by any spatially non-uniformity within the magnetic field. The ferromagnetic elements within the system, our "magnetic objects" thus contribute an additional factor to the natural accumulated phase output as

$$\Delta\phi = \kappa \cdot l + \int_0^r \kappa\left(\vec{H}_m\right) dr$$

Here the additional term is an integration of a new wave vector that is a function of the strength and the direction of the local magnetic field provided by the magnetic object $H_{m,}$ the additional term shows the sensitivity of the output phase to the local magnetic field. The ferromagnetic elements thus are producing spatial non-uniformity locally on the device which results in a determinable phase shift. H_m is a term that is sensitive both to the modes

of the spin wave as well as a variety of other factors. The two predominant modes of spin waves used in device research are those resulting from a tangentially applied magnetic field[51], known as Backwards Volume Magnetostatic Spin Waves (BVWSM) and Magnetostatic Surface Spin Waves (MSSW). Using these modes it can be determined the amount of phase shift that both modes of spin waves will experience, and can be described thusly[52][53]:

$$\frac{\Delta\phi}{\partial H} = \frac{l}{d}\frac{(\gamma H)^2 + \omega^2}{2\pi\gamma^2 M_s H^2} \text{(BVSM)}$$

$$\frac{\Delta\phi}{\partial H} = -\frac{l}{d}\frac{\gamma^2(H + 2\pi M_s)}{\omega^2 - \gamma^2 H(H + 4\pi M_s)} \text{(MSSW)}$$

In the above equation M_s is the saturation magnetization, γ is the gyromagnetic ratio, l is the phase accumulation length and d is the thickness of the device. With the amount of phase shift given above, two questions of great import are how much phase shift is necessary, as well as what is the intensity coefficient for the output signal since that is the typical established measured output of a holographic system. The minimum phase shift necessary is typically thought to be a full radian shift in the phase, though smaller shifts may still be utilized, and is found by taking the derivative of wave vector with respect to κ, resulting in an equation that relates the wave shift to the reciprocal of the group velocity, v_g.[54]

$$\frac{\partial \kappa}{\partial H} = -\frac{\partial \omega}{\partial H}\Big/\frac{\partial \omega}{\partial \kappa} = -\frac{\partial \omega}{\partial H}\Big/ v_g$$

For spin wave interferometry the intensity transmission coefficient can then be written as[54]:

$$I_o = \frac{\sinh(\pi \kappa d)^2}{\sinh(\pi \kappa d)^2 + \sinh(\pi \lambda)^2}$$

In order to make a multi-bit magnonic holographic devices, the operating wavelength should be scaled down below 100nm [44]. The main challenge with shortening the operating wavelength is associated with the building of nanometer-scale spin wave generating/detecting elements. There are several possible ways of building input/output elements by using micro-antennas[10], spin torque oscillators[55], and multi-ferroic elements [56]. So far, micro-antennas are the most convenient and widely used tool for spin wave excitation and detection in ferromagnetic films[47]. An electric current passed through the antenna placed in the vicinity of magnetic film generates a magnetic field around the current-carrying wires, which excites spin waves in the magnetic material. And vice versa, a propagating spin wave changes the magnetic flux from the magnetic waveguide and generates the inductive voltage in the antenna contour. The reducing the size of the antenna will lead to the reduction of the detected inductive voltage. This fact limits the practical application of any types of conducting contours for spin wave detection. The utilization of spin torque oscillators makes it possible to scale down the size of the elementary input/output port to several nanometers. The main challenge for the spin

torque oscillators approach is to reduce the current required for spin wave generation. More energetically efficient are the two-phase composite multiferroics comprising piezoelectric and magnetostrictive materials [57]. An electric field applied across the piezoelectric produces stress, which, in turn, affects the magnetization of the magnetoelastic material. The advantage of the multiferroic approach is that the magnetic field required for spin wave excitation is produced via magneto-electric coupling by applying an alternating electric field rather than an electric current. For example, in Ni/PMN-PT synthetic multiferroic reported in Ref. [58], an electric field of 0.6MV/m has to be applied across the PMN-PT in order to produce 90 degree magnetization rotation in Nickel. Such a relatively low electric field required for magnetization rotation translates in ultra-low power consumption for spin wave excitation [22]. At the same time, the dynamics of the synthetic multiferroics, especially at the nanometer scale, remains mainly unexplored.

1.3 Research Objectives

While research exist on spin wave devices, no current realization of magnonic holographic matrix devices has been done from an experimental viewpoint. It is thus the focus of my research to provide the first experimental works with this focus in mind. The objectives of the research proposed are as follows:

- Carry out experiments pertaining to the development of an appropriate multiferroic substrate and element
- Carry out experiments characterizing such a substrate and/or element
- Further experimental knowledge pertaining to the characteristics of a spin wave cross and spin wave propagation in such a structure
- Obtain first experimental realization of a Magnonic Holographic Matrix Device

- Characterize and study the effects of magnetic objects on an MHM device signal

In conclusion we plan to construct synthetic multiferroics elements that can be used to both excite and detect spin waves. By combining these elements with the well-established technology of the spin wave bus we will be able to build devices in which multiple ME elements interfere and thus are able to form a MHM device. Also included in this research will be the study of the spin waves when excited via this method as well as the exploration of spin wave interference and magnonic holographic techniques. Due to this designs ease of manufacture, great possible efficiency and ability to scale we believe this structure to be a good candidate for a technology to eventually phase out current CMOS processing as we know it and go well beyond 2020.

2 Fabrication of Spin Wave Devices

2.1 Overview of Facilities

Devices were constructed in primarily two facilities. Permalloy style devices were constructed at the University of California – Riverside (UCR), using the shared facilities made available at the Center for Nanoscale Science and Engineering (CNSE). This facility supports both a class 100 and class 1000 cleanroom area and has full support for photolithography, electron beam lithography, metal and dielectric deposition processes, as well as a host of characterization techniques available to users such as Tunneling Electron Microscopy, Scanning Probe Microscopy, Scanning Electron Microscopy and Ellipsometry. The facilities are made available to faculty and staff at UCR using a fee-for-services model, and were the predominant processing location. Additional processing (wafer dicing and focused ion beam) were also done on occassion using the shared facilities at the University of California – Los Angeles (UCLA).

Yttrium Iron Garnett (YIG) device fabrication was performed using the facilities at the Kotel'nikov Institute of Radioengineering and Electronics a facility of the Russian Academy of Sciences located in Saratov, Russia.

2.2 Materials Selection

It should be noted that two different styles of single cross and double cross structures were constructed. The first set of devices were fabricated using YIG while the second devices were fabricated using a Nickel-Iron Compound known as Permalloy ($Ni_{81}Fe_{19}$).

Both materials are commonly used in spin-wave studies and are popular within the community for microwave oriented studies. Each material has advantageous and disadvantageous, some of which it is prudent to mention outright, so as to make some careful distinction in the reasons for size dimensions and fabrication methods in each style

of device. YIG is an insulating, crystalline material. It has very little in the way of scattering defects and is one of the best materials for studying spin wave propagation over a long distance, as spin waves can propagate in the material several millimeters. As such, devices constructed with this technique are constructed to the size of several millimeters in scale, and antennas are added using a unique procedure described below.

Permalloy is also a well-known material for spin wave studies with a near zero coercivity, it has excellent dampening parameters, but it is a conducting material. As such it has more scattering points for spin waves and requires insulation when electrically conductive spin wave excitation methods are utilized. As such additional insulation is used and the devices have been built at a smaller scale (to the order of 10's of microns). Both devices still have their excitation method in common and the use of both materials allow for a comparison of the material properties, and some idea of an ideal material for use in both industry and research. A comparison of devices constructed using both materials are offered in later sections for the interested reader.

2.3 PZT Substrate Preparation

One of the stated goals of the research plan is to establish methods using multiferroics to send dynamic magnetization signals (magnetic spin waves) along a selected route, while affecting and/or detecting magnetic elements along this established route, and to study the interaction of these "spin-wave devices". In our case a magnetic signal would be generated using a small AC signal applied to a multiferroic element and then studying the interaction of elements exposed to the generated waves by reading in subsequent signals received either by an antenna or another multiferroic element. To begin we began producing a piezoelectric substrate on which to make multiferroic devices. This substrate is

made from Lead Zirconate Titinate (PZT) via a spin-coating method followed by an annealing process to allow the coating to align to the correct crystal orientation, in this case a <111> orientation. The substrate was produced by using a fused silica substrate or an n-type Silicon substrate, coated with platinum, and finally covered by a Lead-Zirconate-Titanate (PZT) layer. The recipe followed will be similar if not identical to the recipe provided by the Carmen group at UCLA [19]. This recipe was also confirmed and discussed by Dr. Kin Wong, who had first-hand experience with the recipe and provided many details concerning the making of the PZT sol-gel.

Starting with a quartz substrate, approximately 100nm of Platinum (Pt) is deposited onto the quartz substrate. This is accomplished via e-beam deposition, as it is readily available and fairly wuick when using that technique. The PZT layer is deposited on top of this layer. It should be noted that this differs from the exact Carmen group recipe in that they usually deposit 10nm of Titanium (Ti) before also depositing the PZT. Any problems might be related to that. Heating and annealing were then performed prior to coating, so as to release any thermal stress that might occur later in the process. The wafer was baked at 150^{o}C on hotplate for 5 minutes, then at 300^{o}C for approximately 5 minutes. This can be performed in an open atmosphere. A final annealing at 700^{o}C then occurs and the wafer was allowed to cool down for approximately 10 minutes (until cool). The sol-gel of PZT (10% by weight solution) was then spin coated on at a rpm of approximately 4000rpm – 7000rpm depending on the desired thickness. The higher the rpm's the thinner the coating. This also differs from the Carmen group recipe, as they spin coated at 500rpms for 5s followed by 1500rpms for 30s, before annealing. Necessary times were determined by experiment. Carmen's group repeated the process 4 times to create a 1.28um layer. So it can be assumed that one run using Carmen's recipe will produce a layer of approximately 300-

400nm. Either way, on the first attempt 4000rpm was deemed sufficient, so 500rpm for 5s and then 4000rpm for 30s, before annealing/heating. These higher rpm's do seem to agree with another publication (Processing Effects in the Sol-Gel Preperation of PZT Dried Gels, Powders, and Ferroelectric Thin Films, 1992), though heating times differ, between publications. After spin-coating the material is dehydrated on a hotplate at 150C for 5 minutes, and then pyrolyzed at 350C for 5 min on a hotplate. After this the wafer is annealed in oxygen for 3-5 minutes (depends on thickness) at 700C. This should complete the process of creating the wafer, below is a breakout chart, showing the entire process graphically.

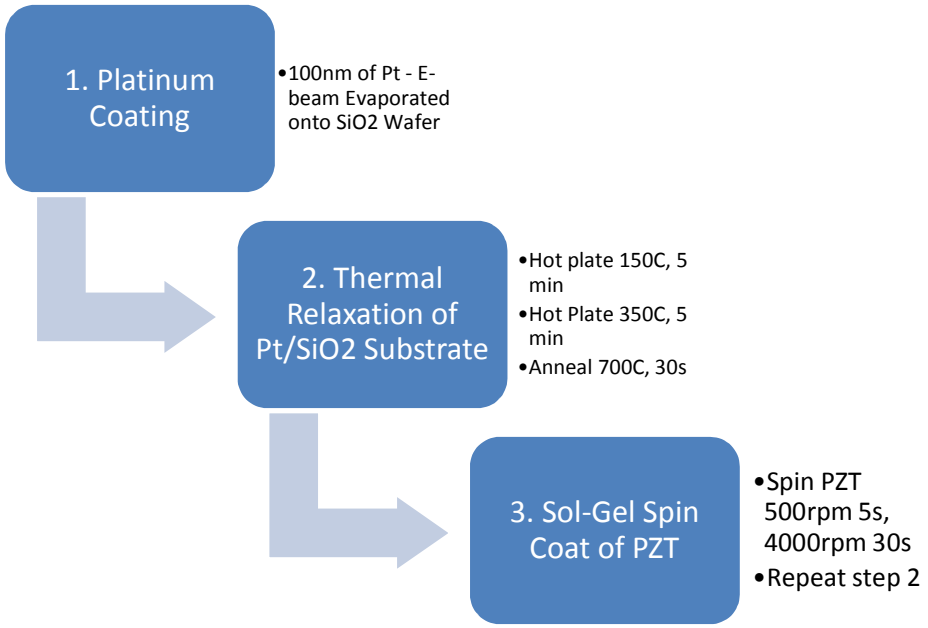

Figure 14 - Graphical Breakout of PZT Substrate, showing the original proposed process from the Pt deposition step onward.

The initial recipe showed several processing problems when completed. The most obvious was due to poor adhesion of the platinum layer to the substrate, whether using fused silica or standard silicon substrates. Pinholes and cracks were very apparent, especially due to the thin nature of the films. In some samples, complete separation of the films was observed. On samples where the film did not completely anneal we attempted to

gain some insight both in quality and composition by utilizing a technique known as ellipsometry. Ellipsometry is a non-destructive [59] [60]non-linear [61], model based technique that utilizes elliptically polarized light to measure properties of samples. In a typical ellipsometry setup, a polarizer is placed in a beam of light; the polarized light has field components in the S and P direction (parallel and anti-parallel). This light, when interacting with the sample, undergoes changes in intensity (due to absorption) as well as changes in phase and polarization well described by Fresnel equations[60]. Ellipsometry is an indirect method that then requires the data be compared to a model, either determined through calculation of the optical effects or through empirical built models obtained by careful measurement of known samples.

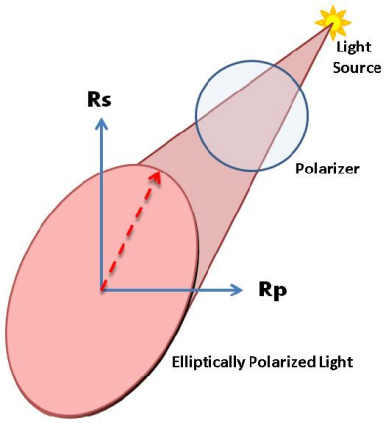

Figure 15 - Diagram showing typical ellipsometry setup as well as orientation of the ellipsometry beam.

Spectroscopic ellipsometry, uses these same techniques; however it can incorporate the use of multiple wavelengths of light. By scanning through a variety of wavelengths it is possible to determine a wavelength dependent factor that can be utilized for better accuracy as well as modeling. This technique has been used for ultra-thin samples in

research [62] as well as clear samples [63]and is somewhat akin to polarimetry measurements.

Ellipsometry is an indirect method, meaning that data will not just be collected from the source machine for direct analysis but will also be compared to models produced by the user through empirical methods. This has the advantage of producing models that match the process being used directly and can account for any discrepancies that the mathematical-based model might not be able to account for. It also means that once a model is developed, all samples can be compared directly to the model and passed/failed based on their performance without having to analyse each sample's individual data.

The advantages of the method are numerous. First, there is the great deal of accuracy due to the fact that ellipsometry is able to measure fractions of a nanometer for ideal samples. Second, there is the ability to distinguish between multiple coatings from one single measurement. Ellipsometry has the ability to simultaneously measure film thickness as well as quality of multiple coatings through a single measurement.

This technique is also high-speed[64] and non-destructive. Each point taken in a measurement can be taken in as little as 20 milliseconds. Measurements taken using the RC2 ellipsometer can be taken in as little as 0.3 seconds.

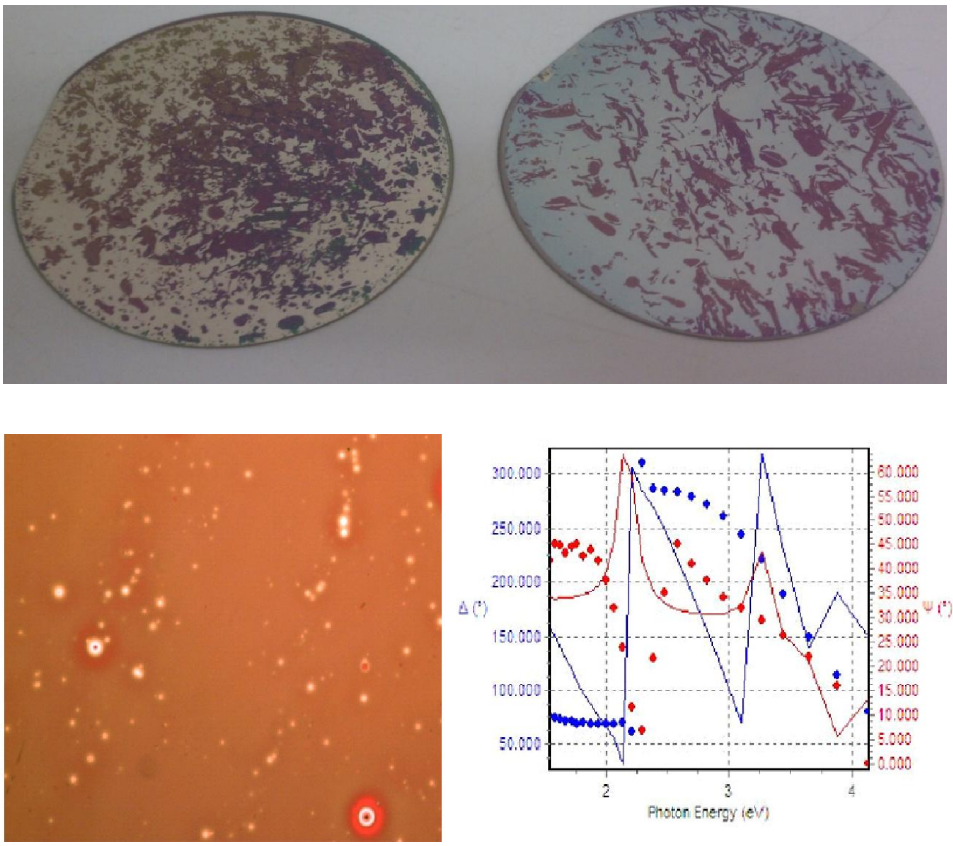

Figure 16 - The image on the left is a microscopy image showing an abundance of pinholes. The figure on the right is the ellipsometry results. The blue line is the Delta results and the red line is the Psi result. The solid line is the expected curve, while the dotted lines represent the measured results.

The processing of the films was improved through superior cleaning protocols as well as the addition of a Titanium adhesion layer with a thickness of 10 nm and through a better heating protocol that allowed for more thermal relaxation in the process. Aggressive cleaning protocols were undertaken, and are outlined below. Wafers were selected with n-type doping in a <100> crystal orientation. This allowed for superior adhesion and growth characteristics for our samples as well as for simplicity in processing as diamond scribing techniques could be used to make smaller substrates without the need of either a scribing machine or wafer dicing apparatus. All Silicon wafers used in these experiments were single sided polished (SSP) with a thickness of 500 micrometers and of Semi-Prime Grade. While

wafers were usually provided in an unhandled, “clean” state to observe best practices as well as gain the utmost control in the later processes, wafers were cleaned using a standard, but aggressive technique to remove any possible contaminants. The wafer cleaning process was as follows. A mixture of Sulfuric Acid (H_2SO_4) and Hydrogen Peroxide (H_2O_2) was mixed with a 4:1 ration. This mixture is colloquially known as a Piranha Etch and is an exothermic acidic reaction with that also performs oxidation. The reaction is noticeable exothermic, producing temperatures in excess of 80 degrees Celsius on some occasions and is an excellent remover of any organic residue that might be contaminating a wafer. The chemical reaction can be written as

$$H_2SO_4 + H_2O_2 \rightarrow H_2SO_5 + H_3O^+ + HSO_4^- + O$$

This reaction utilizes acidity, dehydration, and strong oxidation to remove organics and is even capable of removing carbon residue, and noticeably difficult material to remove. It is a standard chemical mixture used within the microelectronics industry. Wafers were submerged in a fresh mixed Piranha Etching solution for 10 minutes, being placed carefully and slowly in the solution as to avoid possible cracking/damage due to thermal shock. After ten minutes wafers were moved to another cleaning solution this time, Hydrochloric Acid (HCl). Wafers were placed in a solution of HCl to remove any possible metallic residue that might have been contaminated their surfaces. After 10 minutes wafers were removed and placed in the final solution, phosphorous buffered Hydrofluoric Acid (BHF) also known as Buffered Oxide Etch (BOE). This solution is ideal for removing dielectrics that may be on the wafer, but more specifically it removes the approximately 10 nanometer coating of silicon

dioxide that tends to form on the surface of a Silicon wafer over time. The wafers were placed in this solution for approximately 10 seconds, before being removed, rinsed with Deionized water and blown dry using nitrogen gas. If wafers were to be immediately oxidized using PECVD then they were placed in the Ultraviolet Oven to better improve oxide growth and adhesion characteristics, otherwise the wafers went on to other processing step outlined later in this chapter.

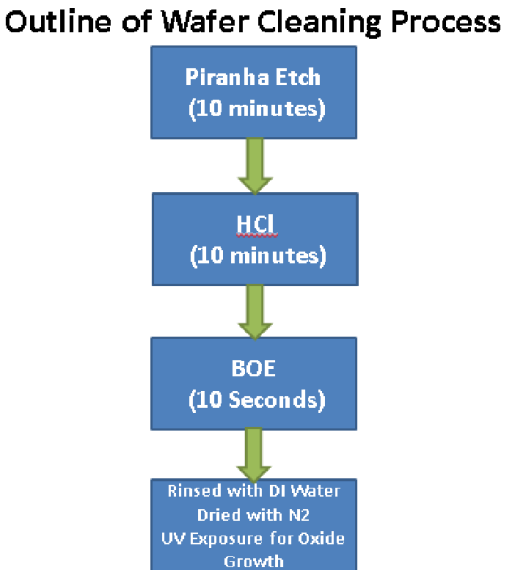

Figure 17 - Flow chart showing the breakout of the wafer cleaning protocol.

This cleaning protocol is a standard within the CMOS setting and while perhaps aggressive under a research setting, did produce remarkably better results. When coupled with better heating temperatures, the use of a Rapid Thermal Annealer (RTA), as well as a Titanium adhesion layer, thin film adhesion was drastically improved. The results (shown below) summarize the improved quality of the film after this process was undertaken.

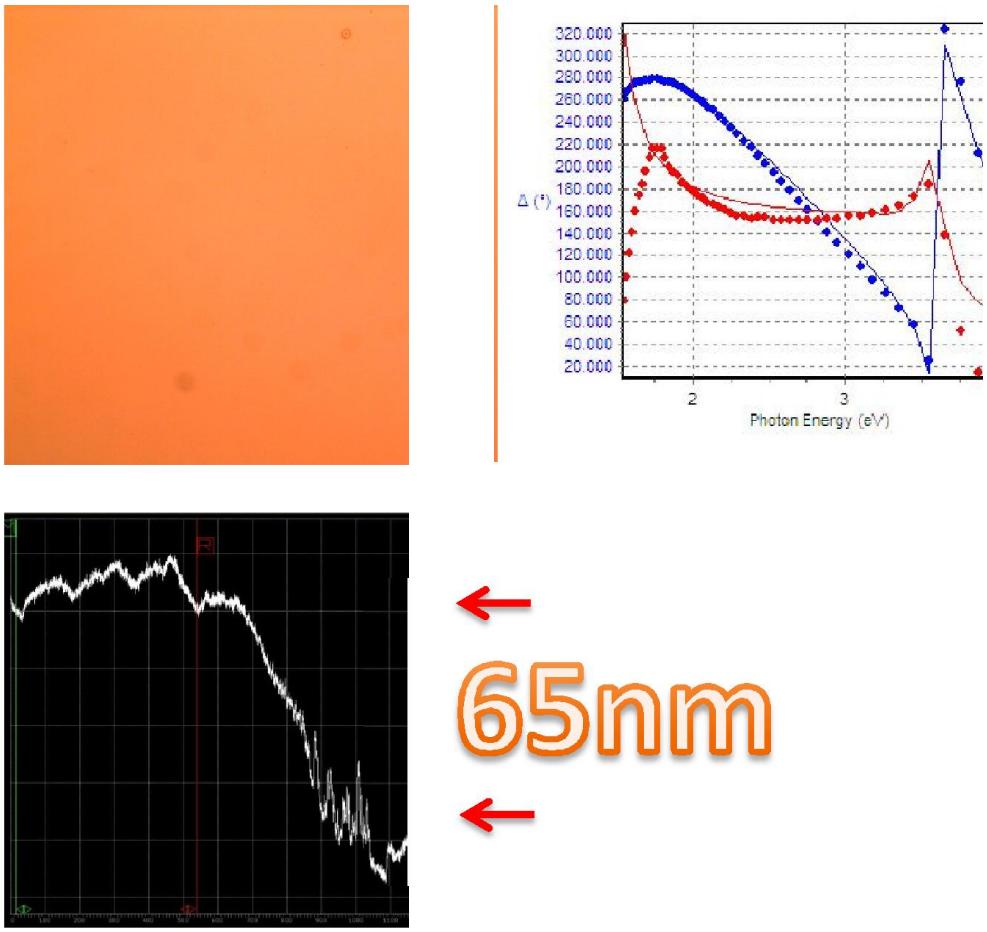

Figure 18 - Top left shows a microscopy result free of deformations, top right shows the ellipsometry result with a X^2 of 9, and an excellent fit. The bottom image is a profilometry result showing a step height of approximately 650 Angstroms, which agree very well with the ellipsometry result.

After establishing the quality of the substrates it was necessary to fabricate nickel magnetic prototype structures using Electron Beam Lithography (EBL). Electron Beam Lithography is a lithographic technique identical to photolithography, except that no mask is necessary to perform the technique and the chemical used are sensitive to electrons instead of light. Photolithographic procedures have a technical limit of about 800 nm, and a fundamental physical limit with respect to the wavelength of the light. While some techniques exist that allow for focusing of light (stepper systems), these systems are expensive and still held to a limit that is on the order of the wavelength of light used. To

overcome this, electron beams can be used, identical to the ones utilized in Scanning Electron Microscopy. Since electrons have wavelength on the order of picometers the fundamental limit to this technique is usually associated with the chemicals used. Patterns are created in standard CAD software and then translated into paths for the electron beam to raster over via a controller and beam blanker. This technique allows for patterns as accurate as 10 nm and due to the fact that no mask needs to be created it is ideal for rapid prototyping of nanoscale devices. After exposure to the electron beam, the resist layer is developed a standard lift-off processing can ensue.

For the deposition of metallic films the most commonly used technique in our process was Electron Beam Physical Vapor Deposition, more colloquially referred to as Electron Beam Evaporation (E-Beam). This technique allows for a material contained within a crucible to be bombarded with electrons produced by an electron gun (anode) and then aimed at a crucible full of the desired material so as to produce a molten, thermally energized solution of material that outputs a vapor of the material into a vacuum chamber. This material then condenses on the top of any substrate that is placed above the melt in the crucible. For our processes graphite crucibles (Fab-Mate) were adequate for deposition of all materials (Gold, Permalloy, Nickel, Titanium). Thickness of the deposited films can be monitored using piezoelectric crystal monitors, which calculate the rate of deposition by monitoring the change in frequency of the piezoelectric element that is also deposited along with the substrate. This method is very accurate, usually resulting in thickness within 10% of the required amount, though even more accurate measurements can be obtained. The method does present one short fall, since the deposition method involves the melting and condensing of a material, alloyed materials are not guaranteed to recombine in the same ratio (due to different melting temperatures of the alloys components) as the alloy. In the

case of Permalloy films, this leads to a potentially unusable film, as the alloy of Nickel and Iron is designed to give the lowest coercivity possible. Due to this, electron beam evaporated films for Permalloy had to analyzed using a Ferromagnetic Resonance technique to insure high quality useable films, the results and nature of this technique are described in later sections.

A test pattern was produced on top of a PZT substrate to see the adhesion of the nickel to the surface as well as to acquire exposure times using the Electron Beam Lithography setup. The pattern was developed in PMMA and then 10nm of titanium and 40nm of nickel were deposited and finally a lift-off was performed using a warm acetone bath. The patterns were then analyzed using Scanning Electron Microscopy (SEM). A scanning electron microscope (SEM) is an imaging tool used to characterize the topology and to some extent some material properties of a sample. SEM's use a focused beam of electron usually produced via a high-voltage applied to a tungsten filament in a high-vaccuum. Much like an optical microscope this beam of electrons is ejected towards the sample and then focused using a set of magnetic "lenses" that act as an objective system, analogous to that of the optical microscope. SEM's then, unlike an optical setup, raster the beam across the sample. Images are not formed by reflected electrons but by electrons emitted from the charged surface caused by interaction with the electron beam. Depending on the material being studied as well as the energy of the primary electron beam several different signal can be excited from the sample, including Auger Electrons, Secondary Electron, X-Rays, and Backscattered Electrons (see diagram below). For imaging purposes secondary electron are of the most interest, and a secondary electron detector is located near the sample to collect this signal and form an appropriate image. Some materials properties can be determined, mostly conductivity of a sample from this signal, though it is mostly used for topological

imaging. SEM's have the advantage of not needing to worry about achromatic dispersion characteristics of their beams, as well as produce images with much deeper depths of focus, creating images in which the entirety of the image is in focus. Also the SEM has the advantage of having much smaller wavelength and therefore can produce images of with much greater magnification, with features as small as 0.6 nm being discernable using in-lens techniques. Prototype structures include a spin wave bridge and some nanomagnetic squares.

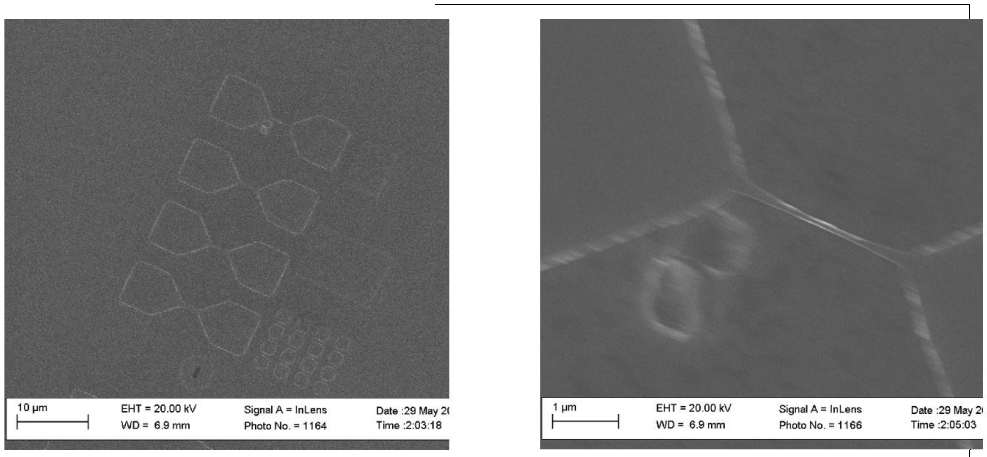

Figure 19 - Top left is SEM image of Ni prototype structures, top right shows 100nm wide bridge between two structures.

We then studied the magnetic properties of the nickel patterns, along a spin wave bridge, to better understand how magnetic domain were laid out along the structures. Atomic Force Microscopy is a technique for determining the topology of micro- and nanostructures. It can have accuracy to the order of several atoms. This technique relies on silicon cantilevers that are extended from silicon cantilever holders. At the end of the cantilever is a tip with a radius of curvature that can be as small as 10's of nanometers. This tip is lightly placed on the surface of the sample and then rastered across. As the tip moves across the surface the cantilever bends depending on high changes within the topology. A

laser is deflected off the back of the cantilever into a photodiode that is then used to measure this deflection. From this laser deflection signal topology can be measured. One technique known as tapping mode differs from standard AFM techniques (known as contact mode) in that a piezoelectric is used to vibrate the cantilever tip at a frequency of several kilohertz. When the tip comes near the surface of the sample attractive forces (Van der Waals and electrostatic being dominant) cause a change in the frequency of vibration. This signal change can then be used to determine the topology of the sample. If the tip is modified with a magnetic coating then magnetic forces from the sample can also be determined. This technique is known as Magnetic Force Microscopy and can image domains as small as 10 nanometers in ideal conditions with appropriate tips. It should be noted that this technique is ideal for imaging domain structures within magnetic microstructures as well as determining magnetic properties of materials. Using Magnetic Force Microscopy we were able to get a clear picture of the magnetic layout of the structures. Domains are clearly visible along the bridge and at the edge of the structure. This technique also allowed us to study some of the AFM properties the substrate which we found to have a roughness less than 5nm, showing a very a high quality substrate.

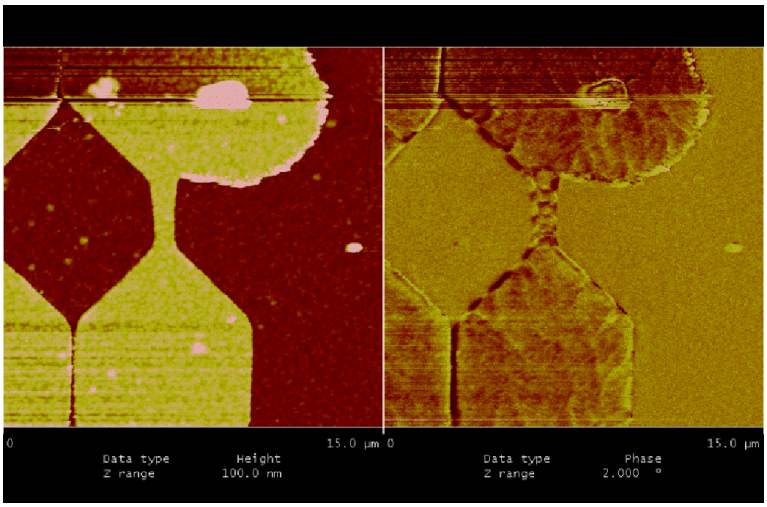

Figure 20 - AFM/MFM result of the structures, the MFM on the right clearly shows magnetic domains.

Once the production of the waveguides as well as the PZT substrates was completed, the next logical step was to attempt to gain insight into the multiferroic capabilities of the system. To do this we explored the magnetic response as DC and AC voltage was applied to a sample. Light when reflected from a magnetic material, has a change in both reflected angle and light intensity based on the magnetization of the media, this phenomena is known as the Magneto-Optical Kerr Effect (MOKE). Because of this magnetic properties can be measured by measuring optical properties while varying an applied magnetic field on the sample. This technique allows for the detection of magnetization, as well as measurements of coercivity and remnance of a magnetic material. The effect can be described by the change in the speed of light using the simple formula:

$$v_p = \frac{1}{\sqrt{\varepsilon\mu}}$$

where Vp is the speed of light, and episilon and mu are material and magnetic permittivity respectively. It has advantages over Vibrating Sample Magnetometry and SQUID

measurements in that it has no moving parts, does not require low temperatures and can accommodate fairly large samples.

Depending on the configuration of the optics as well as the applied magnetic field, several different orientations can be measured, with the UCR setup allowing for Polar MOKE, Longitudinal MOKE, and Focused MOKE studies, though our studies looked at only L-MOKE since the MFM seemed to establish that this was the most likely orientation of the domains.

Samples were prepared on PZT with large nickel pads, placed within a hand-made package to allow for biasing and then mounted inside the MOKE setup.

Figure 21 - Image of a Nickel on PZT sample inside of handmade packaging. Packaging is attached to a standard mini-SNA connector to allow for easy AC or DC biasing/measurement. The connector is attached to a proto-board and connector wires are soldered to the proto-board. To insure good connection between the package and substrate a standard ohmmeter is used to check continuity.

For the DC measurements the hope was that isotropic stress produced by PZT should promote out-of-plane magnetization alignment and hysteresis loops should become more narrow and more tilted (HA like) with applied DC voltage. For AC the though was that perhaps alternating anisotropic stress should promote magnetization switching and coercitivity (hysteresis loops) should shrink with applied AC voltage.

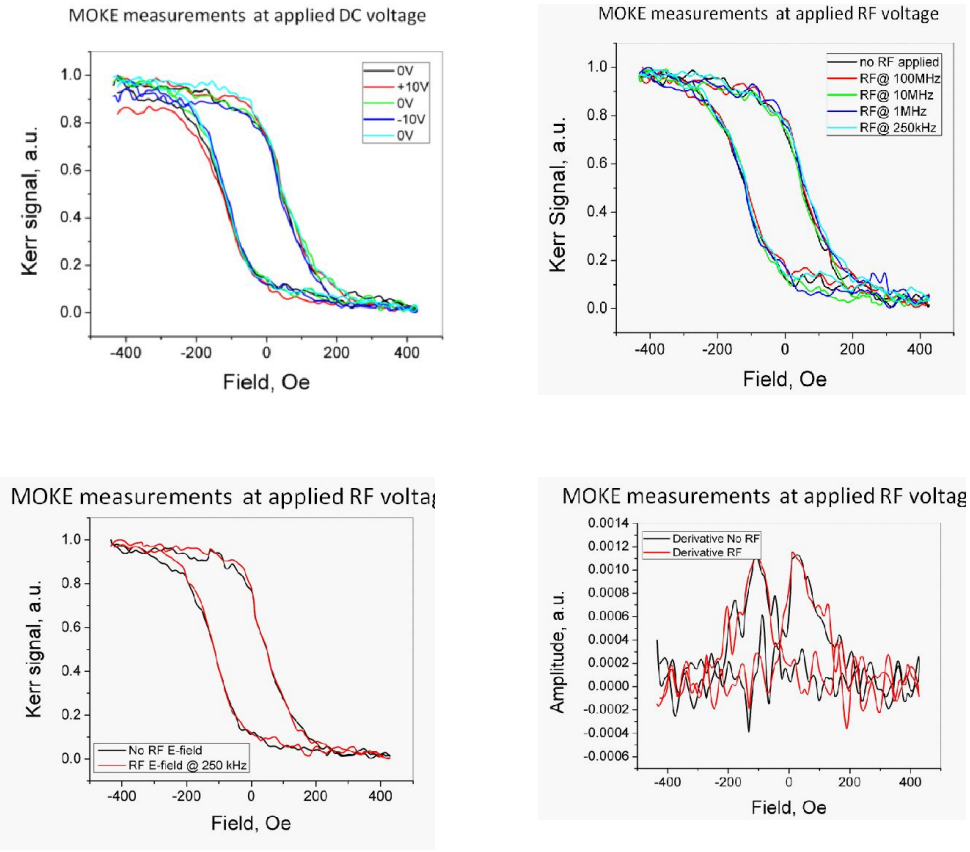

Figure 22 –(top-left) Voltage was applied in sequence 0V – +10V – 0V – -10V – 0V and hysteresis was measure at each voltage. There was almost no visible change with applied voltage. (top-right) RF Voltage was applied at frequency range 1GHz – 250 kHz. (Bottom-left) Similar to the top-right image no obvious change is visible, but only one frequency and control comparison is shown to better highlight the similarity. (Bottom-right) RF Voltage was applied at a frequency of 250 kHz closest to the expected resonance frequency of the structure. The coercitivity is almost the same. A derivative was taken of the data and the peaks stay at almost the same position.

2.4 **Strain Enhanced PZT - Substrate**

In the previous study we had experimented with thin-film PZT systems and determined that the lack in change of magnetic system may be due to substrate clamping, which was preventing the piezoelectric from straining the nickel top layer. We tried to reduce substrate clamping using basic techniques such as patterned surfaces, high aspect ratio devices, and back-etching to remove the substrate.

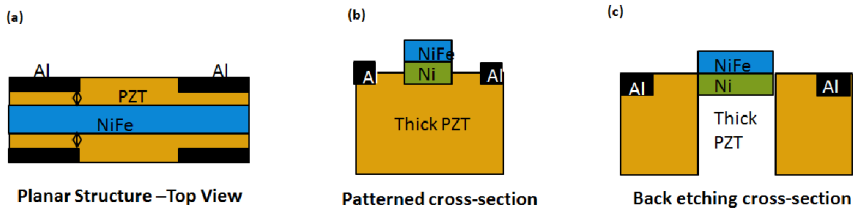

Figure 23 – Examples of proposed technologies for the reduction of substrate clamping. A) A planar structure in which PZT "sandwiches a Nickel of Nickel-Iron layer. B) A Patterned film, where nickel and Permalloy exist as islands on the surface. C) Back etching, which would remove most if not all of the substrate.

The first proposed structure was the planar structure design, which would sandwich Nickel and Permalloy between two layers of PZT. It has sseveral advantages such as it places contacts on the surface of the PZT next to the waveguide. The structure is simpler to bias, and requires no etching. Unfortunately, this was realized to not be feasible, as the PZT layer typically gains it's orientation from the layer underneath it, and in the case of a nickel film, the film would be destroyed by the temperatures required to anneal PZT. Micro-patterning was suggested as it may allow for a reduction in clamping by removing much of the surrounding material. However, this technique had both processing issues as well as a biasing problem once the island type features were created.

Back Etching seemed to be the most promising since substrate clamping is the problem, removing all or most of the substrate seemed an ideal solution, but local processing issues caused problems.

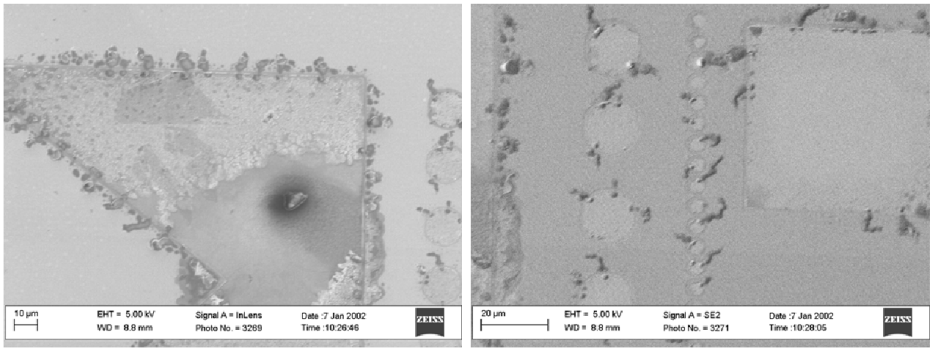

Figure 24 – Mask deformation as a result of local RIE etching techniques at UCR. Deep etching caused a mask breakdown for both Nickel and Nickel-Gold films, as such it would be nearly impossible to create the necessary features desired for the design.

After much consideration a new structure was suggested. This structure envisioned a patterned piezoelectric urface that would both enhance the strain that the piezoelectric could provide but also increase the magnetic anisotropy of the magnetic layer. The hope was to create a geometry with both enhanced strain and magnetic properties using a simple processing technique. Structure is made similar to other samples with a Nickel Layer, Titanium Layer (adhesion), PZT and Pt (Seed and Bottom Electrode). Structures should be easy to create either using EBL or Focused Ion Beam (FIB) Milling Technology, but FIB was selected due to its ability to create high aspect ratio, and it's direct writing capability. FIB Milling is a technique that utilizes energized Gallium ions to remove (mill) away material in a selected area. It is unique as a patterning tool, in that it is a direct patterning method, meaning that the area is directly removed and no further processing is required to remove material in the device/substrate.

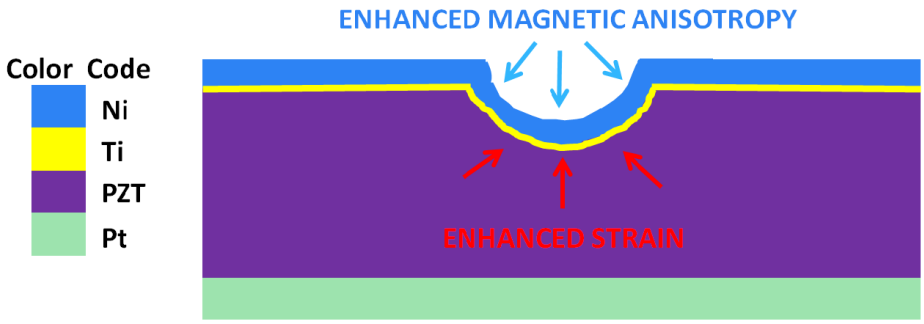

Figure 25 – Diagram depicting the structure refered to as "strain-enhanced" layer. While the technique focuses on the ability to hopefully increase strain to a magnetic layer, for small structure is also has the ability to enhance the shape anisotropy with-in the magnetic film, in this case Nickel

The most interesting results were obtained using a "strain-enhanced" PZT layer, where sub-micrometer scale features were added using Focused Ion Beam milling (FIB) to increase anisotropy of the material. Images were obtained using a SEM which showed quite clearly the pattern of hole that had been added to the surface. These holes or bumps, then required both a topological study to determine depth as well as a magnetic study to see the influence of the enhanced layer on the magnetic layer.

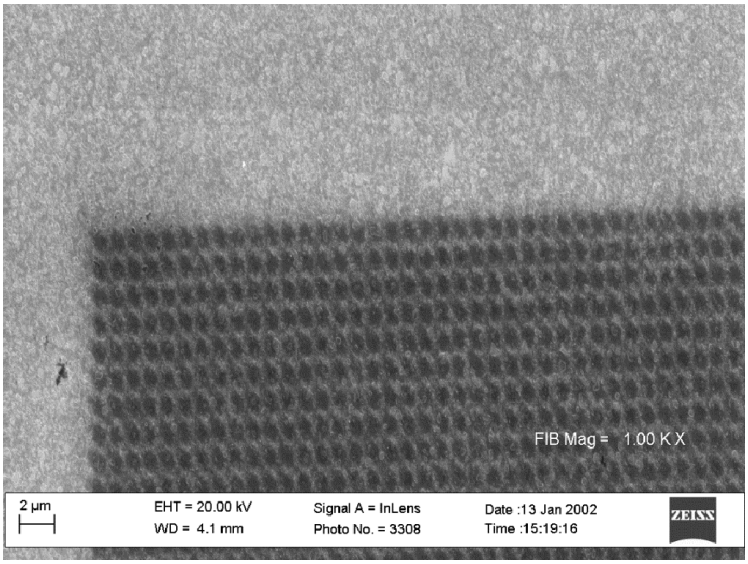

Figure 26 - SEM image showing pattern produced in PZT substrate via Focused Ion Beam (FIB) milling. The intention of these structures is to increase anisotropy in the substrate and nickel pattern placed on top.

After making structures it was necessary to characterize the magnetic properties of the nickel on top of the strain-enhanced PZT substrate. Samples with nickel on top of the strain-enhanced area were produced using electron beam lithography and electron beam evaporation. These samples were then characterized using Atomic Force Microscopy and Magnetic Force Microscopy (AFM/MFM).

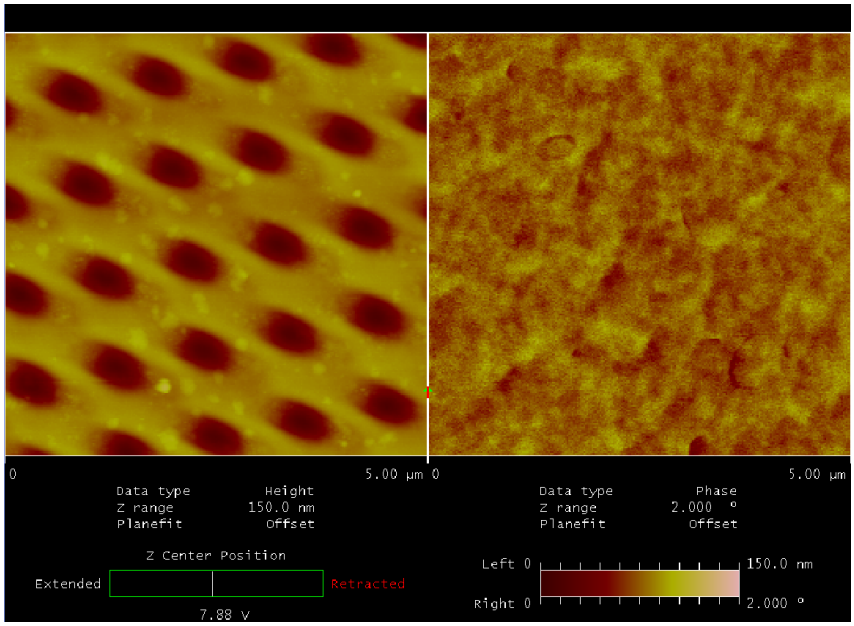

Figure 27 - AFM(left)/MFM(right) image showing strain-enhanced topology on the AFM but no change in the magnetization in the MFM

The first results cleary show a topology that has been modified with bumps or holes that are approximately 100 nm deep. The holes are quite uniform and evenly spaced, however, there appears to be no affect on the magnetic information. The MFM image clearly shows an expected magnetic response from the nickel layer, but no clear magnetic order that coincides with the placement of the bumps. It should be noted here that the magnetic signal is only looking at changes from 0 to 2 degrees, and is therefore experiencing a fairly week signal from the magnetic thin-film. It was expected that the new film may be in a relaxed magnetic state, and so an attempt was made to magnetize the film in an out-of-

plane direction, and thus an applied field of nearly 2 Tesla was applied out-of-plane and the result was then expected under AFM/MFM again.

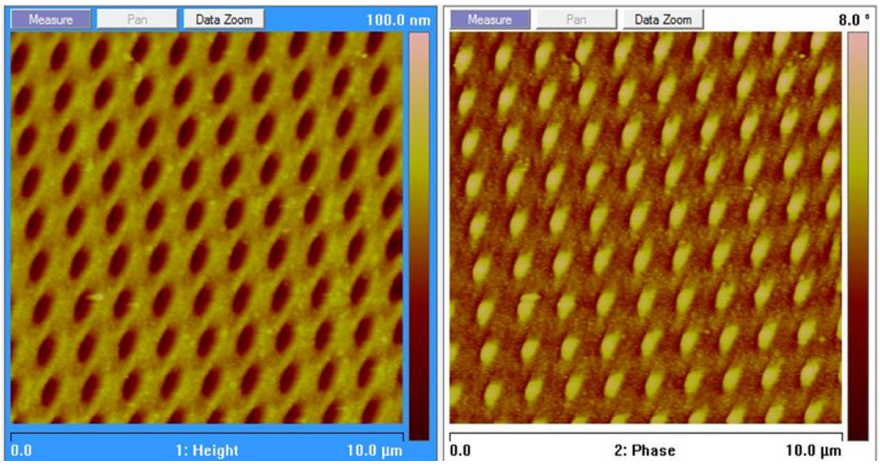

Figure 28 - Same sample as shown in figure 29, but with a 1.5T field applied in plane. After applying field the new magnetic structure becomes apparent, and has good correlation with the AFM topology.

The results from the above figure are very promising as the not only is there an obvious correlation between the placement of the bumps and the MFM response but the MFM signal is much stronger. Figure 31 shows MOKE data from our setup at UCR. It is clear that there is a hysteresis loop meaning the sample is magnetic and measurable we carried out MOKE measurements with DC voltage applied (from 0V to 20V) across PZT. There appears to be some small change in the magnetization of the sample as we apply voltage, and experiments are ongoing.

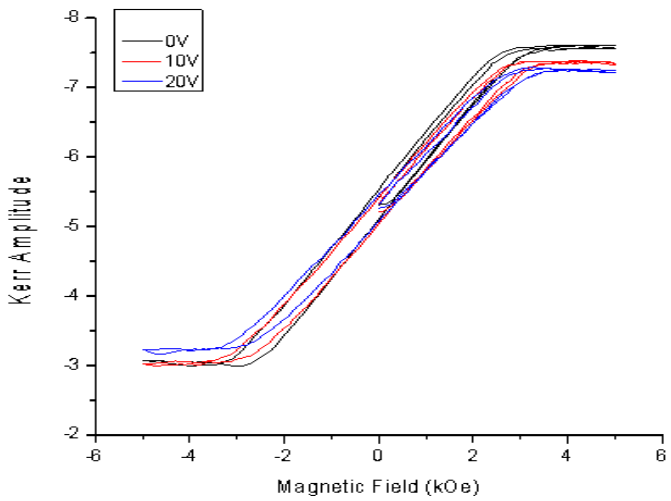

Figure 30 - MOKE data from strain enhanced Nickel/PZT sample showing subtle change as DC voltage is applied across the sample.

From this data we suspect that the magnetic media is longitudinal and we are in the process of reconfiguring the MOKE to make such measurements while still focusing the beam on the patterned area.

2.5 Magnonic Holographic Device Fabrication

2.5.1 YIG Device Fabrication

The $Y_3Fe_2(FeO_4)_3$ YIG used is epitaxially grown on gadolinium gallium garnet $Gd_3Ga_5O_{12}$ substrate with (111) crystallographic orientation utilizing the liquid-phase transition method. Liquid Phase Epitaxy (LPE) is a common method of growth that allows for high quality, large scale growth of pure epitaxial films. Liquid phase epitaxy (LPE) is the most widely used method to prepare garnet films for microwave applications. In this technique the single-crystal garnet substrate (mostly $Gd_3Ga_5O_{12}$ or GGG) is dipped under rotation into a supersaturated, metastable melt, and the garnet film crystallizes on the substrate. Since this method was applied for the first time at the end of the 1960's [3], it has become and been the most widely used preparation technique for epitaxial garnet films.

In the case of the LPE of the YIG films the oxide constituents of the garnet, Y_2O_3 and Fe_2O_3 are dissolved in a solvent, most commonly a mixture of PbO and B_2O_3 oxides of the certain molar ratio where the variation of the melts composition provides growth temperatures in the range of 900-1000 ^{o} C [6, 7]. For a given solution composition, there is a saturation temperature T_s. Typically, the composition is chosen so that T_s is about 1000°C or less to avoid excessive evaporation of PbO from the solvent. Above T_s the solution is unsaturated; additional garnet can be dissolved. Below T_s the solution is supersaturated and garnet tends to crystallize. Fortuitously, the supersaturated state is metastable. A well-prepared solution can be maintained at a temperature considerably below *T,* (say, *5O^{o} C* below) for many hours without spontaneous crystallization. During this period of time, a substrate wafer can be positioned in the furnace, allowed to warm up to the furnace temperature, and immersed in the solution. The substrate acts as a seed on which a garnet film deposits. Removal of the wafer from the solution terminates the film growth. Under this processes the crystallographic orientation of the YIG film defined by the GGG substrate. The GGG(111) substrates with missorientation of the <111> axis and substrates normal to within 0.1° are widely used.

The YIG film has a ferromagnetic resonance (FMR) line width of $2\Delta H \approx 0.5$Oe, saturation magnetization $4\pi M_s$=1750G in accordance with similar devices found in literature. The advantages of using YIG for spin wave research are well known and have been established. The length of the whole structure is 3mm; the width of each arm of the waveguide is 360μm with a thickness of 3.6μm. Laser ablation is a technique in which either a high-energy pulsed laser or in some cases a high-energy continuous wave laser is used to remove material from a substrate. Due to the high-dielectric properties of the YIG material, as well as their millimeter size scale it was a superior method for patterning of the YIG films.

Patterns are designed using standard CAD software and the laser vaporizes any material not in the pattern design. This technique can take several hours for thick films but has the advantage of being a direct patterning technique, ideally suited for relatively quick prototyping of large device designs. To excite spin waves, micro-antenna structures have been fabricated at the edges of each arm. Microwave voltage signals can be transmitted and received using the micro-antenna structures, and spin waves are excited by the well-established inductive voltage method.

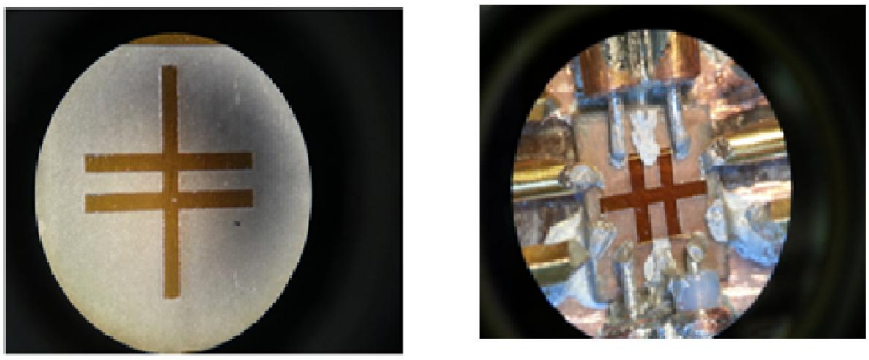

Figure 31 – The figure on the left is an optical microscope image of a YIG device that has not been packaged. The image on the right is a microscope image of a device in finished microwave packaging, ready for testing.

2.5.2 Permalloy Device Fabrication Procedure

Permalloy is a material with unique magnetic properties, but with processing properties almost identical to non-alloyed Nickel. This means that standard deposition and photolithographic procedures can be used to make Permalloy devices without the need for exotic processing such as E-Beam Lithography or FIB milling. This advantage also means that devices designed using permalloy are CMOS (Complementary Metal-Oxide-Semiconductor) compatible, so devices designed as such can be built on silicon substrates, and are possibly compatible with current manufacturing techniques. For the crosses discussed here in standard photolithography techniques were incorporated. A p-type doped silicon wafer was insulated using 100nm of Silicon Dioxide (SiO2) utilizing a Unaxis Model 790 Plasma

Enhanced Chemical Vapor Deposition (PECVD) system. Plasma Enhanced Chemical Vapor Deposition (PECVD) allows for the deposition of materials based on chemical compositions of gases provided to a reaction chamber. To facilitate the deposition of gas-state materials into a solid-state material, RF (AC) plasma is utilized within the reaction chamber, with reacting gases flowing through the gap between plasma electrodes. The gas flowing through the electrodes forms a plasma, meaning a significant portion of its atoms have been converted into ions, which allows for either more efficient conversion of the selected materials into the desired material, or in some cases the creation of these energetic ions is the only way to create certain reaction without using high temperature processing techniques. For the devices presented within the work the PECVD technique was used to create insulating layers of up to 300 nm of SiO2. The chemical precursors used for this technique were Silane and Oxygen gases, with the 100nm of SiO2 being deposited at a rate of 40 nanometer per minute, under Low Vacuum Pressure using an RF plasma set at 300W. Deposition time was two and one-half minutes. The film was evenly applied and was checked for electrical continuity using an ohmmeter and found to offer excellent insulation using this recipe. After this a layer of photoresist (AZ 5120) was deposited on the wafer using a spin-coating technique and a speed of 4000 RPM. The film was settled and dried on the wafer at 110 degrees Celsius hotplate for 1 minute post spin. Lithographic exposure was performed using a Suss Microtec MA6 Mask Aligner. Flood exposure was performed with a 12 second exposure time. After exposure development was performed using (4:1) AZ 400K to water solution with a development time of 1 minute. Features were inspected using a microscope and then a layer of Permalloy was deposited using an E-Beam Evaporator. 100 nm of Permalloy was deposited with 10nm of Titanium used as an adhesion layer. Samples were then placed in an acetone bath overnight (at least 8 hours) to perform liftoff. Since e-beam evaporation is not as commonly used technique as sputtering, there was some

concern for the quality of the magnetic material being deposited, so a witness sample with the same substrate as the devices was placed inside the evaporation chamber, and the magnetic properties were analyzed. Ferromagnetic Resonance was measured in a solid-state EPR measurements system capable of X-Band measurement studies. After deposition of magnetic material it can be important to measure magnetic properties of a deposited film. One of the most accurate methods, that realtes directly to spin wave propogation is to measure the magnetic resonance of the thin film, to understand the magnetic qualities of the deposited film. UCR has an X-Band capable EPR measurements setup as part of the shared facilties attached to the chemistry department. This setup can be modified with appropriate sample holders to make solid state measurements and thus allow for ferromagnetic resonance measurements. The setup consist of a large magnet with a microwave cavity between the poles of the magnet. By using a microwave source, energy is then placed into the cavity a specific frequency while the applied magnetic field is varied. The measurement aims to measure the amount of microwave energy absorbed as a function of the applied magnetic field. These measurements are ideal for pin-pointing the resonance of a magnetic material as well as determining coactivity of the material.

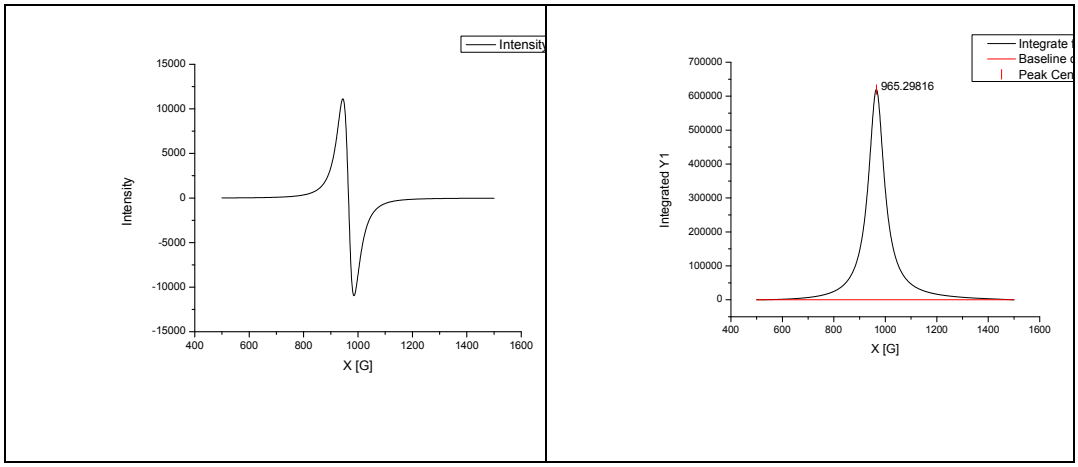

Figure 32 – FMR measurement (image on left) taken using an X-Band EPR setup and solid-state adapter. This graph shows a peak to peak coercivity of 40 Oersted. The derivative (image on the right) of the previous FMR measurement, used to determine the peak magnetization energy.

The first figure shows the intensity of the signal with respect to the applied magnetic field measured in Gauss. This can be used to measure the coercivity which is found to be 40 Oersted, which is a very good result and well within the range necessary for spin wave studies. The second figure is an integration which is used to check the FMR center frequency, here measured to be 965.29 Gauss. These results show that even if there is some small change in the coercivity or alloy of the material, the resulting measured magnetic properties are well within the necessary range needed to perform high-quality magnetics measurements. After the Permalloy orthogonal waveguides are deposited the devices and again insulated using the same technique as described above, with an insulation layer of 40 nm. Afterword's gold contact pads and antennas are deposited using the same photolithographic and evaporation technique as described for Permalloy. Gold is selected because of it's excellent electrical characteristics, also because it is a noble metal and therefore unlikely to experience corrosion due to environmental factors. Devices are then

able to be wire bonded and packaged to appropriate microwave connectors for further study (SNA connectors being the standard connection within our laboratory setup).

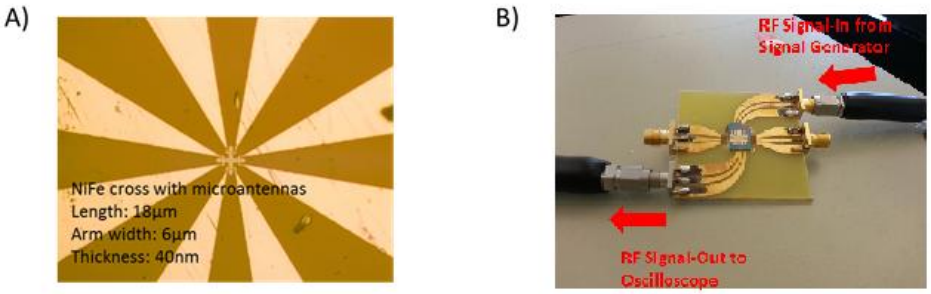

Figure 33 – A) microscope image showing permalloy cross with antennas, inset contains dimensions. B) Fabricated device in microwave packaging, the device is wire bonded to gold plated leads that are connected to mini-SNA connectors.

The image shown in Figure 37 depicts the final packaging of the devices and shows how the packages connect to microwave measurements. After these steps, the devices are done being fabricated and packaged and experimental procedures, outlined in later chapter, may begin.

3 Spin Wave Propagation within Orthogonal Waveguide Structures

The first step to understanding spin wave interference within the framework of the Magnonic Holographic Device structure is to gain an appreciation of a single element of the MHM structure. The simplest element of the structure is a single-cross structure with no magnetic element "object" placed in the junction. This free junction cross structure can be studied as the results of two independent, yet coupled orthogonal waveguides. While spin wave interference is of course an interesting phenomenon capable within this simple structure, it represents an interesting structure simply for some studies of propagation through each waveguide. These studies are necessary for a clear understanding of spin waves within the device structure, which add to our understanding of propagation when interference and magnetic objects are added. Also of interest is propagation of spin waves through arms orthogonal to the first excited waveguide. While discussion of magnetic objects will take a predominant role in later chapters in this work, it should be noted that when a magnetic waveguide passes over another magnetic waveguide it represents a non-uniform magnetic field to a propagating spin wave and thus is a scattering parameter that can have a serious effect on the device performance and spin wave coherence. The single cross spin wave structure has several interesting characteristics, as well as acting as the simplest element within a MHM design. The study of this structure gives important information concerning the interference and propagation properties of Magnonic Holographic Matrix Devices. Previous studies of such a device have not incorporated the

highly efficient YIG material nor have cross like devices yet been explored in literature using Permalloy, so it is of interest to not only explore the material characteristic but to also compare them.

3.1 Experimental Procedure

The design of the initial experiments is as follows: A vector network analyser is used as a microwave source and a signal from the VNA is sent to the gold antenna structures that lay across each arm of the cross. The microwave signal generated by the VNA excites a small, but non-negligible alternating field within the antenna contours and this field excites spin waves within the structure. The structure is placed inside a large electromagnet so that an applied field may be uniformly applied across the device, thus forming a lattice of spins and allowing spin waves to propagate along the lattice. In turn the spin waves are able to propagate along the arms of the cross, and will the alternating magnetic field produced by the spin wave oscillation will induce a voltage change in the receiving antenna structures, this technique is the common inductive voltage technique. This signal is then measured and recorded using the VNA. A diagram, as well as some images of the experimental setup is given below.

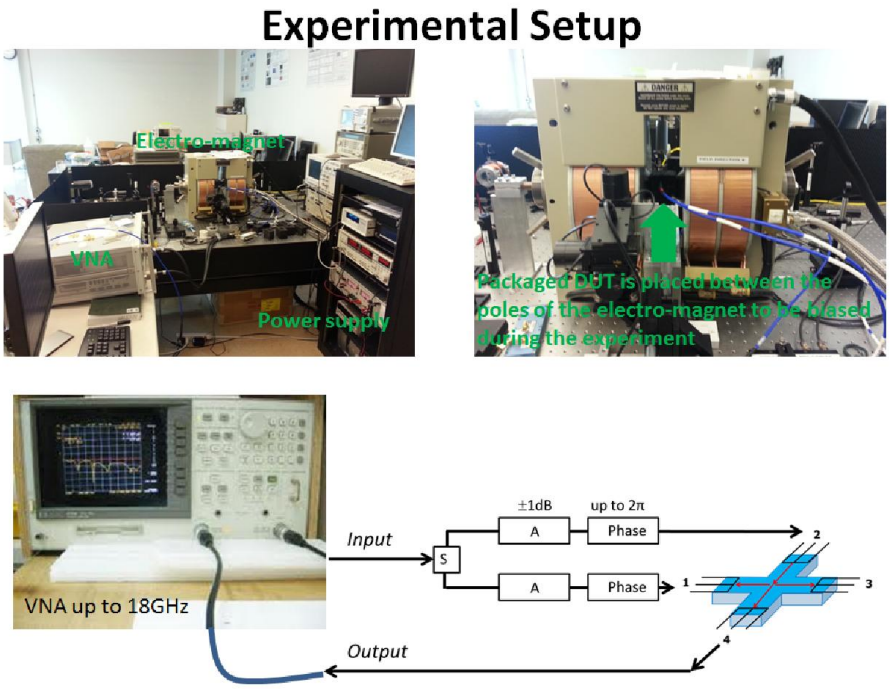

Figure 34 – (Top Left) Shows laboratory setup that includes the Power Rack, electro-magnet, and the Vector Network Analyzer (VNA). (Top Right) Image is a closer picture of the the electromagnet, highlighting where samples are located for measurement. (Bottom) Schematic to illustrate how the VNA is connected to the single cross structure, phase shifters (Phase), splitters (S) and attenuators (A) are also denoted in the schematic.

Let it be noted that the method used for suspending the device in in the electromagnet can also be rotated. This allows for studies of the spin wave propagation through the device at different angles of the applied magnetic field.

3.2 Results

3.2.1 Results of YIG Device

The results for these experiments resulted in a wealth of data, of which a selected portion will be contained in this section of the work. Some amount of the raw data will be presented, though it should be noted that due to the large amount of this data studies concerning it are on going. These results, in figure 39, represent a summary of some of the conclusions obtained from the wealth of raw data that was acquired during these experiments. Much of this data is specifically represented due to how it coordinates either

with the direct research objectives stated or because of the ability to use this data to compare the devices to either current CMOS standards or other spin wave devices.

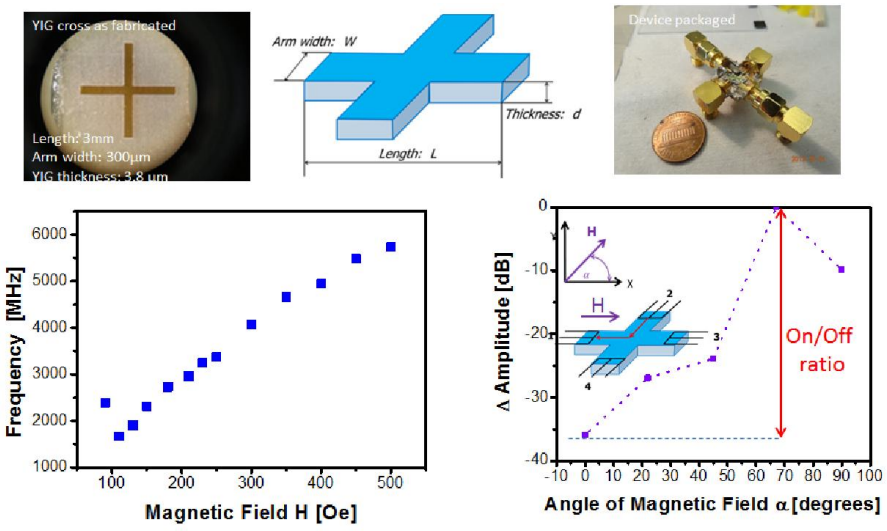

Figure 35 – (Top Left) Microscope image of a single cross design. (Top Middle) Schematic of single cross. (Top Right) Microwave packaging of single cross. (Bottom Left) FMR frequency dependency shown graphed as a function of the applied magnetic field. (Bottom Right) Amplitude in dB as a function of the applied magnetic field angle. On/Off ratio for maximum and minimum amplitude is in excess of 35 dB.

Figure 39 shows some interesting features of the device as well as a schematic and image showing the device and device layout. Also included is an alternative packaging technique, that is somewhat smaller and less noisy than the one originally shown in the fabrication section of this work. An On/Off ratio is given, while these devices are not necessarily intended for Boolean logic, or high speed swithing applications it is interesting to see how they perform when compared to other switching type logic devices. Also, even whe not considering the "On/OFF" ratio the dependence of the magnetic field direction is surprisingly high in these samples, which can open the door to much discussion concerning the "angle of incidence" style of multiplexing within a holographic system.

The vector network analyser produces data that shows the amount of microwave absorption (in either millivolts of dB) in comparison to the frequency of the supplied

microwave signal. For the majority of our data produced we observe changes in this VNA signal by either changing the direction of the signal (what ports we excite and read), the direction of the applied magnetic field, or the strength of the applied magnetic field. Figure 40 shows two VNA outputs that have been overlayed on top of each other. The red signal shows propogation from port 2 to 4 and the black signal from port 4 to 2. Even though the path is the same in these examples the result is a slight change in amplitude and an even smaller change in resonance frequency. This is an important result because it shows that the device is non-reciprocal, an important characteristic for a logic device. This example is also presented here because of it's simplicity and ease of reading.

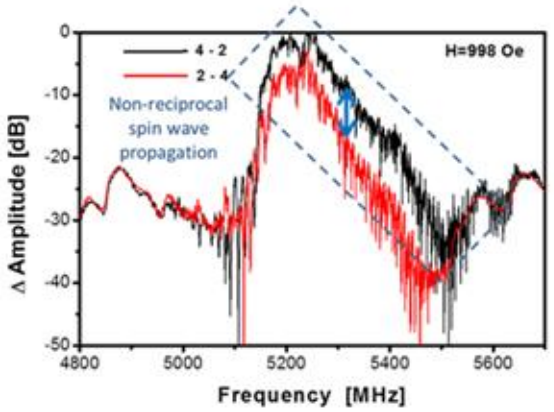

Figure 36 - YIG Device output showing non-recipricol spin wave transport when traveling between arms 3 and 4. The result is several dB in amplitude difference as well as a small shift in resonance

Other features of note are the orthogonal features, especially that exhibited by propagation from port 4 to port 3 and vice versa. At select angles we see a scattered spin wave signal moving orthogonal to the original propagation direction and at a different applied field angle, for the signal from port 4 to 3 the signal can result in a change as high as 40 dB differences at select angles.

Below is a select amount of raw data that is presented even though the current analysis of this data is ongoing. This data is presented with the hope of giving the reader the ability to derive their own conclusion as to what assumptions can be made from these devices. The following data plots show spin wave propagation from one port to all other ports for an applied field of 998 Oersted for YIG devices. The figures denote which port is the port being used to begin propagation of the spin waves, and the measurement port is denoted in the top-left of each individual graph. All YIG results discussed in this section will be for this collection of data at this field strength. The data is collected to show every combination of ports, as well as a variety of applied magnetic field angles. Spin wave signals should change with changes in the direction of the applied magnetic field and is one of the methods used to determine that the signal being measured is indeed caused by propagating spin waves. Changes in the direction and the strength of the applied field cause direct frequency and amplitude affects to the spin wave signal.

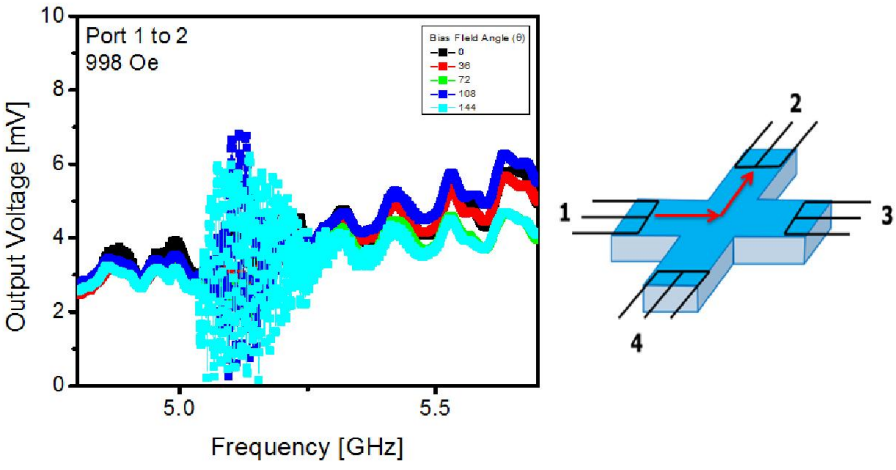

Figure 37 – VNA Output showing Output Voltage in mV with respect to the frequency for signals traveling from port 1 to port 2. Different colors denote different angles of the applied bias field, ranging from 0 to 144 degrees.

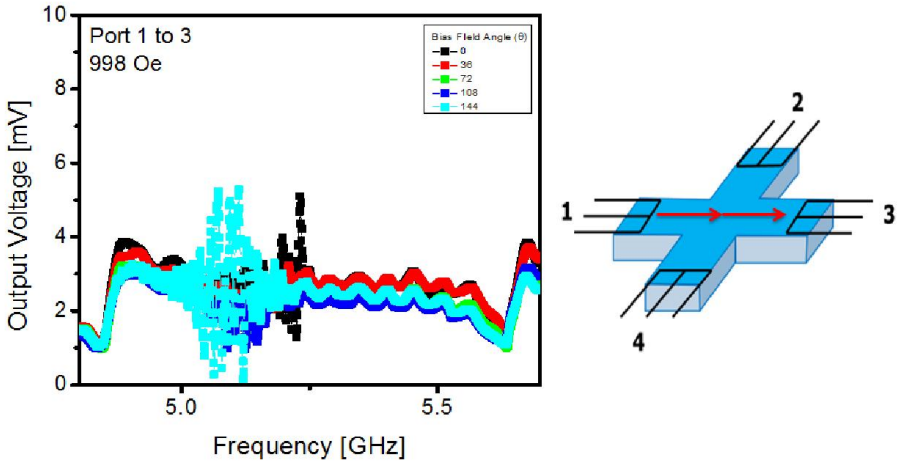

Figure 38 - VNA Output showing Output Voltage in mV with respect to the frequency for signals traveling from port 1 to port 3. Different colors denote different angles of the applied bias field, ranging from 0 to 144 degrees.

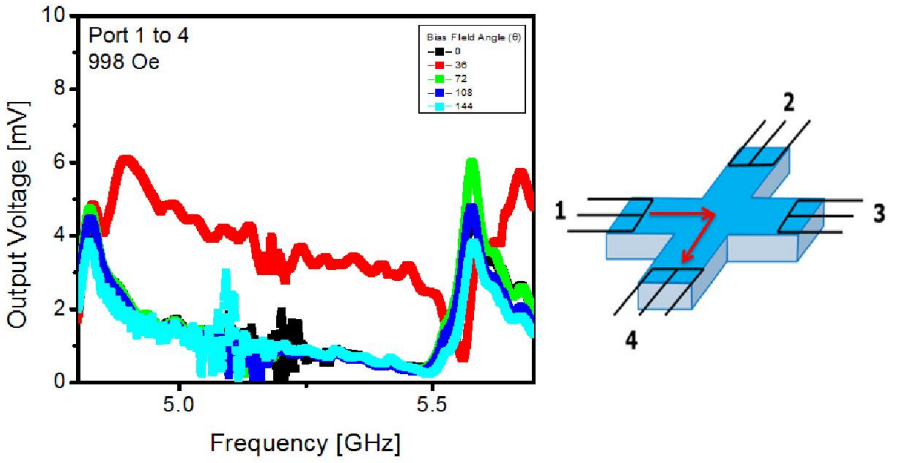

Figure 39 - VNA Output showing Output Voltage in mV with respect to the frequency for signals traveling from port 1 to port 4. Different colors denote different angles of the applied bias field, ranging from 0 to 144 degrees.

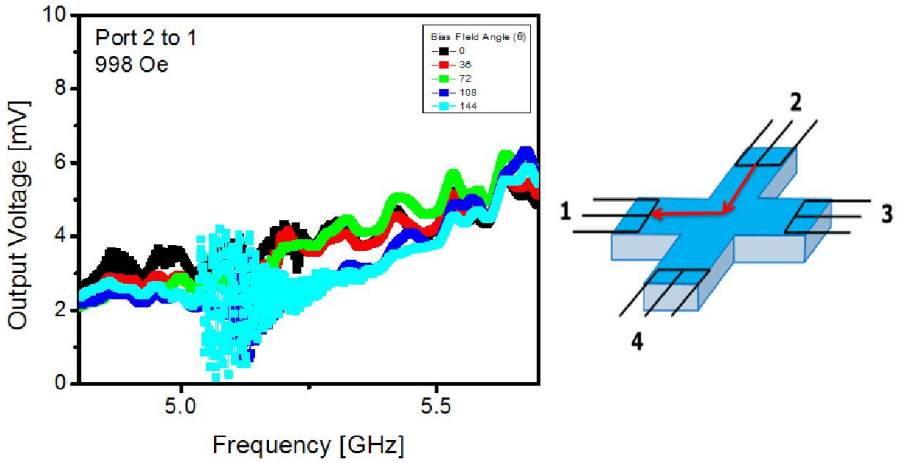

Figure 40 - VNA Output showing Output Voltage in mV with respect to the frequency for signals traveling from port 2 to port 1. Different colors denote different angles of the applied bias field, ranging from 0 to 144 degrees.

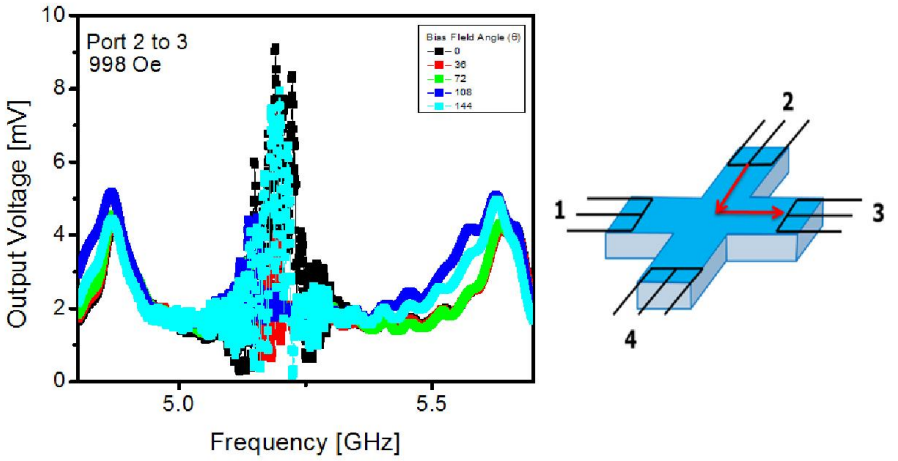

Figure 41 - VNA Output showing Output Voltage in mV with respect to the frequency for signals traveling from port 2 to port 3. Different colors denote different angles of the applied bias field, ranging from 0 to 144 degrees.

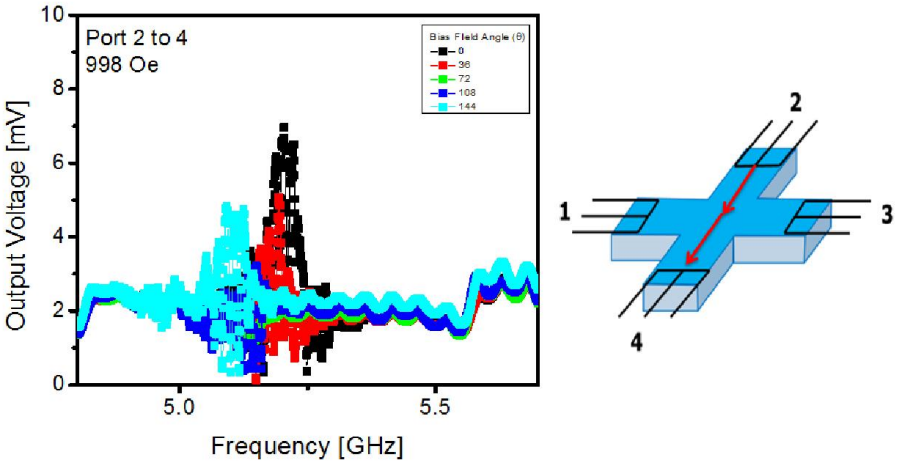

Figure 42 - VNA Output showing Output Voltage in mV with respect to the frequency for signals traveling from port 2 to port 4. Different colors denote different angles of the applied bias field, ranging from 0 to 144 degrees.

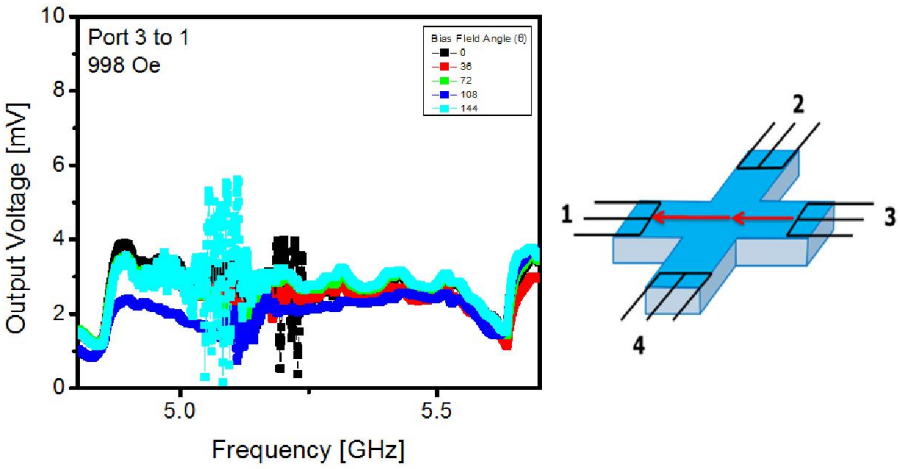

Figure 43 - VNA Output showing Output Voltage in mV with respect to the frequency for signals traveling from port 3 to port 1. Different colors denote different angles of the applied bias field, ranging from 0 to 144 degrees.

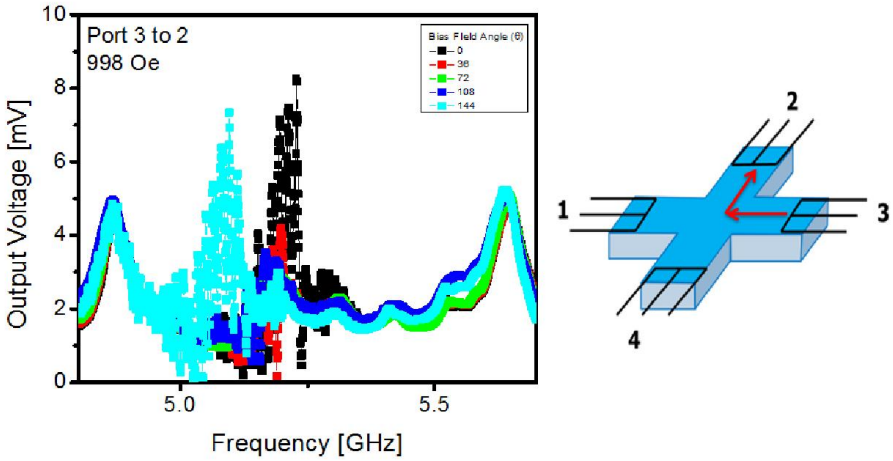

Figure 44 - VNA Output showing Output Voltage in mV with respect to the frequency for signals traveling from port 3 to port 2. Different colors denote different angles of the applied bias field, ranging from 0 to 144 degrees.

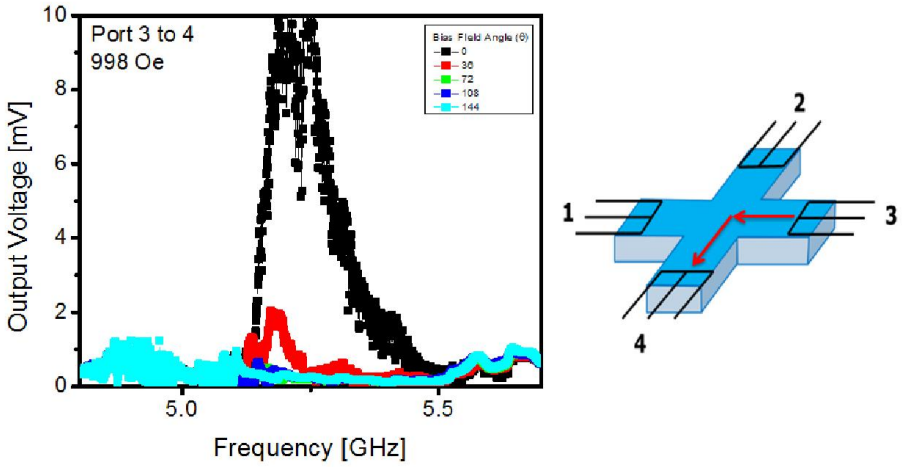

Figure 45 - VNA Output showing Output Voltage in mV with respect to the frequency for signals traveling from port 3 to port 4. Different colors denote different angles of the applied bias field, ranging from 0 to 144 degrees.

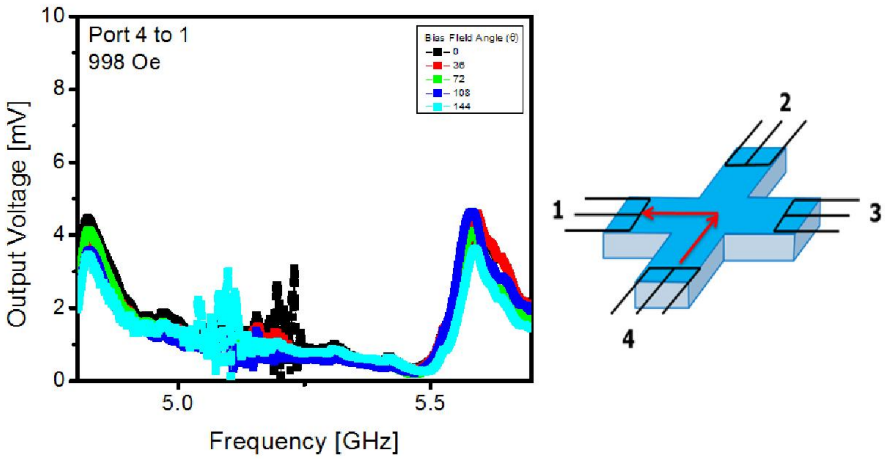

Figure 46 - VNA Output showing Output Voltage in mV with respect to the frequency for signals traveling from port 4 to port 1. Different colors denote different angles of the applied bias field, ranging from 0 to 144 degrees.

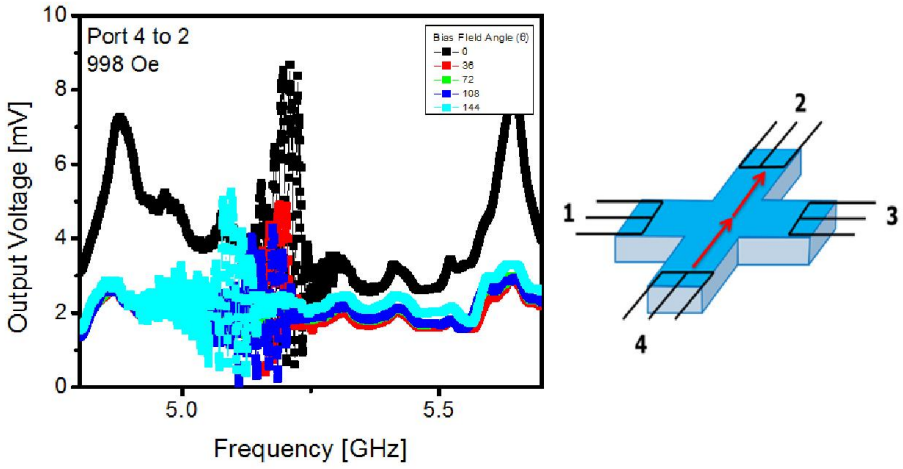

Figure 47 - VNA Output showing Output Voltage in mV with respect to the frequency for signals traveling from port 4 to port 2. Different colors denote different angles of the applied bias field, ranging from 0 to 144 degrees.

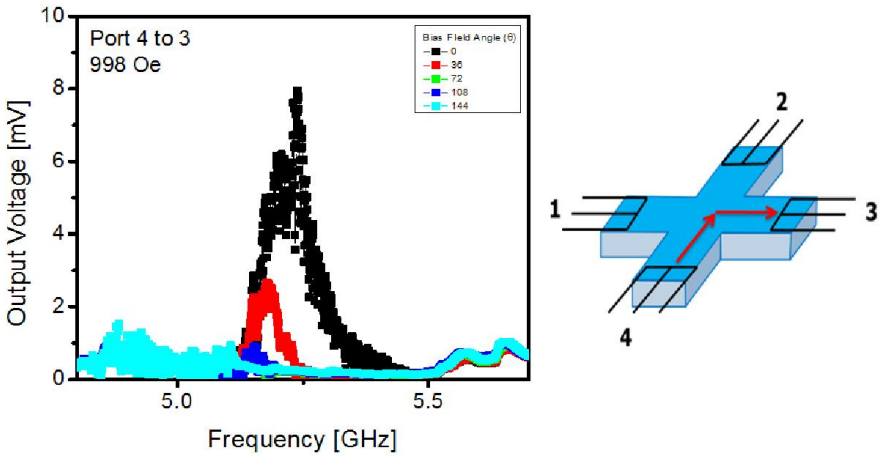

Figure 48 - VNA Output showing Output Voltage in mV with respect to the frequency for signals traveling from port 4 to port 3. Different colors denote different angles of the applied bias field, ranging from 0 to 144 degrees.

3.2.2 Results of Permalloy Devices

Permalloy devices were also measured, and allow for some comparison between YIG and Permalloy devices. Typically Permalloy devices have a lower frequency then YIG devices, but for the selected field strength (998 Oersted, as with the YIG devices) the frequencies are similar. For both devices the frequency of operation can be seen to increase with the strength of the applied field. It should be noted that neither data set is identical though there are definite similarities that will be further explored in the discussion section of this chapter.

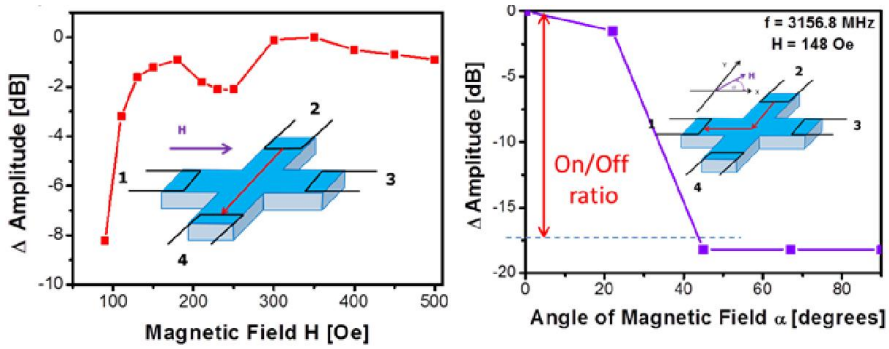

Figure 49 – (Left) Amplitude as a function of magnetic field for a Permalloy cross, from port 2 to port 4. (Right) On/Off ratio which is observed to be in excess of 15 dB for a Permalloy sample for propagation between port 2 and port 1 at an applied field strength of 148 Oe and a frequency of 3156.8 MHz.

Here many of the same effects are observed within the data. There is a distinct "On/Off" ratio observed within the device and the amplitude depends on the strength of the magnetic field. These similarities, and in some cases differences, lead to several interesting questions that we will now discuss.

3.3 Discussion

The raw data that is provided is difficult to interpret and at first glance contains a wealth of information that can be difficult to interpret. Before we delve deeper into analysis of this raw data for better comparison, some important features of this data set should be pointed out. First, with the data sets, it is important to make observations of direct propagation through the device. In this numbering scheme, direct propagation, is represented by any port number that is two ports away, i.e 1 to 3, or 2 to 4 and vice versa These port numbers show the signal as it travels through a single waveguide and past through the junction. For all devices and ports, we see a distinct spin wave signal through the direct propagation direction. This means that spin waves are able to not only be excited in the device but that some part of the spin wave is able to be excited through the scattering junction in the center of the device.

What is also remarkable is that both the YIG and the Permalloy device exhibit this change in the signal, despite extreme differences in device dampening, size, and method of antenna fabrication. This is also important because it allows us to highlight the non-reciprocal feature of the spin-wave cross device. A small but discernable, several dB difference in amplitude is noticed when the direction of propagation is changed between arms 3 and 4. This result is of great interest to the community. Also it is worth noting the on/off features of the device. With such a large difference in the signals on/off state there is much interest in both how the spin wave may turn the 90 degree corner and what exactly are the effects of the junction scattering parameter. Previous literature on the subjects of spin waves and corners has proposed that spin waves under the right conditions will undergo a mode transition change, or a filtering effect when changing their original propagation direction. This may in turn explain why we see a signal shift of such a dramatic size. MSSW waves are characterized typically by a higher signal strength, since the original Spin Wav excitation mode is distinctly a mixed mode method of excitation, if some of the spin waves are converted from the lower signal strength BVSW to the higher signal MSSW this might explain the drastic changes in signal strength exhibited under appropriate conditions.

The results demonstrate prominent change in the amplitude of the transmitted signal [18dB] when the field is applied between 20° and 30°. The main observations of these experiments are the following. (i) Spin wave propagation through the cross junction can be efficiently controlled by the external magnetic field. (ii) Both the amplitude and the direction of the magnetic field can be utilized for spin wave control.

We conducted similar experiments on the YIG single cross device as shown in Figure 39. It was observed prominent signal modulation by the direction and the strength of the external magnetic field. In Fig.39, there is shown an example of experimental data on the spin wave transport between ports 2 and 1. The maximum transmission between the orthogonal arms occurs when the field is applied at 68°, while the minimum when the field is applied at 0°. The On/Off ratio for YIG cross reaches 35dB. Of noticeable interest is also the effect of non-reciprocal spin wave propagation. The two curves in Figure 40 show signal propagation from port 2 to port 4, and in the opposite direction from port 4 to port 2. The measurements are done at the same bias magnetic field of 998 Oe. There is a difference about 5dB for the signals propagating in the opposite direction. The effect is observed in a relatively narrow frequency range (e.g. from 5.2GHz to 5.4GHz). Concluding on the spin wave transport in the permalloy and YIG single cross structures, prominent signal modulation has been observed in both cases. The operation frequency is slightly higher for YIG structure (~5GHz) than for permalloy (~3GHz). The speed of signal propagation is slightly faster in permalloy (3.5×10^6 cm/s) than in YIG (3.0×10^6 cm/s). The difference in the spin wave transport can be attributed to the differences between the intrinsic material properties of YIG and Permalloy as well as the difference in the cross dimensions. It is important to note, that in both cases the level of the power consumption was at the microwatt scale (e.g. 0.1μW-1.0μW for permalloy and 0.5μW-5.0μW for YIG) with no feasible effect of micro heating on the spin wave transport. The summary of the experimental finding for permalloy and YIG single cross junctions is in Table I.

	Permalloy	**YIG**
Cross dimensions	L=18μm, w=6μm, d=100nm	L=3mm, w=300μm, d=3.8μm
Operational Frequency	3GHz-4GHz	5GHz-6GHz
SW group velocity	3.5×10^{6} cm/s	3.0×10^{6} cm/s
Equal splitting between the arms at bias field angle	20^{0}-30^{0}	~45^{0}
Maximum On/Off ratio	20dB	35dB
Power consumption	0.1μW-1μW	0.5μW-5μW
Compatibility with Silicon	Yes	No

In closing these results provide good insight into how spin waves propagate through a single junction. A wealth of data was produced in these experiments and as such it will lend itself to further analysis than what is presented here. While interesting trends appear to exist, the next step is to understand how multiple junction devices will interact with spin waves.

4 Double Cross Magnonic Holographic Matrix Device

Here we present the first application of a Magnonic Holographic Matrix, as well as the first demonstration of spin-wave holography, using a prototype structure with two junctions, which is referred here-in as the double cross structure. This structure represents the simplest form of the matrix in which multiple elements are present in the device. This has dual purposes, it allows for a simple structure to detect multiple junction interference and secondly it allows for the investigation of the holographic detection of multiple objects.

The schematic of the 2-object MHM prototype is shown in Figure, along with an inset of an optical micrograph of the device.

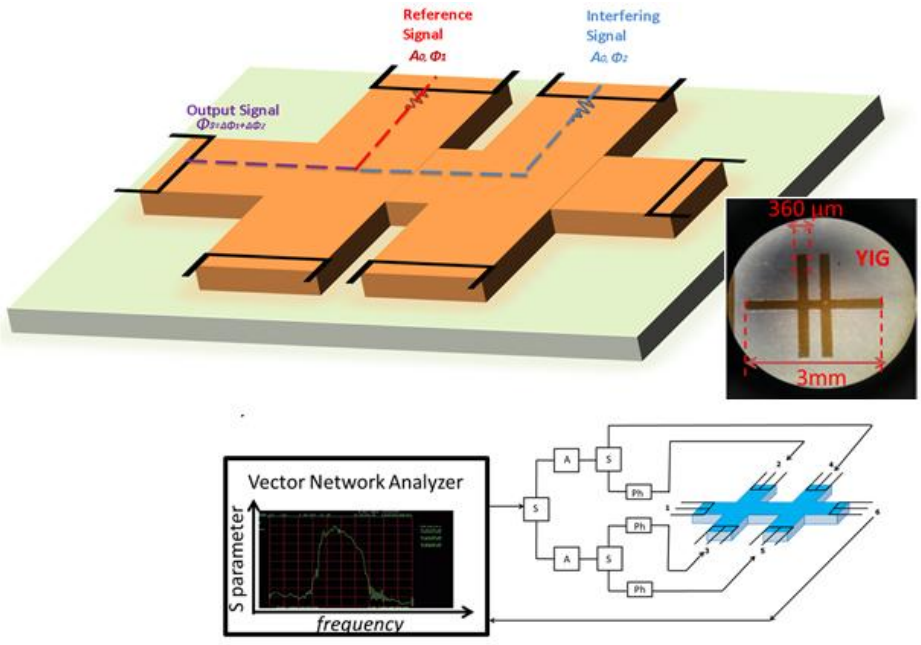

Figure 50 – (Top) Schematic of the YIG double cross device (no magnetic object), along with inset of the device before packaging. (Bottom) Schematic to illustrate how the VNA is connected to the single cross structure, phase shifters (Phase), splitters (S) and attenuators (A) are also denoted in the schematic.

4.1 **Results**

The graph in Figure 54, left image, shows the raw data collected for the structure with just two working micro-antennas. The test experiments are provided for the structure without magnet placed on the junctions. The graph shows the amplitude of the output inductive voltage detected for different excitation frequencies in the range from 5.30GHz to 5.55GHz. The curves of different color depict the output obtained for different phase difference $\Delta\phi$ among the two inputs 2 and 3. These data show the oscillation of the output voltage as a function of frequency and the phase difference between the two generated spin waves. The frequency dependence of the output is attributed to the effect of spin wave confinement within the structure, while the phase-dependent oscillations reveal the interference nature of the output signal. In Figure 54 (right) we show the slice of the data taken at the fixed frequency of 5.42GHz. The experimental data has a good fit with the classical equation for the two interfering waves. The only notable discrepancy is observed for $\Delta\phi=\pi$, where experimental value is non-zero. This fact can be well understood by taking into account all possible parasitic effects (e.g. reflecting waves, direct coupling between the input/output ports, structure imperfections, etc.)

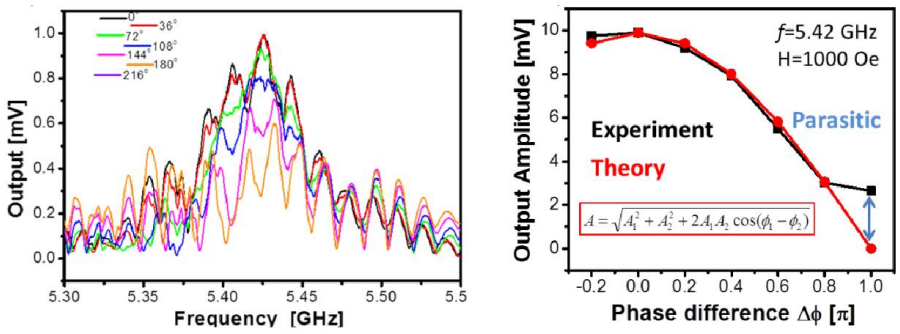

Figure 51 - (Left) Transmitted signal S12 spectra for the structure without micro-magnets. Two input signals are generated by the micro-antennas 2 and 3. The curves of different color show the output inductive voltage obtained for different phase difference among the two interfering spin waves. (Right) The slice of the data taken at the fixed frequency of 5.42GHz (black curve). The red curve shows the theoretical values obtained by the classical equation for the two interfering waves.

The experimental procedure is straightforward. Signals are excited through the input antennas (represented by the input signal and the reference signal in Figure 1), and the spin wave frequency spectrum is determined by varying the magnetic field to ensure that an appropriate frequency range is selected. It is then necessary to determine a base signal that is then removed using a standard subtraction technique built into the VNA. This signal is then subtracted from all subsequent signals in an attempt to remove noise. Figure 56 (A) and (B) shows the first spin wave interactions from the device. It is necessary to obtain a maximum and minimum signal values with respect to a phase shift in the interfering signal, which can be used to determine both in-phase and out-of-phase transmissions in the device. For the experiments discussed here in, a signal will be input to both the input and the reference and an output will be measured from the output signal (see Figure 54). To determine the maximum constructive interference a phase shifter is attached to the input antenna and the reference antenna. It is assumed during the experiment that fully constructive interference ($\Delta\phi = 0$) takes place at a signal maximum, and destructive interference ($\Delta\phi = \pi$), takes place at a signal minimum. Figure 56(A) and (B) shows two graphs, where the red line shows only one port with a signal, while the blue line represents

both ports being excited simultaneously. Both graphs clearly show constructive and destructive interference of the spin wave signal.

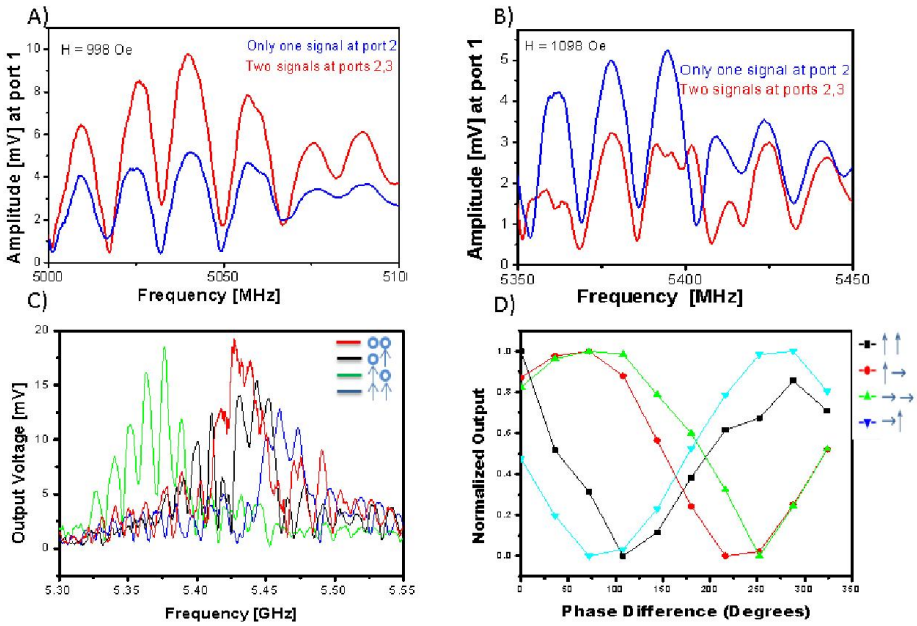

Figure 52 - A) frequency graph showing constructive interference. The blue line (one input) is half the height of the red line (two inputs). B) A frequency graph showing destructive interference, the opposite phenomena from inset a. C) Raw VNA output showing different frequency spectrum for magnetic objects placed on the cross junctions, (O represents no magnet, and an arrow represents the placement of a magnet) D) Magnetic orientations changed with respect to phase difference. Output has been normalized and scaled from 0 to 1.

The results show interesting features for the basic MHM device. First we clearly see spin wave interference within the device over a frequency spectrum. From the results shown we see an approximately 7 mV change in the signal from fully constructive to fully destructive interference. It should be noted that in the graph provided we do not observe the fully destructive interference reaching the 0 point of the graph. This is attributed to the parasitic noise of the system which means that the setup is unable to reach a completely zero state, however, more sensitive equipment should result in an even greater amplitude difference between the constructive and destructive state. Also, spin wave amplitudes are affected by the change in angle, giving credence to the idea that parallelization using phase or angle multiplexing will be possible with any devices created using matrix device method.

Next, experiments were carried out by placing two magnetic objects, as previously discussed, on the junctions of the matrix. Figure 56 shows amplitude and phase information, Figure 56(C) shows raw VNA output, in mV, with different combinations of magnets being added to the matrix. There is a frequency shift in the maximum resonance peak for each combination (note: the symbol O represents no magnet on the junction, thus OO represents a junction with no magnetic objects). Different combinations not only result in distinct amplitude changes for the system, but also result in shifts in the FMR peak, showing a distinct effect caused by the placement of the magnetic objects, and sensitivity to one, two or no magnetic objects.

Figure 56(D) is a graph showing the amplitude of the signal at a fixed frequency, as the magnetic orientations are changed. The amplitudes of each of the signals has been normalized and scaled from 0 to 1, for better comparison. The rotation of the magnetic object appears to clearly correlate with a phase difference dependent on the rotation of the micromagnetic objects. This phase sensitivity is a result of changes in the longitudinal direction of the magnetic film and is most interesting at the two pairs of combinations that represent opposite orientations. When observing the phase of both of the pair (↑↑, →→) and (→↑, ↑→) we see a 180 degree sensitivity in the phase of these two pairs. It should be noted, we clearly see a shift in the wave propagation properties of the spin wave, shown in Figure 56(C). This is clearly evident by the shift in the ferromagnetic resonance measured in the VNA, and is dependent on the placement of one or two magnets.

In both experiments, the output is varied by phase shifting of the input, interfering signal. As with optical holograms this information opens the door to possible multiplexing applications, where by holograms can be constructed and multiple dimensions used. In the optical case this is done by varying the “angle of illumination”, and a parallel process can be

created here, by either varying the frequency, the angle of the applied magnetic field or the phase of the input, interfering wave. Using this information we are able to construct 3D holographic data as an image in Figure 57.

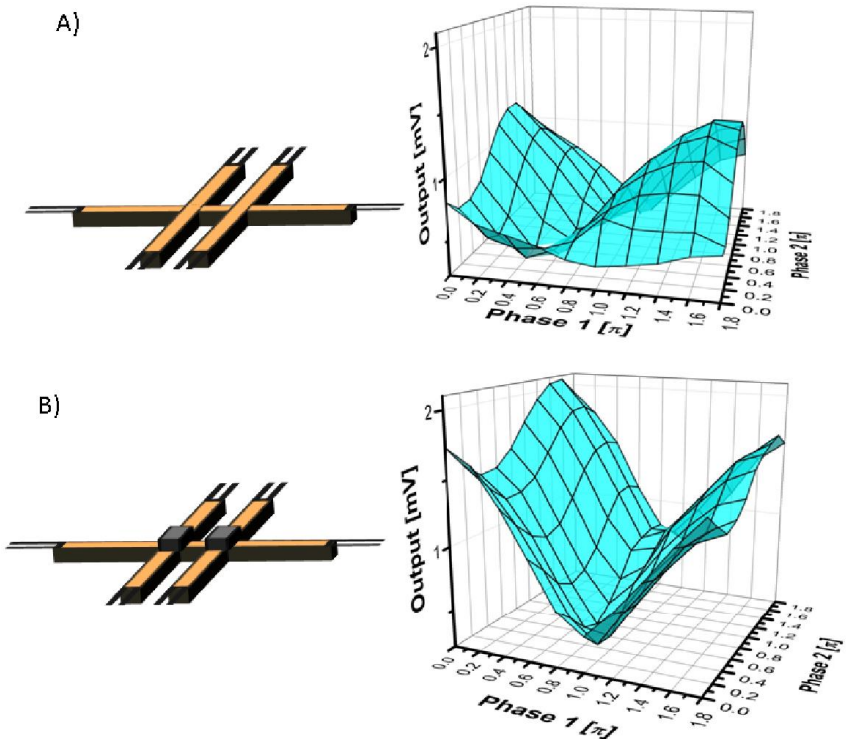

Figure 53 - Spin Wave holograms constructed for both a device with no magnetic object A) as well as a device with magnetic objects on both junctions, B)

For each of the events shown (no magnetic object and both magnetic objects oriented "up") the spin wave holograms show different features over a wide "angle of illumination". It should be noted that this ability means that the system may be very sensitive to even small changes, and the ability to change the angle of illumination to explore new areas of the data may point to the possibility of massive parallelization within the device as well as associative memory applications.

Next, we carried out the experiments placing two micro-magnets with a length of 1.1mm and a width of 360µm, each with a proprietary microscale coating provided by Paramount Sensors and a coercivity of 200-500 Oe on the junctions as illustrated in Figure 58.

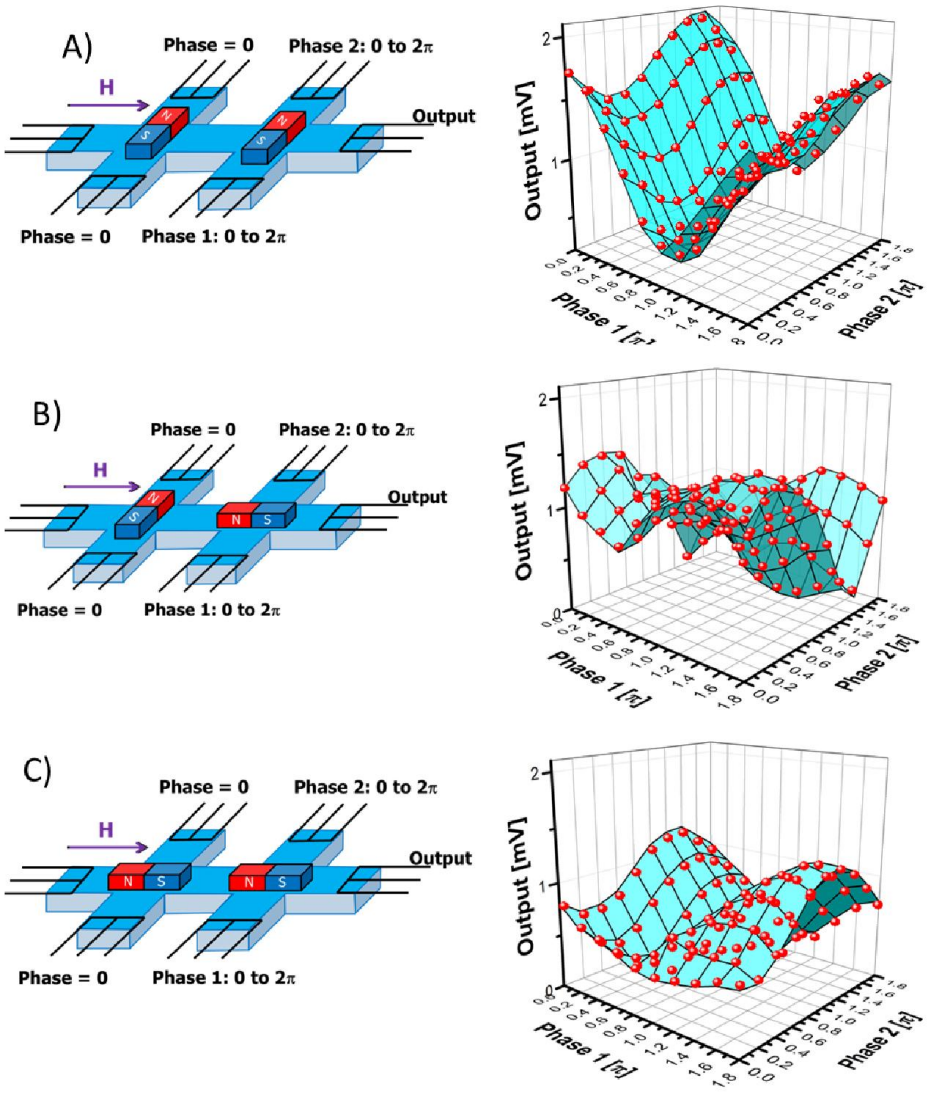

Figure 54 - A set of three holograms obtained for the three configurations of the top micro-magnets as illustrated by the schematics on the top: A) two micro-magnets aligned in the same direction perpendicular to the long axis; B) the magnets are directed in the orthogonal directions; and C) both magnets are directed along the long axis. The red markers show the experimentally measured data (inductive voltage in millivolts) obtained at different phases of the four generated spin waves. The cyan surface is a computer reconstructed 3-D plot. The excitation frequency is 5.4GHz, the bias magnetic field is 1000 Oe

The aim of these experiments is to show the dependence of the output from the magnetic states of the micro-magnets. Figure 58 shows the set of three holograms obtained for the three configurations of the top micro-magnets as illustrated by the schematics: A) two micro-magnets aligned in the same direction perpendicular to the long axis; B) the magnets are directed in the orthogonal directions; and C) both magnets are directed along the long axis. The red markers show the experimentally measured data (inductive voltage in millivolts) obtained at different phases of the four generated spin waves. The cyan surface is a computer reconstructed 3-D plot. The excitation frequency is 5.4GHz, the bias magnetic field is 1000 Oe. All experiments are done at room temperature. As one can see from Figure 58, the state of the micro-magnet significantly changes the output. The three holograms clearly demonstrate the unique signature defined by the magnetic state of the micro-magnet. The internal state of the holographic memory can be reconstructed by the difference in amplitude as well as the phase-dependent distribution of the output.

There are several important observations we want to outline based on the obtained experimental data. The observed interference data are matched well by the classical equation (as shown in Figure 55 (D)). The only feasible deviation is at the point corresponding to the destructive interference, where the experimental data show a non-zero output due to the presence of the additional parasitic coupling (e.g. waveguide eigen modes, reflecting waves, direct coupling among the input/output antennas, etc). Such a good fit shows no feasible sign of the thermal noise. The latter can be explained by taking into account that the flicker noise level in ferrite structures usually does not exceed -130 dBm[66]. At the same time, the direct coupling between the input/output antennas in our case is of the order of -70-80 dBm. So, all possible thermal noise signals are much smaller than the direct coupling, reflections and others parasitic effects.

Phase-dependent output is clearly observed in a relatively long device, where the direct distance from the input to the output exceeds 3mm. In contrast to the initial skepticism on the possibility of using spin wave interference for logic applications [67], it appears to be a robust instrument allowing us to sense magnetic textures at micrometer scale at room temperature. Long coherent is the main physical parameter defining the maximum size of the interference-based devices. Taking into account the typical size of currently used nano-magnetic bits (i.e. ~100 nm x ~100 nm), and with current advances in the patterning of magnetic media spin waves make it possible to sense hundreds of thousands of bits in parallel.

5 Results of Permanent Deformation to Cross Structure

From the aspect of memory devices much of the focus has been on Random Access Memoy (RAM), where in not only the capacity but the speed of the memory is of utmost importance. Longer term, slower, and nonvolatile solutions have focused on magnetic recording technologies such as harddrives and Solid-State Storage solutions that use charge capture methods. Another area of focus is that of write-once read many (WORM) styles of memory recording, of which a prime example is the Compact Disc. This style of memory recording has many applications especially for archival purposes where it is more important that the recorded information last a long time and in a high fidelity state, and speed and even to an extent storage density is a somewhat secondary objective. To date several technologies have been proposed that would allow for huge amounts of data to be stored for archival purposes, with a magnetic technology, in this case referring to magnetic tape[68], being the current popular method used for large scale data storage along with rigid disk technologies. Most recently the company InPhase attempted to introduce optical holographic storage media for use in archival purposes. While some commercial products were released, the technology has since traded hands is still in an evaluation phase. Other technologies have been proposed, but many of them are based on a fuse type system and require exotic materials or nanostructures or in some cases both[69]–[76].

While optical media, for use in holographic storage has some distinct advantages, such as the used of laser based technology as well as the option to use well known glass and plastic technologies, it's short comings, including cost and size may always keep it from being a relevant archival technology. For this purpose it has been proposed that techniques involving permanent features within magnonic holographic devices may allow for a massively parallel technology with WORM capability. In this case a design would

require physical manipulation of the magnetic cross junction, most likely in a permanent manner. These features could be made either during a lithographic process or written to a MHM device grid sometime after the making of the device. To prove the conceptual ability of devices with this design several cross junction were physical modified using Focused Ion Beam technology and the spin wave propagation changes were studied.

5.1 Device Preparation and Description

5.1.1 Single Cross Permalloy Device with Variable Hole Size

Cross devices were fabricated as previously described for Permalloy and YIG devices. Both devices had similar alterations, in both cases holes added to the center of the device at the junction. YIG device holes were fabricated using laser ablation while the device was fabricated. Permalloy devices were measured and then modified using an FIB to add hole structures to the junction. Holes were made going all the way through the spin wave mediation material and into the substrate. The FIB tool used allowed for simultaneous SEM imaging, and holes could be deemed completed when the contrast of the SEM changed. The contrast was a results of going from a conductive material (Permalloy) to a dielectric material (Silicon).

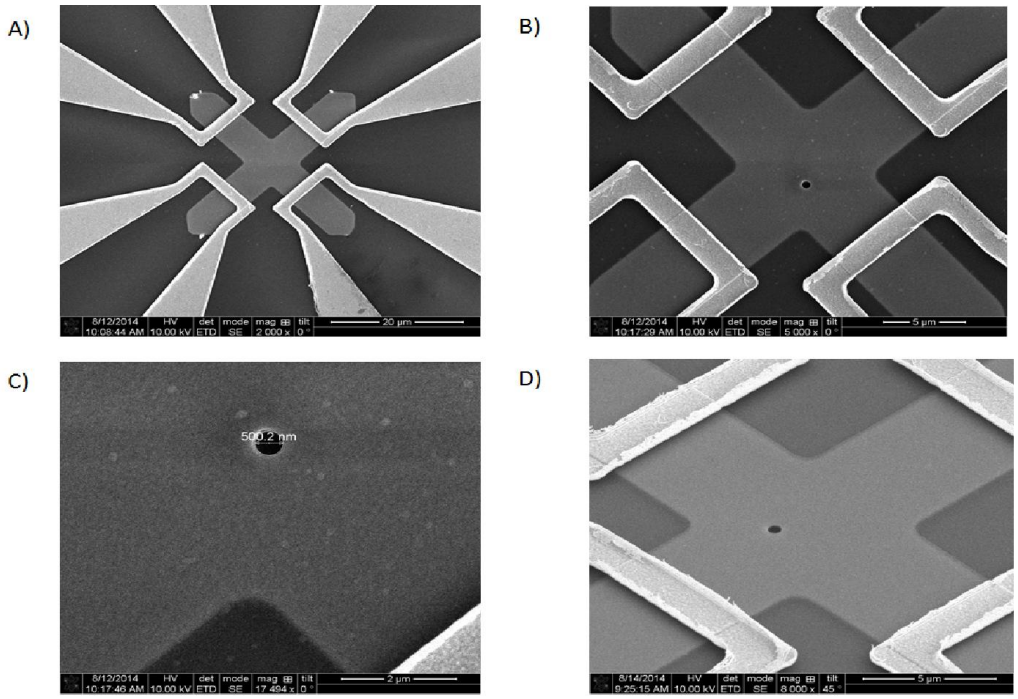

Figure 55 – (A) SEM image of Permalloy cross structure, before milling process. (B) SEM image of the permaloy cross structure after milling. (C) higher resolution image of hole in structure with measurement markers digitally added. (D) Angled image of permalloy cross structure with hole.

The above images shows the cross structure before and after FIB milling. The hole is added to the center of the cross, though it does end up slightly off direct center. The third image of the series (C) shows a measurement made by the SEM system of the hole diameter. Even when the final image of the series shows a tilted angle, it is obvious that the hole goes directly through the Permalloy and leaves a small divot in the substrate.

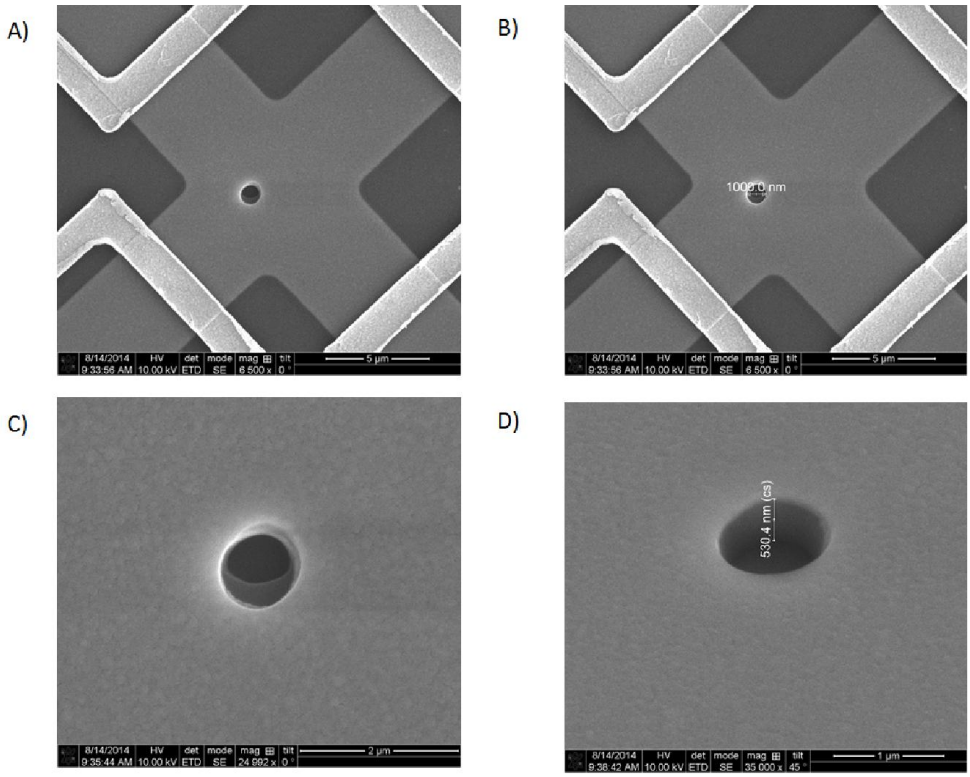

Figure 56 - (A) SEM image of Permalloy cross structure, after hole has been widened. (B) SEM image of the permalloy cross structure with measurement markers added to hole structure. (C) higher resolution image of hole in structure. (D) Angled image of permalloy cross structure with hole, angle allows for depth measurement that insures the hole was milled through to the substrate..

The second set of images is for the 1000 nm (1 um) hole device. This hole is simple a widening of the 500 nm hole, since there was an assumption of continuity between the devices. Since the device is milled while still in the microwave packaging it was expected that all signal changes would be a result of the milling of the wider hole. Since the milling process was not capable of making an accurate donut like shape the hole was milled assuming a circle full circle needed to be milled. For this reason the center of the hole shows a darker contrast change, due to its deeper depth. A careful tilted angle allowed for a depth measurement to be made to ensure that the hole did indeed go through the entire device. With a measured depth of over 500 nm the hole in question is certainly deep enough to penetrate all the layers of the device which should have a stack with the following depths: 100 nm SiO2, 100 nm Py, 10 nm Ti, 100 nm SiO2. With these film thicknesses for the

device, 500 nm should easily penetrate all the layers, and remove all the magnetic material. This image also highlights one of the many advantages of the FIB method, both the ability to directly manipulate a sample as well as the ability to mill walls with very high aspect ratios. There is however some slight drift in the milling process, which is assumed to be caused due to the weight of the packaging and the necessity to mill the device at a 54 degree angle.

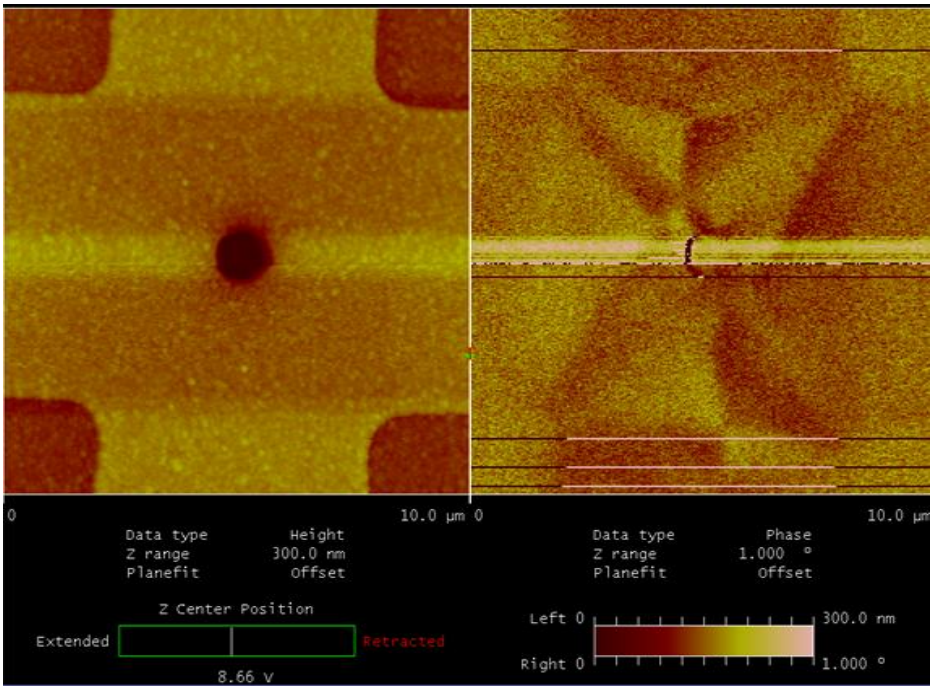

Figure 57 - AFM/MFM image of permalloy hole. A weak MFM isngla on the left shows the change in domain structure, and the AFM shows the topological affect of the FIB milling.

Of much interest is the effect of the magnetic domain structure in a modified domain. The left image shows an AFM topological image of the device with a whole milled through it, and the right image depicts the MFM, showing magnetic domains. Unfortunately due to the 100 nm insulation layer the magnetic signal for this structure is very weak, as well as the fact that Permalloy has a very low coercivity and magnetization, compounding the difficulty for obtaining a clear magnetic signal for the device. What is evident is that there us a clear magnetic domain structure in the device junction that differs from that of the arms. The milled hole unfortunately obscure the MFM directly in the center of the device, however

it is apparent that there are some smaller domain structures that have appeared around the edges of the hole, perhaps due to increased anisotropy from the addition of the hole edges. This is an interesting phenomenon, that may also help account for signal changes resulting in the addition of the whole. If shape anisotropy plays a role in the layout of the magnetic domains in the structure then it may account for signal changes that are observed and noted in the results section of this chapter. It should also be noted that spin wave interference may very well be sensitive to even very small changes in magnetic signal, and is perhaps sensitive to changes in domain and magnetic orientation of magnetic objects. This may very well highlight the sensitivity of the magnonic holographic technique, however, more in-depth studies will have to be done to see the direct influence on physical features such as these with the phase effects of the magnetic oscillations.

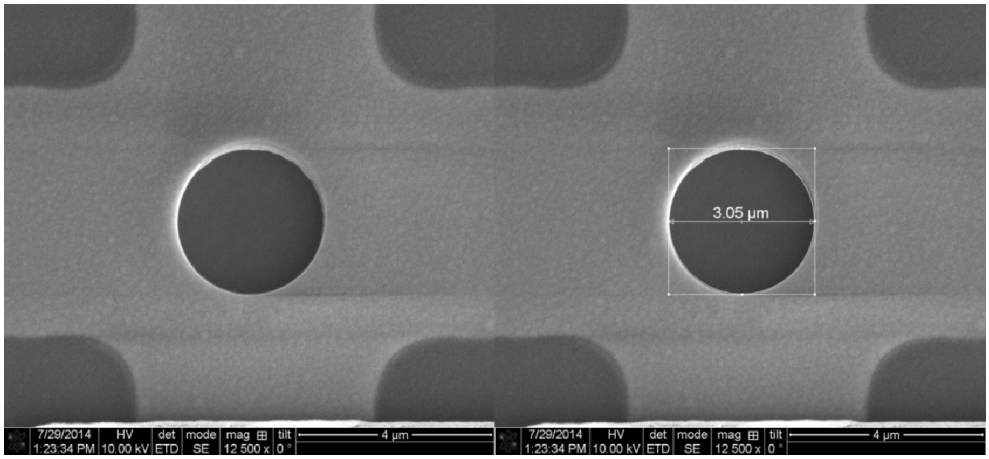

Figure 58 - (Left) SEM image of 3 um hole milled into cross structure. (Right) Same image with digital measurement markers added.

This summarizes the fabrication and simple characterization of these devices. The holes added in the centre should modify the scattering and it was a hoped that there would be some dependence on size. The results of these experiments are below.

5.2 **Results**

The addition of the whole, as an interesting result on the VNA readings for the device. Figure 63 shows a sequence of images for the results obtained for a device as a hole is added and widened.

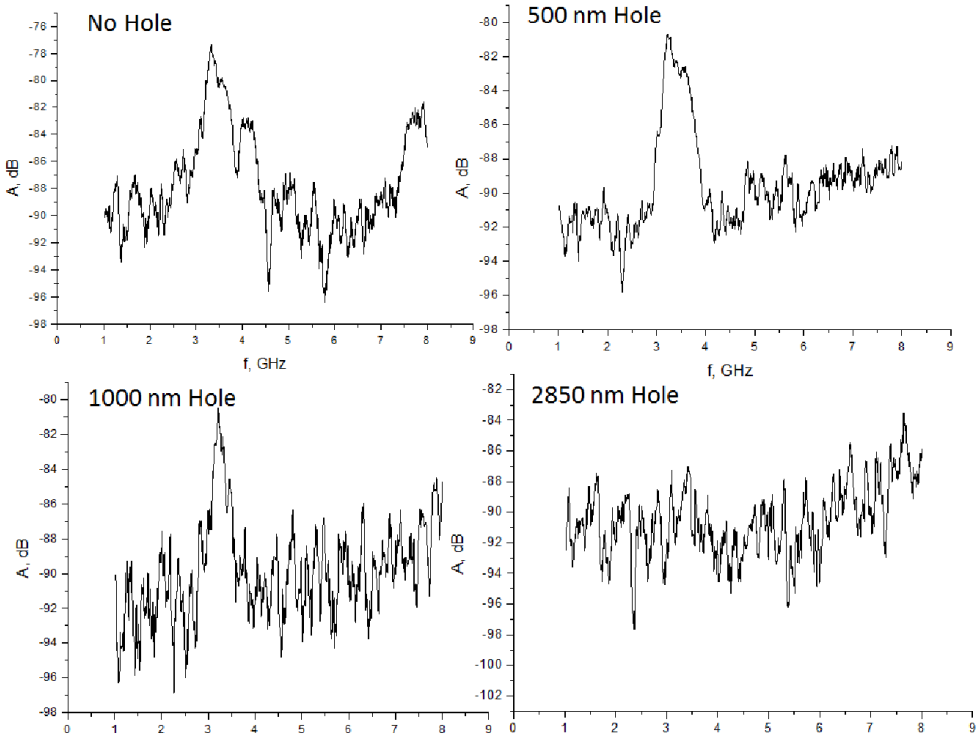

Figure 59 - A sequence of VNA outputs in dB from port 1 to port 3 as the hole structure is widened.

It should be noted that there was an expectation of some drastic change in amplitude as size was increased, which is not readily observed until the whole reaches 2850 nm. What is observed is a slight change in amplitude as wells as what appears to be a narrowing of the frequency band of the resonance peak. Also, while the amplitude of the signal stays mostly the same until 2850, the same cannot be said of the noise level which increases with the size of the hole. While the narrowing of the frequency band cannot be definitely tied to any phenomena from these measurements, and additional measurements will be required it can be hypothesized that the addition of the hole may disallow certain modes and thus frequencies to propagate, in essence acting like a sort of band pass filter for

spin waves. Until more definitive measurements can be made however, it will exist as a question for future research. Below for the interested reader there is also provided some raw data, showing the VNA output for the device as the spin wave propagates from port 1 to the other ports in the device. This data was recently acquired, and has not been fully analysed but does offer some interesting questions, again that can exists as questions for future research.

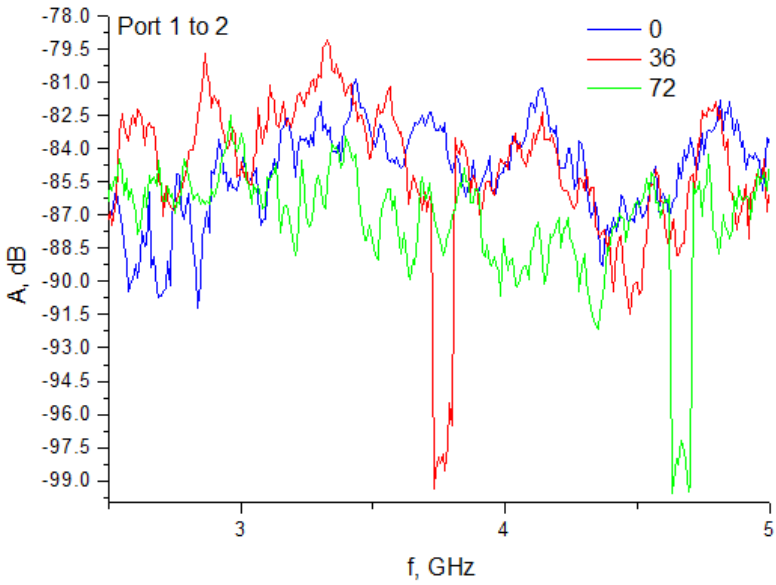

Figure 60 - Output as recorded by the Vector Network Analyser for different applied field angles, with the Y-Axis showing amplitude of the signal in dB, and the X-Axis showing the frequency. The graph shows different applied field angles as different colors, and the signal is a reading from Port 1 to Port 2.

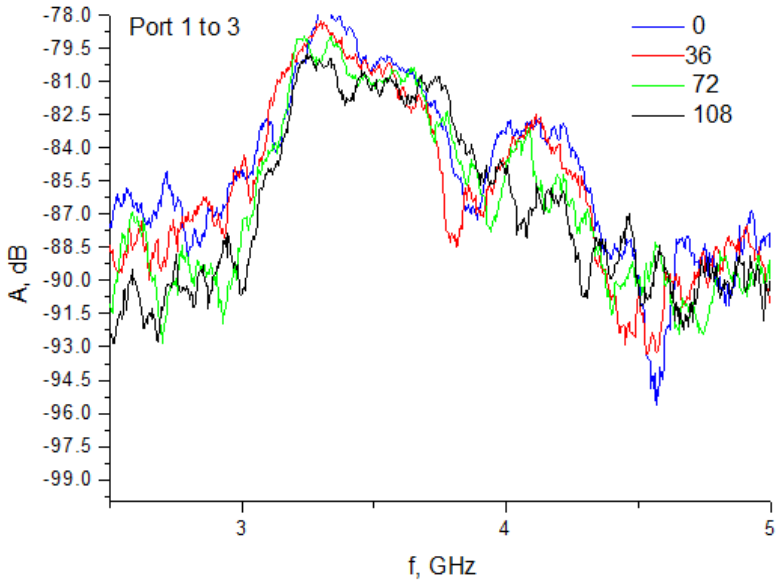

Figure 61 - Output as recorded by the Vector Network Analyser for different applied field angles, with the Y-Axis showing amplitude of the signal in dB, and the X-Axis showing the frequency. The graph shows different applied field angles as different colors, and the signal is a reading from Port 1 to Port 3.

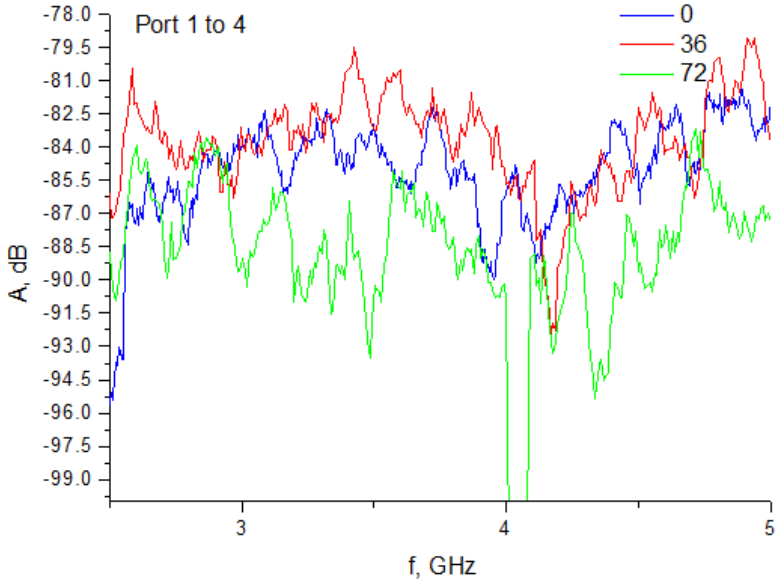

Figure 62 - Output as recorded by the Vector Network Analyser for different applied field angles, with the Y-Axis showing amplitude of the signal in dB, and the X-Axis showing the frequency. The graph shows different applied field angles as different colors, and the signal is a reading from Port 1 to Port 2.

The results from this experiment are compelling in that we do notice several features that will require further inquiry. First, and the most expected result, is there appears to be some modification to the amplitude of the spin wave signal as the hole grows in size. However, the expectation would be that the amplitude might drop off in some linear fashion, i.e. as the hole gets larger the amplitude would decrease. What we observe is in fact some slight increase in the signal, followed by a decrease, and then a sudden "disappearance" of the signal. Also, of great interest, is the information that the signal may in fact be acting in some filtering manner, since the resonance band peak actually decreases in width. All of these questions lend themselves to further study and hopefully will lead further researchers to explore the exact mechanisms of this interaction.

6 Conclusion

In conclusion we demonstrate here the first experimental data of a MHM device. The collected experimental data show rich physical phenomena associated with spin wave propagation in single- and double-cross structures. Prominent signal modulation by the direction rather than the amplitude of magnetic field and the low effect of thermal noise on spin wave propagation at the room temperature are among many interesting findings. The effect of spin wave redirection between the cross arms by the external magnetic field may be further exploited for building a variety of logic devices. Besides, spin waves appear to be a robust instrument allowing us to sense the magnetic state of micro-magnets by the change in the interference pattern. Quite surprisingly, it is possible to recognize the unique holographic output for the different orientations of micro-magnets in a relatively long device at room temperature. Overall, the obtained data demonstrate the practical feasibility of building magnonic holographic devices. These holographic devices are aimed not to replace but to complement CMOS in special type data processing such as speech recognition and image processing. According to the estimates, scaled magnonic holographic devices may provide more than 1×10^{18} bits/cm^2/s data processing rate consuming less than 0.2mW of energy. The main technological challenges are associated with the scaling down the operating wavelength and building nanometer scale spin wave generating/detecting elements. Spin torque oscillators and multiferroics are among the most promising solutions. At the same time, it is expected that reducing the operating wavelength will make spin waves more sensitive to the structure imperfections. The development of scalable magnonic holographic devices and their incorporation with the conventional electronic devices may the pave road to the next generations of logic devices with functional capabilities far beyond current CMOS.

Not only are we able to detect magnetic objects successfully using the device, but independent object orientation as well as parallel detection of objects is observed. These preliminary findings open up the possibility of an entirely new class of magnetic device as well as the possibility for high speed, massively parallelized applications. Furthermore, since the data shows a distinctly nonlinear broadening of the resonance, it can be concluded that there may be a wealth of non-linear phenomena which could have applications in the development of new devices for magnetic resonance imaging, spin-echo effect phenomena, as well as devices for the exploration of interactions with new magnetic phenomena such as topological insulators and skyrmions. As these devices show the same potential as any other spin wave device utilizing interference, they also have the ability to perform spin wave logic operations, work as memory devices and possibly combine memory and logic architectures. It should be noted that these matrix elements can play a prominent role in not only exploring spin wave interference, but also in exploring holographic operations which were not feasible or practical in optical holographic setups. The possible resolution of this technique is governed by both the spatial dimensions of the device as well as the wavelength of the excited spin waves. Since spin wave wavelengths have been measured to less than a micron in wavelength and devices can be manufactured as small as 10 nm we can assume the technique has a similar spatial resolution and could allow for resolutions as high as 10 nm, which competes well with MFM[77] and GMR technologies[78]. Energy efficiency of this technique compares well with other technologies and has been calculated in previous works[44] to be as low as 10 attojoules depending on the excitation method. We present these findings as an exciting new field of study with strong implications both in the field of device physics, as well as possible applications in creating highly accurate spin wave devices to explore spin wave and electron resonance phenomena.

The obtained experimental data show the practical feasibility of utilizing spin waves for building magnonic holographic logic devices and help to comprehend the advantages and the shortcomings of the spin wave approach. There are several important observations we want to outline.

First, spin wave interference pattern produced by multiple interfering waves is recognized for a relatively long device (more than 3 millimeters between the excitation and detection ports) at room temperature. Despite the initial skepticism[67], coding information into the phase of the spin waves appears to be a robust instrument for information transfer showing a *negligible effect of thermal noise* and immunity to the structure imperfections. This immunity to the thermal fluctuations can be explained by taking into account that the flicker noise level in ferrite structures usually does not exceed -130 dBm[66]. At the same time, spin waves are not sensitive to the structure imperfections which dimensions a much shorter than the wavelength. These facts explain the good agreement between the experimental and theoretical data (e.g. as shown in Figure 55).

Second, spin wave transport in the magnetic cross junctions is efficiently modulated by an external magnetic field. Spin wave propagation through the cross junction depends on *the amplitude* as well as *the direction* of the external field. This provides a variety of possibilities for building magnetic field-effect logic devices for general and special task data processing. Boolean logic gate such as AND, OR, NOT can be realized in a single cross structure, where an applying external field exceeding some threshold stops/allows spin wave propagation between the selected arms. The ability to modulate spin wave propagation by the direction of the magnetic field is useful for application in non-Boolean logic devices. It is important to note that in all cases the magnitude of the modulating

magnetic field is of the order of hundreds of Oersteds, which can be produced by the micro- and nano-magnets

Finally, it appears possible to recognize the magnetic state of the magnet placed on the top of the cross junction via the spin waves, which introduces an alternative mechanism for magnetic memory read out. This property itself may be utilized for improving the performance of the conventional magnetic memory. However, the fundamental advantage of the magnonic holographic memory is the ability to read-out a number of magnetic bits in parallel. The obtained experimental data demonstrate the parallel read-out of just two magnetic bits.

In closing presented here are experimental findings and first realization of a magnonic holographic device, as well as findings related to the use of multiferroics for spin wave applications.

7 References

[1] E. Pop, “Energy dissipation and transport in nanoscale devices,” *Nano Research*, vol. 3. pp. 147–169, 2010.

[2] B. Schaller, “The Origin, Nature, and Implications of ‘Moore’s Law,’” 1996. [Online]. Available: http://research.microsoft.com/en-us/um/people/gray/moore_law.html. [Accessed: 10-Sep-2014].

[3] “Semiconductors - A Crazy Industry.” [Online]. Available: http://www.forbes.com/sites/jimhandy/2014/02/11/semiconductors-a-crazy-industry-2/. [Accessed: 10-Sep-2014].

[4] “ITRS 2007 Edition.” [Online]. Available: http://www.itrs.net/Links/2007ITRS/home2007.htm. [Accessed: 10-Sep-2014].

[5] M. M. Mano and C. R. Kime, *Logic and computer design fundamentals, Volume 1*. Pearson/Prentice Hall, 2004, p. 656.

[6] “History of Computing Science: Charles Babbage.” [Online]. Available: http://www.eingang.org/Lecture/babbage.html. [Accessed: 15-Sep-2014].

[7] ITRS, “International Technology Roadmap for Semiconductors, Executive Summary,” *ITRS*, 2011. [Online]. Available: http://www.itrs.net/Links/2011ITRS/2011Chapters/2011ExecSum.pdf.

[8] S. Chikazumi, *Physics of Ferromagnetism*, vol. 1. 1997, p. 655.

[9] C. Kittel, *Introduction to solid state physics*. 2005, p. 703.

[10] M. Covington, T. M. Crawford, and G. J. Parker, “Time-resolved measurement of propagating spin waves in ferromagnetic thin films.,” *Phys. Rev. Lett.*, vol. 89, p. 237202, 2002.

[11] M. P. Kostylev, A. A. Serga, T. Schneider, B. Leven, and B. Hillebrands, “Spin-wave logical gates,” *Appl. Phys. Lett.*, vol. 87, pp. 1–3, 2005.

[12] K.-S. Lee and S.-K. Kim, “Conceptual design of spin wave logic gates based on a Mach–Zehnder-type spin wave interferometer for universal logic functions,” *J. Appl. Phys.*, vol. 104, no. 5, p. 053909, Sep. 2008.

[13] A. Khitun and K. L. Wang, “Nano scale computational architectures with Spin Wave Bus,” *Superlattices Microstruct.*, vol. 38, pp. 184–200, 2005.

[14] A. Khitun, M. Bao, J.-Y. Lee, K. L. Wang, D. W. Lee, S. X. Wang, and I. V. Roshchin, “Inductively Coupled Circuits with Spin Wave Bus for Information Processing,” *J. Nanoelectron. Optoelectron.*, vol. 3, no. 1, pp. 24–34, Mar. 2008.

[15] Y. Wu, M. Bao, A. Khitun, J.-Y. Kim, A. Hong, and K. L. Wang, “A Three-Terminal Spin-Wave Device for Logic Applications,” *J. Nanoelectron. Optoelectron.*, vol. 4, no. 3, pp. 394–397, Dec. 2010.

[16] A. Khitun, M. Bao, and K. L. Wang, “Magnonic logic circuits,” *Journal of Physics D: Applied Physics*, vol. 43. p. 264005, 2010.

[17] B. D. Cullity, *Introduction to Magnetic Materials*. Ma Ling, 1972, p. 666.

[18] T. Wu, A. Bur, J. L. Hockel, K. Wong, T. K. Chung, and G. P. Carman, “Electrical and mechanical manipulation of ferromagnetic properties in polycrystalline nickel thin film,” *IEEE Magn. Lett.*, vol. 2, 2011.

[19] T. K. Chung, G. P. Carman, and K. P. Mohanchandra, “Reversible magnetic domain-wall motion under an electric field in a magnetoelectric thin film,” *Appl. Phys. Lett.*, vol. 92, 2008.

[20] T.-K. Chung, S. Keller, and G. P. Carman, “Electric-field-induced reversible magnetic single-domain evolution in a magnetoelectric thin film,” *Appl. Phys. Lett.*, vol. 94, no. 13, p. 132501, Mar. 2009.

[21] J. Alzate, P. Upadhyaya, and M. Lewis, “Spin wave nanofabric update,” in *International Symposium on Nanoscale Architectures*, 2012, pp. 196 – 202.

[22] A. Khitun and K. L. Wang, “Non-Volatile Magnonic Logic Circuits Engineering,” Dec. 2010.

[23] J. Nitta, F. E. Meijer, and H. Takayanagi, “Spin-interference device,” *Appl. Phys. Lett.*, vol. 75, no. 5, p. 695, Aug. 1999.

[24] P. Rovillain, R. de Sousa, Y. Gallais, A. Sacuto, M. A. Méasson, D. Colson, A. Forget, M. Bibes, A. Barthélémy, and M. Cazayous, “Electric-field control of spin waves at room temperature in multiferroic BiFeO3.,” *Nat. Mater.*, vol. 9, no. 12, pp. 975–9, Dec. 2010.

[25] J. Ding, M. Kostylev, and A. O. Adeyeye, “Magnonic Crystal as a Medium with Tunable Disorder on a Periodical Lattice,” *Phys. Rev. Lett.*, vol. 107, no. 4, p. 047205, Jul. 2011.

[26] V. V. Kruglyak, P. S. Keatley, A. Neudert, R. J. Hicken, J. R. Childress, and J. A. Katine, “Imaging Collective Magnonic Modes in 2D Arrays of Magnetic Nanoelements,” *Phys. Rev. Lett.*, vol. 104, no. 2, p. 027201, Jan. 2010.

[27] B. Behin-Aein, D. Datta, S. Salahuddin, and S. Datta, “Proposal for an all-spin logic device with built-in memory.,” *Nat. Nanotechnol.*, vol. 5, no. 4, pp. 266–70, Apr. 2010.

[28] A. Khitun, D. E. Nikonov, M. Bao, K. Galatsis, and K. L. Wang, “Feasibility study of logic circuits with a spin wave bus.,” *Nanotechnology*, vol. 18, no. 46, p. 465202, Nov. 2007.

[29] E. M. Shapiro, S. Skrtic, and A. P. Koretsky, “Sizing it up: cellular MRI using micron-sized iron oxide particles.,” *Magn. Reson. Med.*, vol. 53, no. 2, pp. 329–38, Feb. 2005.

[30] H.-T. Huang, T.-R. Ger, Y.-H. Lin, and Z.-H. Wei, “Wavy ferromagnetic device as single cell detection,” *J. Appl. Phys.*, vol. 115, no. 17, p. 17E518, May 2014.

[31] H. J. Mamin, M. Poggio, C. L. Degen, and D. Rugar, “Nuclear magnetic resonance imaging with 90-nm resolution.,” *Nat. Nanotechnol.*, vol. 2, no. 5, pp. 301–6, May 2007.

[32] H. Groll and I. Nedkov, Eds., *Microwave Physics and Techniques*. Dordrecht: Springer Netherlands, 1997.

[33] N. Amos, J. Butler, B. Lee, M. H. Shachar, B. Hu, Y. Tian, J. Hong, D. Garcia, R. M. Ikkawi, R. C. Haddon, D. Litvinov, and S. Khizroev, “Multilevel-3D bit patterned magnetic media with 8 signal levels per nanocolumn.,” *PLoS One*, vol. 7, no. 7, p. e40134, Jan. 2012.

[34] S. Tehrani, J. M. Slaughter, E. Chen, M. Durlam, J. Shi, and M. DeHerren, “Progress and outlook for MRAM technology,” *IEEE Trans. Magn.*, vol. 35, no. 5, pp. 2814–2819, 1999.

[35] A. Orlov, A. Imre, G. Csaba, L. Ji, W. Porod, and G. H. Bernstein, “Magnetic Quantum-Dot Cellular Automata: Recent Developments and Prospects,” *J. Nanoelectron. Optoelectron.*, vol. 3, no. 1, pp. 55–68, Mar. 2008.

[36] R. P. Cowburn, “Room Temperature Magnetic Quantum Cellular Automata,” *Science (80-.).*, vol. 287, no. 5457, pp. 1466–1468, Feb. 2000.

[37] D. A. Allwood, G. Xiong, C. C. Faulkner, D. Atkinson, D. Petit, and R. P. Cowburn, “Magnetic domain-wall logic.,” *Science*, vol. 309, no. 5741, pp. 1688–92, Sep. 2005.

[38] S. Mansfeld, J. Topp, K. Martens, J. N. Toedt, W. Hansen, D. Heitmann, and S. Mendach, “Spin Wave Diffraction and Perfect Imaging of a Grating,” *Phys. Rev. Lett.*, vol. 108, no. 4, p. 047204, Jan. 2012.

[39] S.-W. Lee, H.-W. Lee, and K.-J. Lee, “Current-induced modification of spin wave mode interference,” *Curr. Appl. Phys.*, vol. 14, no. 2, pp. 182–186, Feb. 2014.

[40] S. S. Mukherjee, J. H. Kwon, M. Jamali, M. Hayashi, and H. Yang, “Interference-mediated modulation of spin waves,” *Phys. Rev. B*, vol. 85, no. 22, p. 224408, Jun. 2012.

[41] A. Khitun and K. L. Wang, “Spin Wave Magnetic NanoFabric: A New Approach to Spin-Based Logic Circuitry,” *IEEE Trans. Magn.*, vol. 44, no. 9, pp. 2141–2152, Sep. 2008.

[42] A. Kozhanov, A. Anferov, A. P. Jacob, and S. J. Allen, “Spin Wave Scattering in Ferromagnetic Cross,” p. 4, Nov. 2012.

[43] D. Gabor, “A New Microscopic Principle,” *Nature*, 1948. [Online]. Available: http://www.nature.com/nature/journal/v161/n4098/pdf/161777a0.pdf. [Accessed: 14-Jul-2014].

[44] A. Khitun, “Magnonic holographic devices for special type data processing,” *J. Appl. Phys.*, vol. 113, no. 16, p. 164503, Apr. 2013.

[45] A. Khitun and K. L. Wang, “Spin Wave Magnetic NanoFabric: A New Approach to Spin-Based Logic Circuitry,” *IEEE Trans. Magn.*, vol. 44, no. 9, pp. 2141–2152, Sep. 2008.

[46] A. A. Serga, A. V Chumak, and B. Hillebrands, “YIG magnonics,” *J. Phys. D. Appl. Phys.*, vol. 43, no. 26, p. 264002, Jul. 2010.

[47] T. J. Silva, C. S. Lee, T. M. Crawford, and C. T. Rogers, “Inductive measurement of ultrafast magnetization dynamics in thin-film Permalloy,” *J. Appl. Phys.*, vol. 85, pp. 7849–7862, 1999.

[48] M. Bailleul, D. Olligs, C. Fermon, and S. O. Demokritov, “Spin waves propagation and confinement in conducting films at the micrometer scale,” *Europhysics Letters (EPL)*, vol. 56. pp. 741–747, 2007.

[49] V. E. Demidov, J. Jersch, K. Rott, P. Krzysteczko, G. Reiss, and S. O. Demokritov, “Nonlinear propagation of spin waves in microscopic magnetic stripes,” *Phys. Rev. Lett.*, vol. 102, 2009.

[50] T. Schneider, A. A. Serga, B. Hillebrands, and M. P. Kostylev, “Linear and nonlinear phase accumulation of backward volume magnetostatic spin waves in yttrium-iron-garnet spin-wave waveguides,” *Europhys. Lett.*, vol. 77, no. 5, p. 57002, Mar. 2007.

[51] V. V Kruglyak, S. O. Demokritov, and D. Grundler, “Magnonics,” *J. Phys. D. Appl. Phys.*, vol. 43, no. 26, p. 264001, Jul. 2010.

[52] R. W. Damon and J. R. Eshbach, “Magnetostatic modes of a ferromagnet slab,” *J. Phys. Chem. Solids*, vol. 19, no. 3–4, pp. 308–320, May 1961.

[53] M. P. Kostylev, A. A. Serga, T. Schneider, B. Leven, and B. Hillebrands, “Spin-wave logical gates,” *Appl. Phys. Lett.*, vol. 87, no. 15, p. 153501, Oct. 2005.

[54] S. V. Vasiliev, V. V. Kruglyak, M. L. Sokolovskii, and A. N. Kuchko, “Spin wave interferometer employing a local nonuniformity of the effective magnetic field,” *J. Appl. Phys.*, vol. 101, no. 11, p. 113919, Jun. 2007.

[55] S. Kaka, M. R. Pufall, W. H. Rippard, T. J. Silva, S. E. Russek, and J. A. Katine, “Mutual phase-locking of microwave spin torque nano-oscillators,” in *INTERMAG 2006 - IEEE International Magnetics Conference*, 2006, p. 2.

[56] S. Cherepov, P. Khalili Amiri, J. G. Alzate, K. Wong, M. Lewis, P. Upadhyaya, J. Nath, M. Bao, A. Bur, T. Wu, G. P. Carman, A. Khitun, and K. L. Wang, “Electric-field-induced

spin wave generation using multiferroic magnetoelectric cells," *Appl. Phys. Lett.*, vol. 104, 2014.

[57] K. Roy, S. Bandyopadhyay, and J. Atulasimha, "Energy dissipation and switching delay in stress-induced switching of multiferroic nanomagnets in the presence of thermal fluctuations," *J. Appl. Phys.*, vol. 112, 2012.

[58] T. Wu, A. Bur, P. Zhao, K. P. Mohanchandra, K. Wong, K. L. Wang, C. S. Lynch, and G. P. Carman, "Giant electric-field-induced reversible and permanent magnetization reorientation on magnetoelectric Ni/(011) [Pb(Mg[sub 1/3]Nb[sub 2/3])O[sub 3]][sub (1−x)]–[PbTiO[sub 3]][sub x] heterostructure," *Appl. Phys. Lett.*, vol. 98, no. 1, p. 012504, Jan. 2011.

[59] "Spectroscopic Ellipsometry FAQ - J.A. Woollam Co." [Online]. Available: http://www.jawoollam.com/faq.html. [Accessed: 15-Sep-2014].

[60] H. Tompkins and E. A. Irene, *Handbook of Ellipsometry*. William Andrew, 2005, p. 886.

[61] H. K. Kim and M. Cha, "Nonlinear ellipsometric method for measuring second-order cascaded phase shift.," *Opt. Lett.*, vol. 23, pp. 1429–1431, 1998.

[62] "Spectroscopic transmission ellipsometry enables quick measurement of pulp fiber | SPIE Newsroom: SPIE." [Online]. Available: http://spie.org/x14008.xml. [Accessed: 15-Sep-2014].

[63] R. M. Azzam, "Transmission ellipsometry on transparent unbacked or embedded thin films with application to soap films in air.," *Appl. Opt.*, vol. 30, no. 19, pp. 2801–6, Jul. 1991.

[64] C.-C. Tsai, H.-C. Wei, S.-L. Huang, C.-E. Lin, C.-J. Yu, and C. Chou, "High speed interferometric ellipsometer.," *Opt. Express*, vol. 16, pp. 7778–7788, 2008.

[65] "Hysteresis in Magnetic Materials." [Online]. Available: data:text/html,chromewebdata. [Accessed: 15-Sep-2014].

[66] E. Rubiola, Y. Gruson, and V. Giordano, "On the flicker noise of ferrite circulators for ultra-stable oscillators," *IEEE Trans. Ultrason. Ferroelectr. Freq. Control*, vol. 51, pp. 957–963, 2004.

[67] S. Bandyopadhyay and M. Cahay, "Electron spin for classical information processing: a brief survey of spin-based logic devices, gates and circuits.," *Nanotechnology*, vol. 20, p. 412001, 2009.

[68] R. H. Dee, "Magnetic Tape for Data Storage: An Enduring Technology," *Proc. IEEE*, vol. 96, no. 11, pp. 1775–1785, Nov. 2008.

[69] S. Möller, C. Perlov, W. Jackson, C. Taussig, and S. R. Forrest, “A polymer/semiconductor write-once read-many-times memory.,” *Nature*, vol. 426, no. 6963, pp. 166–9, Nov. 2003.

[70] G. Liu, Q.-D. Ling, E.-T. Kang, K.-G. Neoh, D.-J. Liaw, F.-C. Chang, C.-X. Zhu, and D. S.-H. Chan, “Bistable electrical switching and write-once read-many-times memory effect in a donor-acceptor containing polyfluorene derivative and its carbon nanotube composites,” *J. Appl. Phys.*, vol. 102, no. 2, p. 024502, Jul. 2007.

[71] D. Y. Yun, J. K. Kwak, J. H. Jung, T. W. Kim, and D. I. Son, “Electrical bistabilities and carrier transport mechanisms of write-once-read-many-times memory devices fabricated utilizing ZnO nanoparticles embedded in a polystyrene layer,” *Appl. Phys. Lett.*, vol. 95, no. 14, p. 143301, 2009.

[72] B. C. de Brito, E. C. P. Smits, P. A. van Hal, T. C. T. Geuns, B. de Boer, C. J. M. Lasance, H. L. Gomes, and D. M. de Leeuw, “Ultralow Power Microfuses for Write-Once Read-Many Organic Memory Elements,” *Adv. Mater.*, vol. 20, no. 19, pp. 3750–3753, Oct. 2008.

[73] M. A. Mamo, W. S. Machado, W. A. L. van Otterlo, N. J. Coville, and I. A. Hümmelgen, “Simple write-once-read-many-times memory device based on a carbon sphere-poly(vinylphenol) composite,” *Org. Electron.*, vol. 11, no. 11, pp. 1858–1863, Nov. 2010.

[74] J. H. Strickler and W. W. Webb, “Three-dimensional optical data storage in refractive media by two-photon point excitation,” *Opt. Lett.*, vol. 16, no. 22, p. 1780, Nov. 1991.

[75] T. Maruyama and T. Morishita, “Copper nitride and tin nitride thin films for write-once optical recording media,” *Appl. Phys. Lett.*, vol. 69, no. 7, p. 890, Aug. 1996.

[76] L. Dhar, K. Curtis, and T. Fäcke, “Holographic data storage: Coming of age,” *Nat. Photonics*, vol. 2, no. 7, pp. 403–405, Jul. 2008.

[77] G. N. Phillips, M. Siekman, L. Abelmann, and J. C. Lodder, “High resolution magnetic force microscopy using focused ion beam modified tips,” *Appl. Phys. Lett.*, vol. 81, no. 5, p. 865, 2002.

[78] R. Wood, “The feasibility of magnetic recording at 1 Terabit per square inch,” *IEEE Trans. Magn.*, vol. 36, no. 1, pp. 36–42, 2000.